FLEXIBLE FILM AND BREATHABLE TEXTILE ELECTRODES FOR ELECTRODERMAL ACTIVITY MONITORING

by

Peter Alexander Haddad

B.Sc., McGill University, 2011

M.A.Sc., University of Ottawa, 2014

A DISSERTATION SUBMITTED IN PARTIAL FULFILLMENT OF

THE REQUIREMENTS FOR THE DEGREE OF

DOCTOR OF PHILOSOPHY

in

THE FACULTY OF GRADUATE AND POSTDOCTORAL STUDIES

(Biomedical Engineering)

THE UNIVERSITY OF BRITISH COLUMBIA

(Vancouver)

August 2018

Committee Page

The following individuals certify that they have read, and recommend to the Faculty of Graduate and Postdoctoral Studies for acceptance, the dissertation entitled:

Flexible Film and Breathable Textile Electrodes for Electrodermal Activity Monitoring

submitted by Peter Alexander Haddad in partial fulfillment of the requirements for the degree of Doctor of Philosophy
in Biomedical Engineering

Examining Committee:

Peyman Servati, Electrical and Computer Engineering
Co-supervisor

Frank Ko, Materials Engineering
Co-supervisor

Janice Eng, Physical Therapy
University Examiner

Robert Rohling, Electrical and Computer Engineering & Mechanical Engineering
University Examiner

Additional Supervisory/Examining Committee Members:

John Madden, Electrical and Computer Engineering
Supervisory Committee Member

Shahriar Mirabbasi, Electrical and Computer Engineering
Supervisory Committee Member

Hani Naguib, Mechanical Engineering
External Examiner

Abstract

The field of research on wearable systems that monitor human biological responses for healthcare applications is constantly advancing. Electrodermal activity (EDA) is related to the neurological system and is a result of the autonomic nervous system being stimulated, which produces sweat on the surface of the skin, thereby changing its electrical characteristics. The current clinical devices used to monitor EDA utilize rigid and non-breathable silver/silver chloride (Ag/AgCl) electrodes, possibly in combination with gels and irritating adhesives. The research detailed in this dissertation is focused on advancing our understanding of the design and development of comfortable, flexible and breathable EDA electrodes.

Flexible dry Ag/AgCl electrodes were fabricated on a compliant substrate with various surface areas, distances between and geometries. The flexible electrodes were systematically characterized to determine their ability to detect EDA stimulus responses and these were compared to the responses simultaneously collected by rigid dry Ag/AgCl electrodes. The data demonstrated that surface area, spacing and geometry of electrodes affected the detection of the EDA stimulus response. The minimum number of sweat glands to be covered by flexible EDA electrodes has been estimated at 140 to maintain functionality. The optimal design of flexible electrodes is a serpentine geometry (0.15 cm^2 surface area, 0.20 cm distance).

Ag/AgCl electronic yarns were developed through a novel roll-to-roll system and integrated into textile substrates of cotton, nylon and polyester. The EDA stimulus responses detected by dry electronic textile (e-textile) electrodes at various locations on the hand were compared to the EDA signals collected by dry solid Ag/AgCl electrodes. The cotton textile substrate with e-textile electrodes (0.12 cm^2 surface area, 0.40 cm distance) was the optimal material to detect the EDA stimulus responses. Also, differences with EDA waveforms

recorded on various fingers were observed. Trends of long-term measurements showed that skin surface temperature affected EDA signals recorded by non-breathable electrodes more than when e-textile electrodes were used. The effects of electrode design and material for flexible and breathable EDA electrodes detailed in this dissertation can promote the development of effective and wearable EDA monitoring systems, which can help improve our knowledge of the human neurological system.

Lay Summary

The electrodes associated with biological signal monitoring systems in the healthcare setting are critical components that are required to provide accurate and precise data to the user and healthcare providers. Electrodermal activity (EDA), a measurable feature of the human neurological system through sweat, is normally monitored by electrodes on the surface of the skin which are rigid, non-breathable and can be uncomfortable. The work presented in this dissertation compared EDA signals collected by fabricated flexible film and breathable textile electrodes to signals recorded by standard rigid electrodes. The sweat gland coverage, textile material properties and location of the electrodes were shown to affect the detection of EDA signals by flexible and breathable electrodes. This information can provide guidance for the design and development of functional, comfortable and wearable electrodes for long-term EDA monitoring systems, which in turn can promote better understanding of the human neurological system.

Preface

Aspects of the material in chapter 3 of this dissertation were presented as a poster at the 2015 Material Research Society Spring Meeting and Exhibit, as well as at the 2016 Engineering Medical Innovation Global Competition, which also included a full presentation:

P. A. Haddad, A. Servati, S. Soltanian, F. Ko, and P. Servati, "Flexible electrodes for electrodermal activity monitoring," *Materials Research Society Spring Meeting and Exhibit*, San Francisco, California, United States, 2015.

P. A. Haddad, A. Servati, S. Soltanian, E. Hosseini, E. Alhabshi, G. Su, F. Ko, and P. Servati, "Flexible wearable system for electrodermal activity monitoring," *Engineering Medical Innovation Global Competition*, Sha Tin District, East New Territories, Hong Kong, 2016.

A version of chapter 3 has been published in IEEE Transactions on Biomedical Engineering:

P. A. Haddad, A. Servati, S. Soltanian, F. Ko, and P. Servati, "Effects of flexible dry electrode design on electrodermal activity stimulus response detection," *IEEE Trans. Biomed. Eng.*, vol. 64, no. 12, pp. 2979–2987, Dec. 2017.

Research detailed in chapter 4 has been submitted as two manuscripts to journals for review and potential publication as of July 20, 2018:

Submitted Manuscript for Review: P. A. Haddad, A. Servati, S. Soltanian, P. Servati, and F. Ko, "Roll-to-roll electrochemical fabrication of non-polarizable silver/silver chloride coated nylon yarn for biological signal monitoring," 2018.

Submitted Manuscript for Review: P. A. Haddad, A. Servati, S. Soltanian, F. Ko, and P. Servati, “Breathable dry silver/silver chloride electronic textile electrodes for electrodermal activity monitoring,” 2018.

In reference to IEEE copyrighted material which is used with permission in this thesis, the IEEE does not endorse any of the University of British Columbia’s products or services. Internal or personal use of this material is permitted. If interested in reprinting/republishing IEEE copyrighted material for advertising or promotional purposes or for creating new collective works for resale or redistribution, please go to http://www.ieee.org/publications_standards/publications/rights/rights_link.html to learn how to obtain a License from RightsLink.

The author of this dissertation conducted the literature review, structured the design of the research, prepared all testing protocols, experimental setups, collected data, analyzed the data, prepared the posters and presentations for conferences, and wrote the manuscripts.

All other individuals listed in the aforementioned posters, presentations and manuscripts contributed by providing guidance on aspects of the experimental design and analysis, as well as revising submitted work. Supervision was provided mainly by my co-supervisors Prof. Peyman Servati and Prof. Frank Ko, while additional feedback was provided by Dr. Amir Servati and Dr. Saeid Soltanian.

Table of Contents

List of Tables

List of Figures

List of Symbols

Symbol	Description
%	Percent
°	Degree
°C	Degrees Celsius
µ-	Micro-
A	Ampere
a	Ionic activity
C	Coulomb
c-	Centi-
D	Distance
d-	Deci-
E	Half-cell potential
E^0	Standard half-cell potential
F	Faraday's constant
g	Gram
h	Hour
Hz	Hertz
I	Current
J	Joule
K	Kelvin
k-	Kilo-
K_s	Solubility product
L	Litre
L or l	Length
m	Meter
M	Moles per litre
m	Mass
m-	Milli-
min	Minute
mol	Mole
MW	Molecular weight
n	Number of valence electrons
n	Number of trials
N	Newton
N	Number
n-	Nano-
p	Vapor pressure
Pa	Pascal
pH	Power of hydrogen
R	Universal gas constant
R_n	Resistance

RH	Relative humidity
R_K	Contact resistance
S	Siemen
s	Second
SA	Surface area
S_p	Saturation pressure
t	Time
tex	Linear mass density in grams per 1000 meters
V	Voltage
W	Watt
W	Weight
X	Magnification multiple
Ω	Ohm

List of Abbreviations

Abbreviation	Description
AC	Alternating current
Ag	Silver
AgCl	Silver chloride
ANS	Autonomic nervous system
ASTM	American Society for Testing and Materials
Bio-signal	Biological signal
BLE	Bluetooth low energy
CAD	Canadian dollar
Cl	Chlorine
CNS	Central nervous system
Cu	Copper
DC	Direct current
DI	Deionized
e^-	Electron
ECG	Electrocardiogram
EDA	Electrodermal activity
EDS	Energy-dispersive X-ray spectroscopy
EEG	Electroencephalogram
EMG	Electromyogram
EOG	Electrooculogram
ESEM	Environmental scanning electron microscope
e-textile	Electronic textile
FE-SEM	Field emission scanning electron microscope
FPS	Feet per second
GB	Gigabyte
IEEE	Institute of Electrical and Electronics Engineers
IrDA	Infrared
Li	Lithium
MICS	Medical implant communication service
Na	Sodium
NaCl	Sodium chloride
PCG	Phonocardiogram
PVDF	Polyvinylidene fluoride
RPM	Revolutions per minute
SEM	Scanning electron microscope
SNS	Sympathetic nervous system
SWS	Smart wearable systems
US	United States
USD	United States dollar
WLAN	Wireless local area network

WVT	Water vapor transmission
XRD	X-ray diffraction

Acknowledgements

I would first like to thank my co-supervisors Prof. Peyman Servati and Prof. Frank Ko for providing me with the opportunity to work on interdisciplinary research that is both exciting and thought-provoking. Prof. Servati, your critical and analytical approach to experimentation has helped me effectively evaluate the motivations and importance of every aspect of conducting research. Prof. Ko, your expertise on navigating extensive amounts of information in a variety of research fields has assisted me in understanding how to approach a challenging question that is yet to be answered. I would also like to thank Prof. John Madden and Prof. Shahriar Mirabbasi, who both kindly accepted to be on my supervisory committee and provided me with supportive knowledge and direction. Thank you to Prof. Martin McKeown for providing insight about the clinical environment.

This work was supported by the Natural Sciences and Engineering Research Council of Canada Strategic Project and Discovery Grants and the Canada Foundation for Innovation. I would like to acknowledge support from the UBC Biomedical Engineering Graduate program through the Engineers in Scrubs and the Faculty of Applied Science Graduate Student awards.

Dr. Saeid Soltanian and Dr. Amir Servati, thank you for continually providing me with valuable help and insights on experimental aspects, as well as on overall research approaches. Also, thank you, Mr. Jacob Kabel, for your help in obtaining scanning electron microscopy images and energy dispersive x-ray spectroscopy analyses, and Ms. Anita Lam for the x-ray diffraction analyses. For the guidance on electrical aspects of the work, many thanks to Ms. Elnaz Hosseini, Ms. Esra Alhabshi, Ms. Grace Su and Mr. Hossein Soltanian.

Finally, thank you to my wonderful wife Tara, family and friends for always being there for me; it means the world to me.

To my wife, Tara, who always gives me a reason to smile.

Chapter 1: Introduction

A significant component in enhancing the delivery of healthcare for a variety of patients is the development and improvement of medical devices. More specifically, progress in the field of biomedical engineering and smart wearable systems (SWS) can aid in providing vital and timely information on patients, regardless of their location [1]–[6]. The continuous data from these wearable biological monitoring devices can help extend healthcare beyond the clinical environment [1], [2], [5]–[7]. This information can also enable clinicians and other specialists to make important decisions on the delivery of care for patients with a more comprehensive and longer-term understanding of their health status [1], [2], [5]–[7]. At this time, wearables for healthcare do have their challenges and limitations which generate obstacles for effective implementation of these devices in everyday life. However, if there is sustained commitment from interdisciplinary research and sufficient financial resources, it is believed that the benefits will significantly outweigh the investment [2], [4]–[6], [8]. In particular, research into breathable and flexible electrodes can promote the successful integration of wearable monitoring devices in healthcare, which has the potential to increase the quality of life for numerous individuals and reduce overall healthcare costs by reducing patient time in the clinical setting [2], [4], [5], [8].

In order for SWS to be safe and effective means of enhancing healthcare delivery to patients, further progress must be made in terms of functionality of current devices being researched and used. Some of the specific challenges in regards to wearable devices include developing an unobtrusive system [3], [9] while maintaining functionality [10], which drives research into novel flexible sensors and wearable systems. In addition to these challenges, like in many other fields, cost and ethical aspects are equally important factors associated with any

developmental process [2], [10]. By finding effective solutions to these challenges, SWS can be utilized in a variety of applications for patients suffering from acute or chronic conditions [2], [11]. These wearable healthcare technologies can be used to help individuals with cardiovascular [12], [13], pulmonary [14], musculoskeletal [15] and neurological [13] health issues. The focus for this research will be on the design and development of flexible electrodes based on flexible polymers and of breathable electronic textile (e-textile) electrodes.

E-textiles are developed through various methods for end-user comfort and functionality, and hold great promise for the field of wearable technology [16]–[21]. Textile sensors for health monitoring is an area of particular interest for many researchers due to the potential these devices have for making a positive socio-economic impact [13], [22]. For example, using e-textiles to monitor the neurological health of an individual for a known indicator like electrodermal activity (EDA) [23], [24], [33]–[36], [25]–[32] can potentially help diagnose a medical condition and monitor progress throughout treatment.

EDA is directly related to different states of emotional, cognitive or physical stress [35]. This response is the result of the sympathetic nervous system (SNS), which is a division of the autonomic nervous system (ANS) [35]. A state of stress causes an increase of sweat on the skin surface and therefore the electrical properties of the skin change [35]. It is this variation of electrical characteristics of the skin that, when monitored, is called electrodermal activity [35]. The development of flexible and breathable EDA electrodes, as well as further exploration of the effects of design and material selection on the accuracy and precision of detecting EDA, are the main areas of interest of this research. The scientific contributions of this dissertation focus on characterizing the material properties of polymer-based and textile-based electrodes and understanding how they can impact EDA monitoring.

1.1 Objectives and Hypothesis

The objectives of this research are focused on the development and functionality of flexible and breathable electrodermal activity electrodes. In particular, specific design aspects of the electrodes will be assessed and optimized in regards to the ability to effectively monitor EDA. The following are the specific objectives in the form of questions for the EDA research:

1. Flexible Polymer Objectives:
    a. How can we fabricate flexible macroscale silver/silver chloride (Ag/AgCl) electrodes with varying surface areas, geometries and distances between electrodes?
    b. How does surface area of the electrode affect the EDA recording?
    c. How does distance between electrodes affect the EDA recording?
    d. How does the geometry of the electrode affect the EDA recording?
2. Flexible and Breathable Electronic Textile Objectives:
    a. How can we fabricate flexible and breathable Ag/AgCl e-textile electrodes?
    b. How can we prototype functional flexible and breathable EDA electrodes?
    c. How does the material of textile substrates affect the EDA recording in terms of breathability, wettability and bendability?
    d. How does the location of electrodes on the hand affect the EDA recording?

It is believed that through this research, the design of flexible and breathable Ag/AgCl electrodes can be optimized in order to accurately and precisely monitor EDA signals when compared to the signals recorded by current clinical standard Ag/AgCl electrodes.

1.2 Rationale

The main obstacle for long-term EDA monitoring is the lack of understanding of the accuracy and precision of breathable and flexible electrodes when compared to current commercial Ag/AgCl electrodes, which are rigid and at times require the use of gels and strong adhesives on the surface of the skin. In addition, the conventional electrodes are not breathable, preventing the sweat from evaporating or being reabsorbed in a natural way, and possibly causing irritation on the skin. This dissertation provides a novel engineering research approach to the design and development of wearable electrodes suitable for monitoring EDA that are flexible and breathable, enabling further knowledge generation in the area of EDA. In particular, the fabrication of flexible and breathable non-polarizable Ag/AgCl EDA electrodes requires novel methods and optimization. The fundamental understanding of the impact of surface area, geometry and distance between electrodes for EDA monitoring has not been explored systematically. In addition, optimal designs and materials for polymer-based and textile-based EDA electrodes have not been identified in previous literature.

1.3 Scope

The scope of this research will focus on specific and current technical challenges in the area of EDA monitoring. In particular, fabrication approaches for flexible Ag/AgCl electrodes for EDA monitoring will be explored to identify an ideal production method to yield a variety of electrode designs. This will allow for the development of a fundamental understanding of the effects of surface area, geometry and distance between electrodes for EDA monitoring, which have not been explored systematically. The fabrication and functionalization of conductive e-textiles will also be researched. More specifically, e-textile Ag/AgCl electrodes

will be fabricated with a novel experimental approach in order to then determine optimal designs, materials and locations on the fingers for flexible and breathable e-textile EDA electrode straps. Long-term wearability aspects will also be evaluated to determine the potential benefits of e-textile electrodes compared to the current non-breathable and rigid electrodes most commonly used.

1.4 Organization of Thesis

Chapter 1 is the introduction which outlines the field of interest for this dissertation while identifying the objectives, hypothesis, rationale and scope of the work. Chapter 2 is focused on reviewing existing literature on flexible substrates and e-textiles for biological signal monitoring in conjunction with research conducted on EDA monitoring with e-textiles. Chapter 3 describes the design and development of flexible electrodes fabricated on a polymer substrate with a discussion on optimizing and understanding the effects of electrode design on EDA stimulus response detection. Chapter 3 details the fundamental effect of electrode geometry on recording EDA signals. Chapter 4 then utilizes the understanding developed in chapter 3 and further explores the impact of material properties of e-textiles and substrate textiles on EDA monitoring. Chapter 5 is the conclusion which integrates all of the knowledge gained throughout the experimental work and highlights the contributions of this work to the field of biomedical engineering. In addition, recommendations for future work will be discussed.

Chapter 2: Literature Review

Wearable sensors have been researched for a variety of applications. In healthcare, the SWS must be wearable, comfortable and flexible, as well as be safe, effective and enhance the quality of care that a clinician or specialist can provide for the patient [9], [37]. All of these requirements need to be met in order for SWS to be successfully integrated into the current methods of delivering healthcare. There are many biological signals that sensors are capable of detecting on the skin of the human body and the main ones are listed in Table 2.1 to demonstrate the wide range of applications possible. This information has been extracted from multiple sources and specific studies utilizing commercial system are indicated in Table 2.1 [3], [8], [13], [16]–[18], [22], [38]–[40].

Table 2.1 Biological signals measured by sensors on the skin of the human body

Biological Signal	Sensor	Reference
Body temperature	Thermal and Optical	[41]
Blood pressure	Pressure and Optical	[42]
Respiration rate	Piezoelectric / Piezoresistive and Optical	[43]
Blood oxygen saturation	Optical; Pulse Oximetry and Photoplethysmography	[44]
Heart electrical activity and rate	Electrodes; Electrocardiogram (ECG)	[45]
Brain electrical activity	Electrodes; Electroencephalogram (EEG)	[46]
Muscle electrical activity	Electrodes; Electromyogram (EMG)	[47]
Eye electrical activity and movement	Electrodes; Electrooculogram (EOG)	[48]
Body movement and acceleration	Stress, Strain, Accelerometer, Gyroscope	[49]
Sweat / skin conductance	Moisture / Electrodermal Activity	[50]
Heart and respiration sounds	Acoustic; Phonocardiogram (PCG)	[51]
pH, electrolytes, biological markers	Chemical	[52]

Review papers on SWS for healthcare have focused on many aspects of wearable sensors [5], [16]–[18]. Where this review will differ is that it will have an emphasis on electrodermal activity sensors. This review will outline the complications associated with wearable sensors on the human body and where the current research is in terms of finding solutions to these challenges. The fabrication methods will also be discussed in addition to the current and potential uses of SWS in healthcare. Finally, the areas in which further studies need to be conducted to progress the field towards implementation will be described.

2.1 Characteristics and Complications of Wearable Sensors on the Human Body

The main areas in which progress is still necessary for SWS in healthcare include developing devices that are unobtrusive and comfortable [3], [9], energy efficient for secure wireless communication [5], [53], as well as functional and effective over long periods of time [10]. Cost for developing the device is also an important factor, which will determine whether SWS will be implemented successfully [2], [10]. However, this aspect, in addition to energy efficiency and wireless communication, will not be a focus of this review or research.

Patient acceptance and comfort level with wearable sensors are important and have to be a major focus during the design and development phases, as these aspects could directly impact the functionality of SWS. There is currently a deficiency in understanding the factors associated with patients accepting wearable sensors for biomedical applications [9]. Fensli et al. in 2008 constructed a model to assess the level of patient acceptance of a wireless ECG device compared to the commonly used Holter recorder, which is a wired and at times cumbersome technology that is considered a portable ECG monitor [9]. Previous research on user acceptance of technology [54], [55] guided Fensli et al. to outline specific aspects that

should be considered when developing wearable devices, which include: hygiene, physical activity, skin reactions, anxiety and equipment [9]. In addition, other areas of study included pre-trial expectations and patient characteristics [9]. By evaluating user experiences based on the above-mentioned factors, one can utilize the qualitative information collected to make conclusions on the possibility of integrating the wearable technology seamlessly into the lifestyle of individuals. Defining a device as wearable is a very subjective task, as wearability is determined by the user, however various research groups have demonstrated that devices in the form of rings [56], bands [57], adhesive patches [58], and types of clothing such as shirts [59]–[62] can be viewed as wearable. Flexible electronics have the potential to be successfully utilized in long-term healthcare monitoring due to the possibility of creating comfortable solutions without compromising functionality [3].

The multitude of biological signals outlined in Table 2.1 that can be measured on the human body create many opportunities to further understand the biological system. Long-term functionality of SWS to measure parameters such as temperature, electrodermal activity, movement, ECG and heart rate will require one to assess multiple factors to ensure effective monitoring of signals [10]. These aspects include, but are not limited to, location and material of the sensor, signal processing methods and data analysis, as well as electronic components, wireless communication, and optimal energy utilization [10]. Whether the sensor is contactless, such as ECG e-textile SWS that uses a capacitive bio-potential electrode [63], or requires direct contact with the skin, such as adhesive thermocouple sensors for measuring skin temperature [64], limitations arise for the two scenarios. For example, with contactless sensors, motion artifacts become a significant issue in relation to filtering out the signal of interest [63] and some studies have attempted to determine adaptive cancellation methods for

specific wearable devices like photoplethysmography ring sensors [65]. For direct contact fixed sensors, skin contact is of utmost importance when detecting the signal on the skin, and therefore some solutions have even investigated implanting or tattooing the sensor onto the skin to eliminate the need for skin preparation, adhesives, and gels [66]. The general components of SWS are shown in Figure 2.1, however, it is important to note that this dissertation is focused on the sensors of the system.

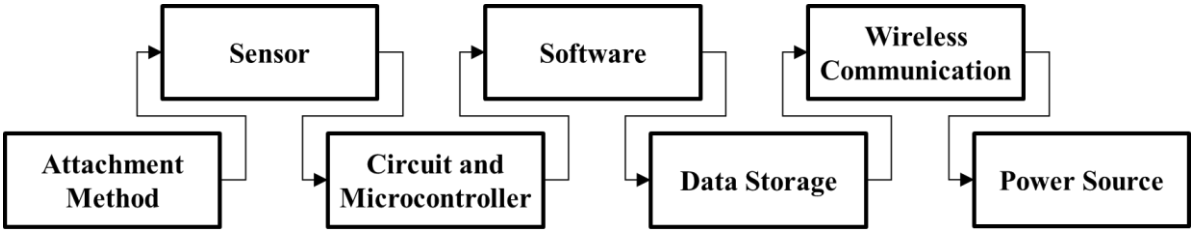

Figure 2.1 Schematic showing the general components of a smart wearable system.

Although not a focus of this research, it is still essential to outline that power consumption and wireless communication are two important factors when developing a long-term wearable healthcare monitor [53]. These two aspects of SWS are directly related, as wireless communication is what requires the majority of power [8]. The two most prominent methods of low-power wireless communication for SWS include ZigBee (IEEE 802.15.4) [67] and Bluetooth (IEEE 802.15.1) enabled devices [68], while other methods such as intra-body area network communication include infrared (IrDA) and the medical implant communication service (MICS), as well as wireless local area network (WLAN) (IEEE 802.11) [8]. The wireless communication standards information mentioned by Pantelopoulous et al. is shown in Table 2 [8]. A more recent wireless communication method that SWS for healthcare can use is Bluetooth low energy or 4.0 (BLE) (IEEE 802.15.1) [69] and is also included in Table 2. Researchers have also investigated methods to reduce power consumption with wearables [70].

Table 2.2 Wireless communication standards [Adapted from [8] with additions]

	Range	Maximum Data Rate	Power Consumption (sending/receiving)	Cost per Chip (USD)	Frequency
Zigbee	10-75 m	20 kbps/ 40 kbps/ 250 kbps	30 mW	$2	868 MHz/ 915 Mhz/ 2.4 GHz
Bluetooth 3.0	10-100 m	1-3 Mbps	2.5-100 mW	$3	2.4 GHz
Bluetooth LE	50 m	1 Mbps	0.15 mW	$3	2.4 GHz
IrDA	1 m	16 Mbps	0.16 mW	$2	Infrared
MICS	2 m	500 kbps	25 µW	-	402-405 MHz
WLAN	200 m	54 Mbps	1 W	$9	2.4 GHz

The cost of developing a smart wearable system for healthcare applications is a necessary assessment, as it is directly related to the accessibility of the device. Also, evaluation of cost savings in healthcare is equally as important, since finding a market need promotes successful integration into the healthcare delivery process. In the United States (US), based on a 2013 report, approximately 75% of their annual $2 trillion USD medical budget is spent on management of chronic disease outcomes [71]. Smart wearable systems can help lessen the burden of chronic disease costs by extending healthcare beyond the clinical setting, relieving strain on resources in hospitals and other institutions [2]. Chronic diseases account for 7 out of 10 deaths annually in the US [71], and SWS can provide timely and more relevant information on their current health status, which can then allow healthcare professionals to establish more effective preventative care plans and treatments [2], [6].

2.2 Physiology of Electrodermal Activity

The first documented observations of quantifiable changes due to emotions happened over a century ago [72], [73]. The term electrodermal activity was introduced by Johnson and

Lubin in 1966 and provided the foundation for further research in the field [74]. EDA was used as a general term for all electrical phenomena on the skin until Brown in 1967 established additional ways to classify specific electrical activities on the human skin [75]. The EDA phenomena and research on the topic are expertly summarized and then discussed in detail by Boucsein in 2012 [35]. Only selected concepts in regards to EDA will be described in this review to highlight important parameters specific to SWS for healthcare.

Electrodermal phenomena origins include the central nervous system (CNS), epidermal features and sweat gland features [35]. With different states of arousal or stress, there are various physiological responses that present themselves, such as changes in blood pressure, heart rate and sweating due to a stimulus that triggers an SNS response, which is a division of the ANS [35]. With increased sweat on the skin surface, various electrical characteristics of the skin change and can be monitored through EDA electrodes. It is important to note that EDA is a complex topic and is still not fully understood [35]. For instance, placement of EDA electrodes is still an aspect that requires more research, but currently the most common placements are on the palmar region, on the medial or distal phalanx of the index and middle finger due to the abundance of sweat glands on the hand [35].

EDA is most likely a result of the stimulation of the efferent postganglionic sudomotor nerves of the sympathetic system [35]. The ulnar nerve primarily innervates the little finger, while the median nerve innervation is dominant on the index and middle fingers. This was shown by evaluating nerve injuries and comparing skin surface electrical resistances at the different locations on the palmar side of the human hand [76]. In addition, surgical anatomy research shows that the ulnar and median nerves can have communication branches in various arrangements, adding to the complexity of human anatomy [77]. It is also currently known that

the distal phalanx of the fingers will have higher EDA baseline signal levels [78], which can be due to the higher density of sweat glands at these locations [79].

After a stress stimulus, the increase in skin conductance, which can be measured in units of micro-Siemens (μS), is due to the significant changes in the sweat on the surface of the skin [35]. There have been electrical models that have tried to describe EDA on the skin in terms of resistive and capacitive circuits, however, there is still much that is unknown, making it difficult to assess the validity of these models [35]. EDA monitoring could be applied to detect ANS dysfunction [35], which can have direct impacts on the quality of life of individuals with Parkinson's disease [80], epilepsy [32] and autism [81]. Therefore, EDA recordings can be an important measurement when evaluating the neurological health status of an individual [35]. A more comprehensive monitoring system for neurological health can include sensors that detect EDA signals in combination with sensors that record blood pressure in mmHg and heart rate in beats per minute, as these biological signals are related to SNS responses [35].

2.3 Electrodermal Activity Sensors

EDA monitoring can be conducted using two different methods, endosomatic and exosomatic [35]. Electrodermal recordings that do not use an external energy source are called endosomatic, which utilize the electrical signals originating from the human body [35]. An EDA signal obtained when using an external power source, be it direct current (DC) or alternating current (AC), is called exosomatic [35]. For DC, when voltage is constant or current is constant, the EDA recorded is skin conductance or skin resistance, respectively [35]. For AC, when voltage is constant or current is constant, the EDA recorded is skin admittance or skin impedance, respectively [35]. This information from Boucsein in 2012 [35] is simplified

and presented in Table 2.3 for the purposes of this review. In addition, EDA is separated into tonic or phasic responses in which there are response-free recordings or a response-to-stimulus relationship observed, respectively [35]. Exosomatic DC measurement with constant voltage, which measures skin conductance, is the most commonly used method to date [35]. However, there is research on the comparison of DC and AC methods for EDA monitoring [82].

Table 2.3 Methods of electrodermal activity recordings [Adapted from [35]]

Methods of Recording	**Endosomatic**	**Exosomatic**			
Applied Current	**None**	**Direct Current**		**Alternating Current**	
		Current Constant	**Voltage Constant**	**Current Constant**	**Voltage Constant**
Term	Skin potential	Skin resistance	Skin conductance	Skin impedance	Skin admittance

The assessment of electrical circuitry components is outside the scope of this dissertation. However, it is important to briefly outline aspects associated with the hardware for EDA measurements. Relatively recent work by Schmidt et al. in 2016 on the evaluation of a low-cost EDA measurement system highlights the basic electronic hardware required for effective EDA monitoring [83]. The focus was on an EDA system that utilized the DC method with a constant voltage of 0.5 V to measure skin conductance [83], which was based on a more detailed description of requirements previously published [35], [36]. In particular, one of the major challenges associated with EDA monitoring is the technical ability to record the whole signal range of the tonic level of EDA, in addition to maintaining resolution of the phasic responses of EDA [83]. An EDA monitoring system generally includes operational amplifiers or a voltage reference to apply a stable 0.5 V to the skin in which the sweat glands act as variable resistors [83]. Another operational amplifier then produces the skin conductivity

values, which are proportional to the inverse of the measured signal [83]. The produced signal is then separated between two channels, where one channel applies a low-pass filter for noise reduction in the tonic EDA signal [83]. The other channel processes the phasic EDA responses with an active band-pass, where a high-pass filter eliminates the baseline EDA signal and a low-pass pass filter reduces noise [83]. Each of the channels also include additional amplifying inverting operational amplifiers [83]. The sensitivities and amplifications of the EDA monitoring system depend on the maximum voltage and input range of the microcontrollers [83]. Also, a sampling rate of 20 Hz is appropriate for EDA signals, as the timing of the EDA responses is in the magnitude of seconds [35], [36]. Importantly, the general range of values for skin conductivity are from 0 to 100 μS and the EDA responses can be from 0.05 to 5 μS in amplitude [35], [36]. With the basic understanding of EDA and the terms utilized, one can now review the research in relation to EDA and e-textiles.

Monitoring sweat and EDA with the use of e-textiles to develop wearable devices is a relatively recent development when compared to many other fields of research. One can observe this through the current research that exists on the topics of sweat, EDA and textiles [23], [24], [34], [84]–[88], [26]–[33]. These papers are summarized in Table 2.4 and a variety of observations can be made by assessing the studies. The most apparent observation is that the electrical properties of skin, which vary by sweat levels, is not the only method researchers are utilizing to assess sweat. For example, enzymatic properties [84], vapour pressure [86], and fluid mass [87] are all methods by which sweat can be monitored. However, researchers have also measured sweat content as a unit of skin conductance [23], [24], [34], [88], [26]–[33] while others have looked at conductivity of sweat [85]. Another interesting aspect associated with previous research is that there has not been a significant amount of work

focused on the understanding of the effects of design and materials of e-textile electrodes on EDA monitoring. There have been fabrics developed for patient beds [85] and wheelchairs [26], but none that have been truly functional for SWS. Poh et al. in 2010 attempted to utilize fiber-based EDA sensors, but it was shown to provide a weaker skin conductance signal after a stimulus when compared to a standard EDA monitor that is commonly used called the FlexComp Infiniti by Thought Technologies Ltd. [34]. It was suggested that the difference in signal strengths between the conductive fabric and standard electrodes may be due to the stretchable nature of the fabric preventing the electrical properties of the e-textile to be maintained when in contact with the user [34]. In addition, the e-textile integrated into a terrycloth textile substrate would absorb sweat more readily than Ag/AgCl electrodes, and after physical exertion, the e-textiles would have a higher baseline EDA signal [34]. Hence, further understanding and improvements in e-textile development are required to fabricate a structure with the desired characteristics for monitoring EDA. In addition, the knowledge gap in the understanding of EDA monitoring with e-textiles has been highlighted in previous literature [23], [28], [34].

Other studies not concerning e-textiles directly could also have positive impacts on advancing research in regards to monitoring EDA and sweat with SWS. Utilizing low-power wireless communication methods like ZigBee could allow for monitoring of patients outside of the healthcare setting [89]. In addition, Bluetooth low energy technology is being integrated into wearable EDA systems, which includes utilizing flexible circuity, with a focus on reducing the overall form factor and power consumption [90]. In particular, one of the smallest footprints for a prototype wearable EDA monitoring system was shown to be 72 mm by 30 mm by 10 mm with a weight of 11 g [90]. This prototype system put a current load of 30 mA

at 3 V on a coin battery and the power consumption was shown to be 90 mW, which resulted in only 2 hours of data recording time [90]. This limited performance, in addition to the current commercial devices using rigid materials, demonstrates that more research is required to minimize the complete form factor of a wearable EDA monitoring system. Also, systems are being researched that can automatically label phasic and tonic signals associated with EDA, facilitating assessment of longitudinal EDA monitoring [91]. Combining sensors into SWS that monitor cardiovascular and respiratory parameters in addition to EDA can provide a more comprehensive understanding of an individual's overall health status [92]–[94].

Table 2.4 Research on monitoring electrodermal activity and sweat using textiles

Experimental Method	Material Structure	Standard Method used to Compare	Duration of Recording	Power and/or Data Storage Specifications	Major Results and Conclusions	Ref. / Year
E-textile electrodes at fingertips of glove to test EDA over frequency sweep	80% polyester yarn knitted with 20% steel wire (Smartex), with a dimension of 1 x 2 cm	Comparison of e-textile electrodes to standard electrodes previously done (see information below for reference [28]), focus on frequency sweep on EDA	15 minutes	4 equal groups with different parameters: DC, AC with 10 Hz, AC with 100 Hz and AC with 1 kHz Power supply of 3.7 V and a capacity of 750 mAh Xbee module for wireless communication	Frequency of the external electrical source affects accuracy of arousal recognition and AC at 100 Hz had the highest average recognition accuracy of 71%	[23] / 2016
Evolon nonwoven fabric microfluidic device to measure enzymatic activity (lactate) of sweat	Spunbonded and hydro-entangled nonwoven fabric made from split polyester / nylon microfibers	Biochemical response of sweat enzymes, specifically lactate	10 minutes	N/A Chemical reaction	Able to fabricate a wearable biochemical analysis of sweat utilizing textiles	[84] / 2014

Experimental Method	Material Structure	Standard Method used to Compare	Duration of Recording	Power and/or Data Storage Specifications	Major Results and Conclusions	Ref. / Year
E-textile electrodes on arm rest of wheelchair to measure skin conductance on fingers	Composite textile made of fibers coated with conductive polymer and silver	Similar to Biopac system (Skin Resistance Trans, TP-TSD203)	120 seconds	DC, 12 V, 7 Ah Wi-Fi connection utilizing LabVIEW	Able to distinguish EDA response to pain stimuli, however no details on methodology	[26] / 2014
E-textile electrodes (textrodes) integrated into gloves on index and middle fingers to measure skin conductance	Conductive fabric (Shieldex Fabric P130+B, STATEX), 78% polyamide, 22% elastomer, 99% silver plated	None mentioned	2 minutes	0.5 V, 900 mAh lithium ion batteries, 2 kΩ, 250 Hz sampling freq. Data stored on a 4 GB microSD card	EDA measure-ments were variable even with filtered data	[24], [27] / 2013, 2014
Integrated Ag/AgCl electrodes within wrist-band textile as well as conductive fabric sensors which measures skin conductance for short and long-term continuous monitoring	Conductive fabric used was silver plated nylon 92%, dorlastan 8%, surface resistance < 1Ω/cm^2, contact area 3.5 cm^2	Commercial-ly available EDA monitoring device, FlexComp Infiniti (Thought Technolo-gies)	25 minutes per stressor task 24 hours or 7 day test with Ag/AgCl integrated into textile wearable device	DC, Single lithium polymer battery with a nominal voltage of 3.7V and a capacity of 1100 mAh Utilized 2GB microSD card for data storage or IEEE802.15.4 wireless standard	Integrated Ag/AgCl electrodes into wrist-band results were comparable to FlexComp Infiniti but EDA signal was poor when using conductive fabric; long-term tests showed functional wearable device	[33], [34] / 2010

Experimental Method	Material Structure	Standard Method used to Compare	Duration of Recording	Power and/or Data Storage Specifications	Major Results and Conclusions	Ref. / Year
E-textile electrodes at fingertips of glove to test EDA monitoring capabilities	Lycra substrate glove, electrodes are 80% polyester yarn knitted with 20% steel wire (Smartex), with a dimension of 1 x 1 cm	Signal processing analysis and comparison of e-textile electrodes to standard Ag/AgCl electrodes MP35 (Biopac)	4 minutes or 18 minutes and 20 seconds	DC voltage source Wireless module for data communication	Textile electrodes have been electrically character-ized and show comparable EDA recordings to standard electrodes, however there is no analysis on the structure and material of fabrics on EDA results	[28], [31] / 2012, 2010
Two-layer striped fabric woven alternating cotton yarn with electrical conductive yarns and wires to measure sweat conductivity for bed-rest	Bekintex 50/2 conductive yarn (80%/20% polyester/ stainless steel) and 50 µm stainless steel monofilament wire (Bekaert)	Standard sodium chloride (NaCl) solution used to have a conductivity of 8 µS/cm	4.5 hours	0-11 V Wired information transfer	Textile sensor provides a good indication of moisture / sweat content and its spatial distribution	[85] / 2011
Shimmer EDA system integrated into socks with fabric electrode from Polar Wearlink on ball and heel of foot to measure EDA	35% polyester, 35% polyamide, 30% polyurethane, conductive material not stated	ProComp2 sensor (Thought Technolo-gies)	2 hours	Shimmer wireless sensor (450mAh Li-ion battery, Bluetooth Radio – RN-42)	EDA recordings from developed device similar but slightly weaker to standard monitor, however walking produces inaccurate results	[30] / 2011

Experimental Method	Material Structure	Standard Method used to Compare	Duration of Recording	Power and/or Data Storage Specifications	Major Results and Conclusions	Ref. / Year
Two humidity sensors integrated into textile at different heights to measure the vapour pressure gradient on lower back of human	Commercial humidity capacitive sensors, Philips H1	Vapometer (Delfin Technolo-gies)	45 minutes	15 V (DC or AC unspecified) Bluetooth interface, developed by Centre Suisse d'Electronique et de Microtechnique	Wearable sweat-rate sensor integrated into textile was comparable to commercial unwearable Vapometer, however wearable required gel to be functional	[86] / 2010
Textile-based fluid handling platform using a passive pump to collect sweat and analyze it through pre-defined channels where sweat rate is also measured	Textile is composed of a polyester/lycra blend (115 g/m^2 polyester 92% lycra 8%) to wick sweat into channels with absorbent Absorbtex (Smartex)	Compared to average sweat rate of 17 mg/min for males during exercise	1 hour	N/A (Passive components)	Sweat rate measured with developed sensor was on average 11 mg/min below the known average for males	[87] / 2009
Textile sensor to measure electrical resistance varied by sweat	Steel textile	Utilized adaptive ESPRIT algorithm	10 seconds	LabVIEW interface with Bluetooth	Demon-strates adaptive algorithm, details of the experimental methodology are lacking	[88] / 2008

2.4 Fabrication Methods

The most popular sensors used to monitor electrical bio-signals of the human body are Ag/AgCl electrodes [95], [96]. The two most common fabrication methods for Ag/AgCl electrodes include electrochemical deposition and sintered bulk [95]. A simple procedure to

produce a layer of AgCl on Ag is through the use of an electrochemical cell with an electrolyte solution containing Cl^- [95]. The two chemical reactions are as follows [95]:

$$Ag \rightleftarrows Ag^+ + e^- \quad (1)$$

$$Ag^+ + Cl^- \rightleftarrows AgCl \downarrow \quad (2)$$

This allows for a layer of AgCl to be formed on the Ag electrode. In order to develop a sintered Ag/AgCl electrode, an Ag lead wire and a mixture of powdered Ag and AgCl are used [95]. The powder is put in a die, then compressed and a pellet is formed and finally baked [95]. These electrodes are more durable than the ones which only have a layer of AgCl deposited on them, and are therefore the most commonly used for acquiring bio-signals [95].

The solubility product of AgCl is 1.77×10^{-10} at room temperature (25 degrees Celsius (°C)) and is an important value for determining the half-cell potential of AgCl [97]. The standard half-cell potential of AgCl, a known non-polarizing material, in relation to the standard hydrogen electrode, is 0.222 V at 25 °C [97]. The governing Nernst equation for the half-cell potential for Ag/AgCl electrodes is as follows [95]:

$$E = E_{Ag}^0 + \frac{RT}{nF} ln \frac{K_s}{a_{Cl^-}} \quad (3)$$

Where E is the half-cell potential of Ag/AgCl in V, E^0_{Ag} is the standard half-cell potential of Ag in V, T is the temperature in Kelvin (K), R is the universal gas constant of 8.314 J/mol·K, n is the number of valence of electrons involved which is 1 in this case, F is Faraday's constant of 9.65×10^4 C/mol, K_s is the solubility product of AgCl and a_{Cl^-} is the ionic activity of Cl^-. At room temperature of 25 °C (298.15 K), the standard half-cell potential of Ag is 0.799 V, the solubility of AgCl is 1.77×10^{-10} and the ionic activity of Cl^- is assumed to be 1.00 mol/L.

Therefore, at room temperature, the half-cell potential of Ag/AgCl electrodes is calculated to be 0.222 V. The reaction associated with the half-cell potential of Ag/AgCl is the following:

$$Ag + Cl^- \rightleftarrows AgCl + e^- \quad (4)$$

When Ag/AgCl electrodes are placed in an electrolyte solution that contains Cl^- as the main anion, which is known to be the case for biological sweat, the half-cell potential of the electrode remains quite stable [95].

Non-polarizing electrodes allow current to cross the electrode-electrolyte interface, while polarizing electrodes have no actual charge cross the electrode-electrolyte interface when a current is applied, instead a displacement current causes the electrodes to function like a capacitor [95]. The type of electrode is very important when considering recording biological signals [95]. Specifically, Ag/AgCl was shown to have a low Faradaic resistance, which infers a lower electrode-skin impedance in regards to using Ag/AgCl electrodes to record biological signals [98]. Briefly, a Faradaic process is one in which there is an electron transfer at an electrode-electrolyte interface [98]. When considering the surface of the skin, the electrolyte is sweat which contains many ions, therefore using a material with low Faradaic resistance allows for a better and more stable bio-signal monitoring [98]. The properties previously characterized for Ag/AgCl demonstrate that this material is non-polarizing and that the electrical signals recorded with Ag/AgCl electrodes on the surface of the skin are mainly Faradaic in nature in regards to when sweat is involved [95], [97], [98].

Currently, the miniaturization of Ag/AgCl electrodes through various techniques is of interest for biomedical applications [99], as well as for developing flexible sensors. The need for electrodes that are flexible is growing as wearable technology advances, meaning that practical and scalable fabrication methods for these types of sensors are necessary [3]. Many

flexible and stretchable sensors have been fabricated on various substrates through inkjet-printing, screen printing, transfer printing, photolithography, as well as many other methods [3]. An example of these sensors are epidermal electronics, in which electrodes have been developed through photolithography and transfer printed onto a silicon substrate with similar mechanical properties to that of human skin to allow for conformability [66]. Also, inkjet-printing has been used to develop Ag/AgCl electrodes on polyethylene terephthalate (PET) as a low-cost method [100]. There is a significant amount of research on flexible electrodes [3], [101], however, the translation to commercial devices has been limited. While there is an increasing interest for the optimization of EDA monitoring [23], [102], existing wearable EDA monitoring devices in the market such as the Embrace and E4 wristbands by Empatica [103], the Moodmetric ring by Moodmetric [104] and the edaMove ambulatory monitoring system by Movisens [105], rely on rigid and non-breathable electrodes, significantly limiting the potential for wearability of these devices and integration with daily apparel. Therefore, developing e-textiles is a promising approach to the fabrication of flexible and breathable EDA electrodes [18].

The development of e-textiles can be accomplished with many different methods, some of which include integrating or embroidering conductive wires or fabrics within the textile, as well as utilizing conductive inks or polymers [18]. To create the conductive fibres, one can extrinsically modify textiles with coatings through inkjet-printing, electrodeposition, electroless plating, dip-coating and sputtering, in addition to other methods [18]. Also, intrinsic modifications to textiles, which can provide inherent functionality to the fibre, yarn or fabric, can be accomplished through methods which include, but are not limited to, wet-spinning, self-assembly, die extrusion and electrospinning [18]. Electrospinning is an increasingly attractive

approach for developing conductive fibres at the nanoscale level, which utilizes a conductive polymer, electromagnetic field and counter electrode in addition to controlling many other parameters [106]. These fibres can be formed into a yarn and then developed into a fabric with various structures, which include woven, non-woven, knitted, nets, braided or tufted [18], [106]. An example of utilizing intrinsic and extrinsic modifications to develop a conductive fibre is the fabrication of Ag-plated polyvinylidene fluoride (PVDF) to be formed into a textile electrode [107]. In terms of monitoring physiological signals, the fabrication of e-textiles coated with silver has been a major area of interest [108]–[112]. There is a current gap in understanding how textiles and e-textiles impact the accuracy and precision of monitoring specific signals; a topic discussed in previous studies focused on the fabrication and implementation of e-textiles [111], [113]. In addition, there are very few studies of note in which Ag/AgCl e-textiles were fabricated, and their ability to monitor biological signals subsequently evaluated [114], [115]. This lack of research on developing comparable e-textile materials to current clinical standard Ag/AgCl solid electrodes shows a significant gap in this field of study.

2.5 Potential for Clinical and Home Applications

Smart wearable systems have the potential to be utilized for many applications, specifically for healthcare delivery to help patients with cardiovascular [12], [13], pulmonary [14], musculoskeletal [15] and neurological [13] health problems. Some examples include monitoring neonates [116]–[118], rehabilitation progress [119], as well as determining the effectiveness of treatments for people with Parkinson's disease [120]–[123]. The applications for SWS in healthcare are seemingly endless, as there are many individuals with specific health

conditions that would benefit from long-term monitoring methods of relevant vital signs and activity. In many cases, a significant portion of a clinician's diagnosis is based on the patients' subjective understanding of their current health status.

For example, patients who have undergone invasive surgery may have a rehabilitation program that they must follow to regain their optimal physical activity level or motion in a certain limb [119]. It is possible for SWS to monitor the patient's progress in the clinical setting or at home to determine how effective the rehabilitation program is for the patient and to adapt it if other options are more appropriate [119]. In addition, for people with Parkinson's disease, tremor frequency and intensity, as well as gait analyses, are important aspects to monitor when determining the effectiveness of treatments [35], [120]–[123]. Being able to quantify information currently unavailable can allow for a more critical and thorough assessment of a patient's response to treatment or progression of a disease. In terms of EDA monitoring, there are many applications that are being explored and they are identified in Table 2.5.

Table 2.5 Applications for electrodermal activity monitoring

Application	Reference(s)
Seizure Detection	[29], [32]
Athletic Performance Monitoring	[86], [87]
Psychological Monitoring	[36]
Wheelchair and Bed Rest Monitoring for Moisture	[26], [85]
Military Stress Monitoring	[24], [27]
Neuromuscular Rehabilitation Monitoring	[119]
Daily Life Stress Reduction	[23], [33], [124]
Teaching and Learning Effectiveness	[125]
Monitoring of Autistic Adults and Children	[81], [126], [127]
Monitoring Stress of Caregivers	[128]
Parkinson's Disease Monitoring	[80], [129]
Traumatic Brain Recovery Monitoring	[130]
Dementia Monitoring	[131], [132]
Pain Monitoring	[133], [134]
Sleep Monitoring	[135]

2.6 Summary

In order to successfully introduce novel and improved SWS in healthcare, solutions to the different challenges discussed need to be effectively and seamlessly integrated. Through a collaborative effort between individuals from a variety of disciplines, there could be great strides in the field of research for smart wearable systems with applications in healthcare. Further research is needed for flexible film and breathable textile electrodes in order to develop unobtrusive, yet safe and effective SWS that patients and healthcare providers would be eager to accept.

Chapter 3: Flexible EDA Electrode Development Based on Polymer Substrate

This chapter is based on work that has been previously published [136]. A major obstacle to comfortable long-term EDA monitoring is the lack of accurate and precise flexible and wearable sensors, since the current commercial Ag/AgCl electrodes are rigid and require the use of gels and strong adhesives [35], [36]. The work discussed in this chapter presents engineering and fabrication of flexible electrodes with systematic investigation of the effects of design parameters including the surface area, spacing and geometry of dry flexible electrodes for EDA monitoring. While there are detailed recommendations for EDA measurements [35], [36], to the best of our knowledge the approach we are proposing to explore has not yet been accomplished to date and the results have the potential to further promote the understanding of parameters for wearable EDA monitoring devices and flexible sensors. It is hypothesized that the surface area, distance between and geometry of electrodes have an effect on the detection of EDA response waveforms, which are induced by a specific stimulus, and can be optimized with a preliminary understanding of the results. Appendix A provides additional data figures and tables for this chapter.

3.1 Materials and Methods

3.1.1 Fabrication of Flexible Electrodes on Polymer Substrate

Custom electrode patterns were created and the designs were printed on copper (Cu) coated (0.035 mm thickness) polyimide film (0.051 mm thickness) with a tensile strength of 138 MPa (Jiu Jiang Flex Co. Ltd., China) using a Xerox ColorQube 8580DN solid ink printer

(Xerox, Canada) and then cured by heating at 115 °C for 1 minute to ensure proper coverage of the Cu by the wax ink. To etch the Cu not covered by the solid ink patterns, the electrodes were immersed in sodium persulphate (MG Chemicals, Canada) with gentle mixing. Electrodes were then cut and sections were encapsulated with electrical tape. The materials and methods used to develop custom electrode patterns are similar to what is done in the industry of fabricating printed circuit boards.

Each electrode was individually secured to a glass microscope slide after being cleaned by sonicating in deionized (DI) water, detergent (3%; EMD Millipore, Germany), acetone (99.7%; Fisher Scientific, United States) and finally in hydrochloric acid (0.2 M; Allied Chemical, United Kingdom). The electrode was then placed inside an electrochemical chamber with a silver (Ag) counter electrode. The electroplating solution was prepared through an adapted protocol of previous studies [137]–[139] and contained 5,5-dimethylhydantoin (1 M; Acroc Organics, United States), nicotinic acid (1 M; Acros Organics, United States), potassium carbonate (1 M; Fisher Scientific, United States), silver nitrate (0.1 M; Fisher Scientific, United States) and potassium hydroxide (until pH of 10-14; Fisher Scientific, United States). A Keithley 2400 SourceMeter (Keithley, United States) was used as the power source in which the program LabTracer (Keithley, United States) was used. The SourceMeter was set to function as a resistor and provided a constant voltage of 1.25 V and a current based on the surface area of the electrode being electroplated (10 mA per cm^2 of surface area). Electroplating lasted 15 minutes and a stir bar mixed the solution at 700 revolutions per minute (RPM).

The electrodes were then cleaned again by sonicating in DI water, then isopropanol (99.5%; Sigma-Aldrich, United States) and finally acetone. To form Ag/AgCl on the surface

of the electrode, the electrodes were secured to a glass microscope slide and the copper portions were covered with electrical tape. The Ag portions of the electrodes were immersed in sodium hypochlorite (12% available chlorine; Advance Chemicals Ltd., Canada) for 5 minutes with a stir bar mixing at 700 RPM. Electrodes were rinsed in DI water and then dried with nitrogen. Copper wires and connectors were then soldered to the electrodes to allow for ease of use during experimentation.

3.1.2 Characterization of Flexible Electrodes on Polymer Substrate

The fabricated flexible electrodes were imaged with an optical microscope equipped with a digital camera (9.0 MP, OMAX, United States) and a field emission scanning electron microscope (FE-SEM, Zeiss Sigma, Germany). The micrographs of the surfaces of electrodes were taken at different stages of the fabrication process: the surface of copper after etching, silver after electroplating, and silver/silver chloride after chemical treatment.

X-ray diffraction (XRD) patterns of the surface of the fabricated Ag/AgCl flexible electrodes were obtained by a D8-Advance X-ray diffractometer (Bruker, United States). To observe the layers of the fabricated electrodes, a cross-section of a sample was prepared by securing it in resin and then polishing the cross-section. The analysis of the layers was conducted with an environmental scanning electron microscope (ESEM, FEI, United States) with energy-dispersive X-ray spectroscopy (EDS, Bruker, United States). Also, the stability of the fabricated flexible Ag/AgCl electrode with a 0.15 cm^2 surface area was determined by placing it in a 3 M sodium chloride (VWR International, United States) solution with a known reference Ag/AgCl electrode (BASi, United States) with a 5 cm distance between. Both electrodes were then connected to a multimeter (Agilent U1232A, United States) to measure

the difference in voltage. The bending moment versus curvature curves were plotted for the flexible electrodes and the bending rigidity and hysteresis (recoverability) were determined with a KES-FB2-S bending tester (Kato Tech, Japan) and associated software (KES-FB Measurement Program, Version 8.07, Japan) with a sensitivity of 20 gram force·cm [140]. The bending tests were done on Ag/AgCl electrodes with a 0.15 cm^2 surface area and a 0.50 cm distance, which were fabricated on the flexible Cu and polyimide substrate (n = 3). Also, there was 0.10 cm of only polyimide on each side of the electrodes, therefore samples tested had a width of 1.00 cm. The bending displacement velocity was 0.5 cm^{-1}/s and the sample size in the bending direction was 1.00 cm. The electrodes were bent in the middle on an axis perpendicular to the longer length of the electrodes, similar to how the electrodes would be placed to curve on the finger. The thickness of the Ag/AgCl on the Cu and polyimide was measured with a Mitutoyo Digimatic micrometer (MDC-1″ SX, Japan).

3.1.3 EDA Monitoring Testing Protocol

To monitor EDA responses, specifically skin conductance, a common method called the Stroop color test [141], [142] has been adapted and utilized for this research. Briefly, the Stroop color test is when cognitive stimuli are presented to the subject through the use of words of different colors which are either conflicting (word and color of text are different, i.e. ‘blue’ is written in green color) and non-conflicting (word and color of text are the same, i.e. ‘blue’ is written in blue color). The subject is required to state the color of the word and not read the text. The experiments assessed EDA for a 15 minute time period, which includes a 22.5 second time period to confirm that the electrodes are connected properly and then an initial rest period of 4 minutes. The Stroop test then begins and lasts for 5 seconds followed by another 2 minute

rest period. There are 3 cycles of a 5 second Stroop test and 2 minute resting period. After the 3 cycles, there is a final 4 minute rest period and another 22.5 seconds to observe and confirm that the electrodes are still recording data.

3.1.4 Systematic Testing of Designs of Flexible Electrodes on Polymer Substrate

To assess the various custom fabricated electrodes of different surface areas, spacings and geometries, the dry flexible Ag/AgCl electrodes are compared to standard rigid dry Ag/AgCl electrodes simultaneously. One group of flexible Ag/AgCl rectangular electrodes had a 0.15 cm^2 surface area with distances of 0.025 cm, 0.20 cm, 0.50 cm and 1.00 cm. Another group of flexible Ag/AgCl rectangular electrodes had a 0.20 cm distance with surface areas of 0.04 cm^2, 0.15 cm^2, 0.52 cm^2 and 0.74 cm^2. The third group of fabricated flexible electrodes were of circular and serpentine shapes with 0.15 cm^2 surface area and 0.20 cm distance. 12 electrodes of each design were fabricated to assess success rate of fabrication process (n = 12). The flexible electrodes designed and used in this study are shown in Figure 3.1.

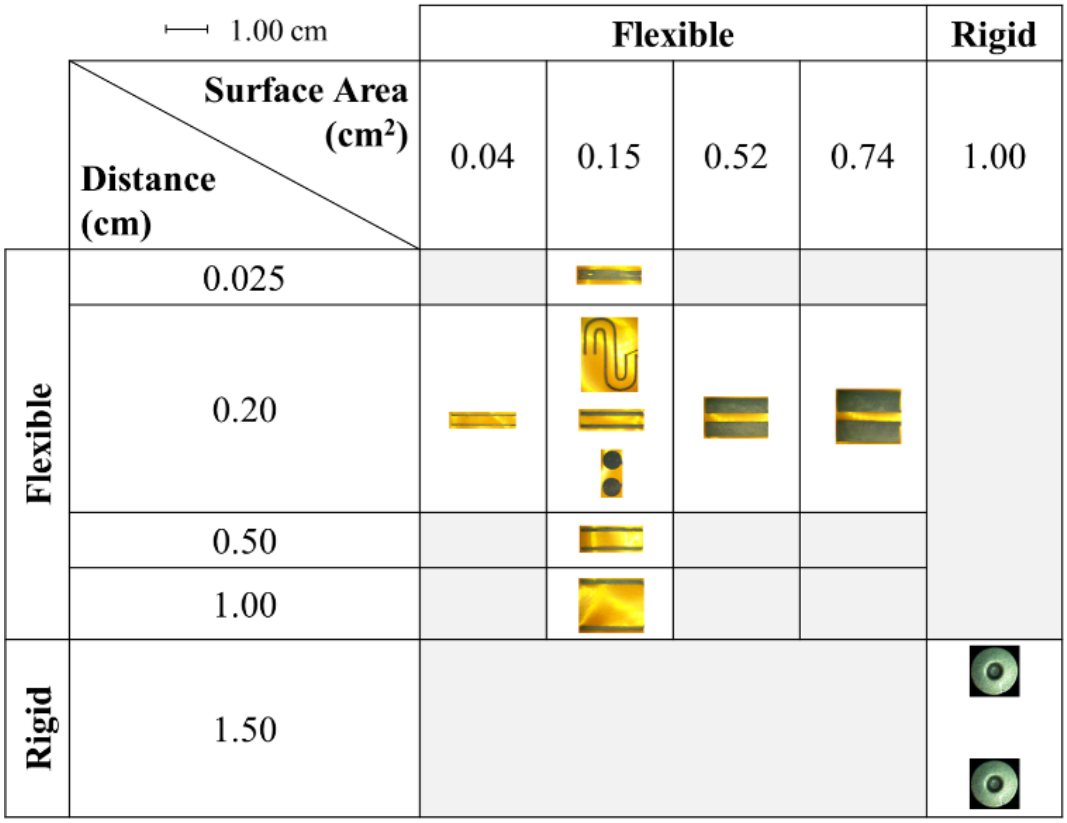

Figure 3.1 Overview of flexible electrode designs with different geometries, distances between and surface areas, as well as specifications for rigid, commercially available electrodes that were used as standard test electrodes (© 2017 IEEE) [136].

Each set of flexible electrodes was attached on the index finger with breathable cloth tape (Johnson & Johnson, United States) and compared against a set of commercially available standard sintered solid Ag/AgCl electrodes (Thought Technology, Canada), with approximately 1.00 cm^2 surface area. The standard solid Ag/AgCl electrodes were attached on the middle finger using straps with a constant distance of 1.50 cm between. To measure the compressive force applied on the electrodes by a strap or tape, a 0.51 cm diameter force sensor (Pololu, United States) was placed at each sensor location shown in Figure 3.2, and an Arduino UNO R3 (Arduino, Italy) was utilized as the data collection system (n = 3).

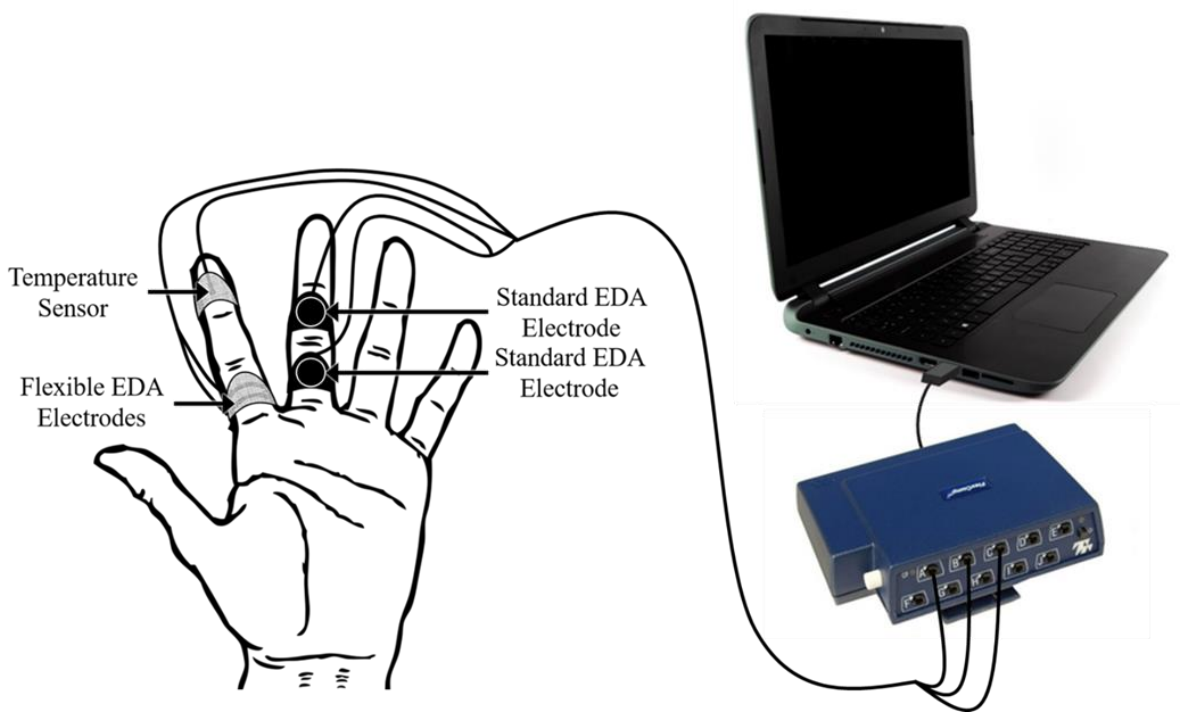

Figure 3.2 A schematic showing the location of sensors, as well as the connection to the FlexComp Infiniti system and computer (© 2017 IEEE) [Adapted from [136]].

For EDA monitoring, the flexible electrodes and standard electrodes were connected to the FlexComp Infiniti (Thought Technology, Canada), which measures skin conductance as it utilizes DC and constant voltage with 0.01 µS sensitivity [34]. The experimental set-up for monitoring EDA is most closely related to the simplified Montagu-Coles model of EDA [35], [143], [144]. This model considers the equivalent circuit of the surface of the skin and the electrode to contain a variable resistor for sweat glands, a constant resistance value for the stratum corneum (the outermost layer of the epidermis), as well as a constant resistance value for the inner dermis with the body core [35], [143], [144]. The simplified Montagu-Coles also purposely lacks a capacitive element [35], [143], [144]. The FlexComp Infiniti was subsequently connected to a computer in which the EDA data would be collected with the use of the BioGraph Infiniti software at a sampling rate of 256 Hz. The EDA stimuli response

monitored with the standard electrodes was compared to the EDA signal recorded with each design of flexible electrodes ten times, where each test utilized newly fabricated flexible electrodes (n = 10). All tests were conducted on one subject. A temperature sensor (Thought Technology, Canada) was used to monitor skin surface temperature during every experiment and the average between experiments was calculated (n = 90). The EDA signal detected with standard electrodes were also compared to the signal recorded simultaneously by another set of standard electrodes to confirm the reliability of the test method (n = 1).

The estimation of total coverage of sweat glands of the flexible electrodes was completed by using the average number of 233 sweat glands per cm^2 that was established for the palmar region of the hand in previous literature [144], [145].

3.1.5 Statistical Analysis

The statistical analysis for the comparison of EDA stimulus responses collected was done on signals recorded during the same experiment. The data utilized in the statistical analysis was selected by visual analysis of the three EDA responses to the Stroop test stimuli. The data selected for further analysis was based on identifying one apparent EDA response with the standard electrodes, which was then sectioned 10 seconds before and 10 seconds after the stimulus. The EDA data of the fabricated EDA electrodes was then sectioned at the same time points and statistically compared to the standard EDA electrode data. This allowed for the inclusion of important components of the signal response as previously described [35].

The correlation between EDA response signals recorded by flexible and rigid electrodes was assessed by utilizing the Pearson correlation coefficient [146], which has been previously done when comparing EDA signals [34], [147]. A one-tailed paired t-test was

completed to compare the means and the standard deviations of the Pearson correlation coefficients of different electrode designs. The significance level (p-value) is less than 0.05 and a correlation coefficient value of 1 means perfect positive correlation between the signals, while a value of -1 means perfect negative correlation. A one-tailed paired t-test, with a p-value of less than 0.05, was also done to assess significant differences between the force test results of cloth tape and straps with standard deviations between tests stated.

3.2 Results

3.2.1 Evaluation of Fabrication of Flexible Electrodes on Polymer Substrate

The fabrication process developed for flexible electrodes proved to be quite repeatable. The success rate of fabricated electrodes was assessed visually for uniformity of the surface and was approximately 94%. An aspect which caused many of the complications for the electrode fabrication resulted from the solid ink not adhering properly to the surface of the Cu, allowing the etchant to penetrate the protective layer, damaging the surface of the electrode to be electroplated. In addition, after electrodeposition of Ag, it was observed that some surfaces were uniformly layered with Ag while others exhibited defects. The Ag adherence to the Cu after electrodeposition proved to be quite robust, as it was very difficult to remove the layer of Ag. Finally, the conversion of Ag to Ag/AgCl also resulted in the presence of slight defects on the surface, however defects in general were a rare occurrence at approximately 6%.

3.2.2 Characterization Results of Flexible Electrodes on Polymer Substrate

The optical microscope and SEM images of the Cu, Ag and Ag/AgCl surfaces are shown in Figure 3.3. The Cu surfaces have visible indentations as a potential result of the

original manufacturing of the Cu films. The Ag surfaces after electrodeposition on the Cu show a smoother surface with uniform distribution. This uniform distribution is also observed when the conversion of Ag to Ag/AgCl is completed through chemical treatment. It is important to note the structural and morphological changes on the surface between the key fabrication steps of Ag deposition and Ag/AgCl chemical treatment, which could impact the results during monitoring EDA. The nanostructures present on the Ag/AgCl could allow for a greater effective surface area when monitoring EDA, however, further evaluation of these effects is beyond the scope of this research. It is also important to note that the surface of the deposited Ag and Ag/AgCl layers are uniformly distributed, which is the desired outcome.

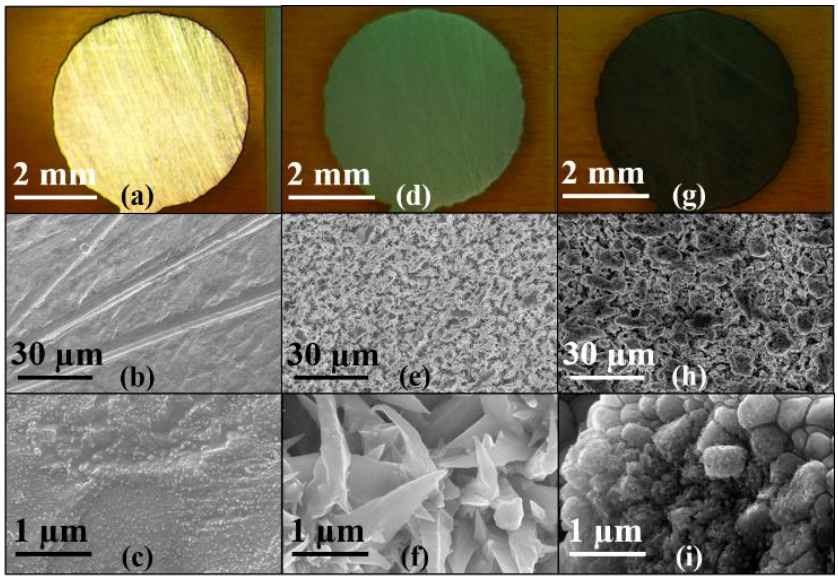

Figure 3.3 Typical optical microscope micrographs (top row) and SEM micrographs with different magnification (1 kX for middle row and 30 kX for bottom row) of the EDA electrodes at different stages of the fabrication process: (a), (b) and (c) initial surface of copper film, (d), (e) and (f) surface of silver electroplated electrodes, and (g), (h) and (i) surface of final silver/silver chloride electrodes (© 2017 IEEE) [136].

The XRD pattern of a typical fabricated flexible electrode is shown in Figure 3.4. The peaks are identified, confirming the electrode surface to contain Ag and AgCl by having the same diffraction pattern as what has been previously shown [148], [149]. The presented Cu

peaks are due to the Cu layer of the sample being exposed when the electrode was cut and prepared for the XRD analysis [150]. Figure 3.4 also includes the cross-sectional SEM micrograph of a fabricated flexible electrode with the line and mapping EDS analysis results. These results confirm that the bottom layer is composed of Cu, the middle layer is Ag and the top layer contains Ag and Cl. Also, when determining if there was a difference in potential between a fabricated flexible Ag/AgCl electrode (0.15 cm^2 surface area) and a reference Ag/AgCl electrode, the voltage measured was 0.0 mV when in a 3 M solution of sodium chloride. This suggests full coverage of the Ag/AgCl surface layer on the developed flexible electrodes, which is the area that will be in contact with the surface of the skin.

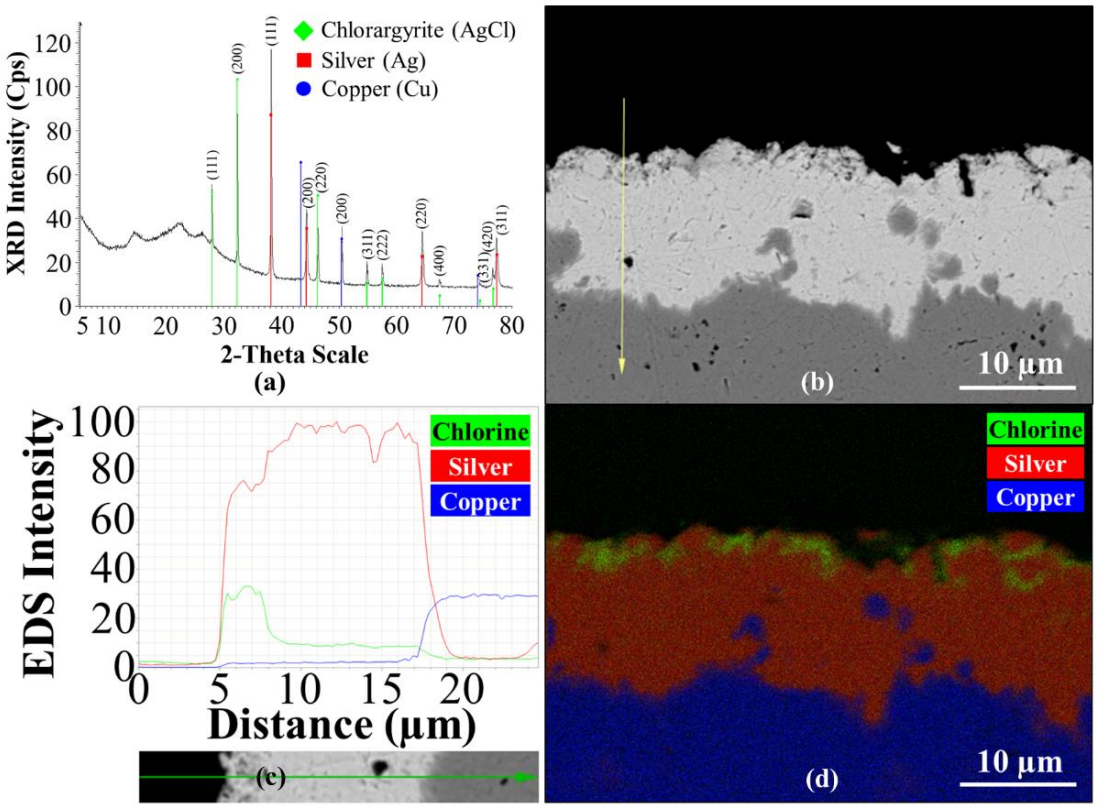

Figure 3.4 (a) The XRD pattern of the surface of a typical fabricated flexible electrode with peaks corresponding to AgCl, Ag and Cu. (b) Cross-sectional SEM micrograph at 2.5 kX magnification of a fabricated flexible EDA electrode with EDS line analysis indicated. (c) EDS line analysis results indicating chlorine, silver and copper peaks. (d) EDS mapping analysis indicating chlorine, silver and copper layer distribution (© 2017 IEEE) [136].

The bending momentum per unit width versus the curvature during a load unload cycle curve is shown in Figure 3.5, which demonstrates the flexible and recoverable nature of the fabricated flexible Ag/AgCl electrodes. The average bending rigidity and hysteresis values for the flexible Ag/AgCl electrodes (0.15 cm^2 surface area, 0.50 cm distance) were measured to be 1.32 x 10^{-4}±0.01 x 10^{-4} Nm/m and 1.12 x 10^{-2}±0.02 x 10^{-2} N/m, respectively. Generally, lower values for bending rigidity and bending hysteresis means that the material being tested is less rigid and has good recoverability, respectively [140]. The Ag/AgCl layer on the Cu and polyimide had a thickness of 0.093 mm and there was 0.10 cm of polyimide on each side of the electrodes with a thickness of 0.051 mm. Importantly, the solid standard Ag/AgCl electrodes are rigid and do not have the ability to conform to the surface of the skin [96].

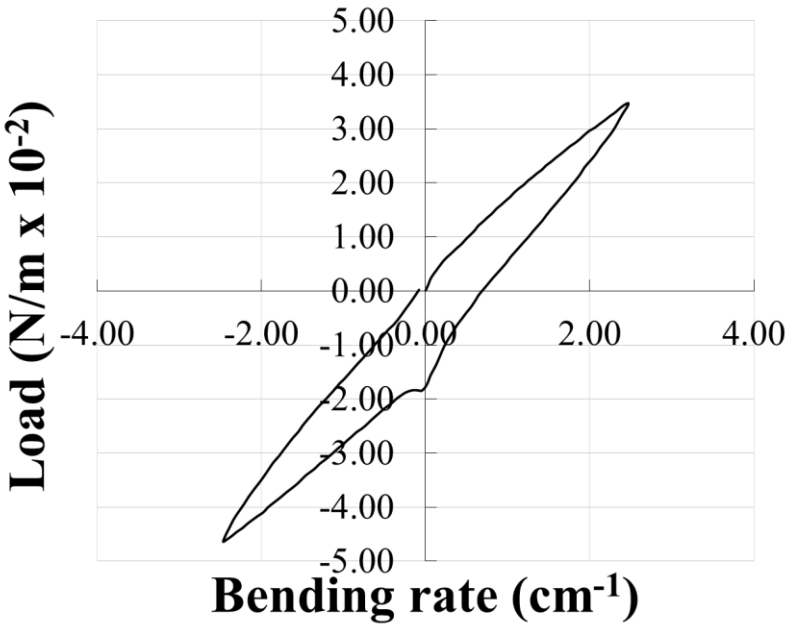

Figure 3.5 The average bending moment versus curvature curve for the fabricated flexible silver/silver chloride electrodes (0.15 cm^2 surface area, 0.50 cm distance) with 0.10 cm of only polyimide on each side of the electrodes. Samples tested had a width of 1.00 cm (n=3).

3.2.3 Analysis of EDA Stimulus Response Data for Flexible Electrode Designs on Polymer Substrate

The average pressure force test results with standard deviations between trials demonstrated that the cloth tape at the distal phalanx of the index finger exhibited 0.08±0.02 N and at the proximal phalanx of the same finger the force was 0.09±0.01 N. The straps at the medial phalanx of the middle finger exhibited 0.13±0.02 N of force and at the proximal phalanx of the same finger it was 0.15±0.01 N. Overall, the straps were observed to have a statistically significant (p-value<0.05) larger average force on the sensors than the cloth tape, which is shown in Figure 3.6. Also, the average skin surface temperature recorded with a standard deviation between the EDA monitoring trials was 26.96±4.17 °C.

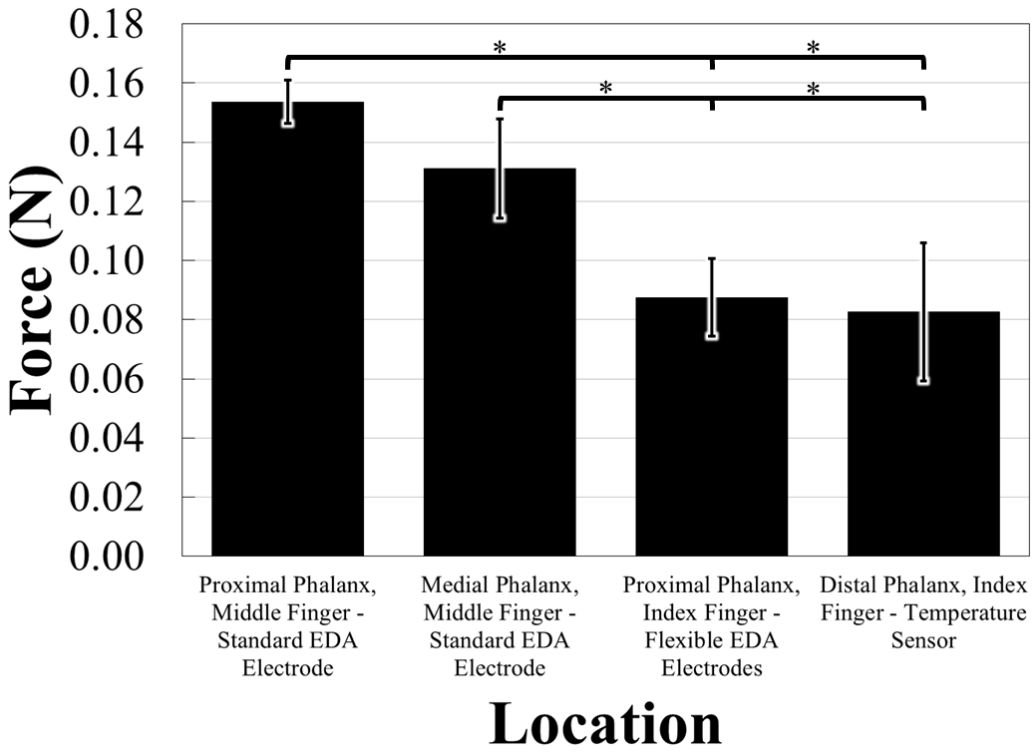

Figure 3.6 The compressive force test results for the different attachment methods and locations of sensors. Standard deviations are shown and one-tailed t-test results with p-values<0.05 are indicated (*). For each value n=3.

The comparison of two sets of standard electrodes resulted in a Pearson correlation of 0.998, confirming the reliability of our testing method. A typical EDA stimulus response is shown in Figure 3.7 and illustrates the waveforms that are being compared. The average Pearson correlation coefficients and standard deviations for the rectangular electrodes of different surface areas and distances are shown in Figure 3.8. The highest average Pearson correlation coefficient among the rectangular electrodes with constant distance between (0.20 cm) and varying surface area is the design with the largest surface area of 0.74 cm^2 (0.979±0.026). The correlation coefficient of the largest surface area electrode of 0.74 cm^2 (0.979±0.026) was statistically significantly greater than the correlation coefficient of the smallest surface area electrode of 0.04 cm^2 (0.925±0.094) with a p-value of 0.04.

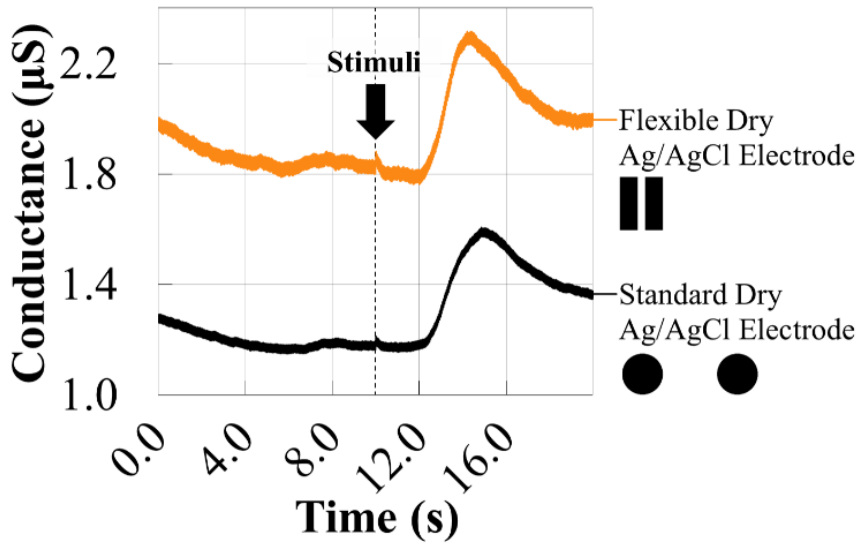

Figure 3.7 Example EDA stimulus response for dry flexible electrodes (0.74 cm^2 surface area, 0.20 cm distance) compared to dry commercial electrodes (1.00 cm^2 surface area, 1.50 cm distance) (© 2017 IEEE) [136].

For the rectangular electrodes with constant surface area (0.15 cm^2) and varying distance between, the highest average Pearson correlation coefficient is the design with the largest distance of 1.00 cm (0.979±0.020). The correlation coefficient of the largest distance

of 1.00 cm between electrodes (0.979±0.020) was statistically significantly greater than the correlation coefficient of the smallest distance of 0.0025 cm between electrodes design (0.828±0.256) with a p-value of 0.04. It is also important to note that generally, as the surface area and distance between the electrodes increase, the standard deviations of the Pearson correlation coefficients decrease, which demonstrate increasing accuracy and precision. There is a high repeatability between trials of electrodes with surface areas equal to or greater than 0.15 cm^2 and distances equal to or greater than 0.20 cm between electrodes. When the surface areas and distances are below these values, there is more variability of the results between trials. The rectangular electrode design with a surface area of 0.15 cm^2 and a distance of 0.20 cm has a high average Pearson correlation coefficient of 0.966±0.027, but is also the most reduced form factor while still maintaining high accuracy and precision when compared to the commercial electrode EDA stimulus response. This is the justification for using these parameters when modifying the geometry of electrodes.

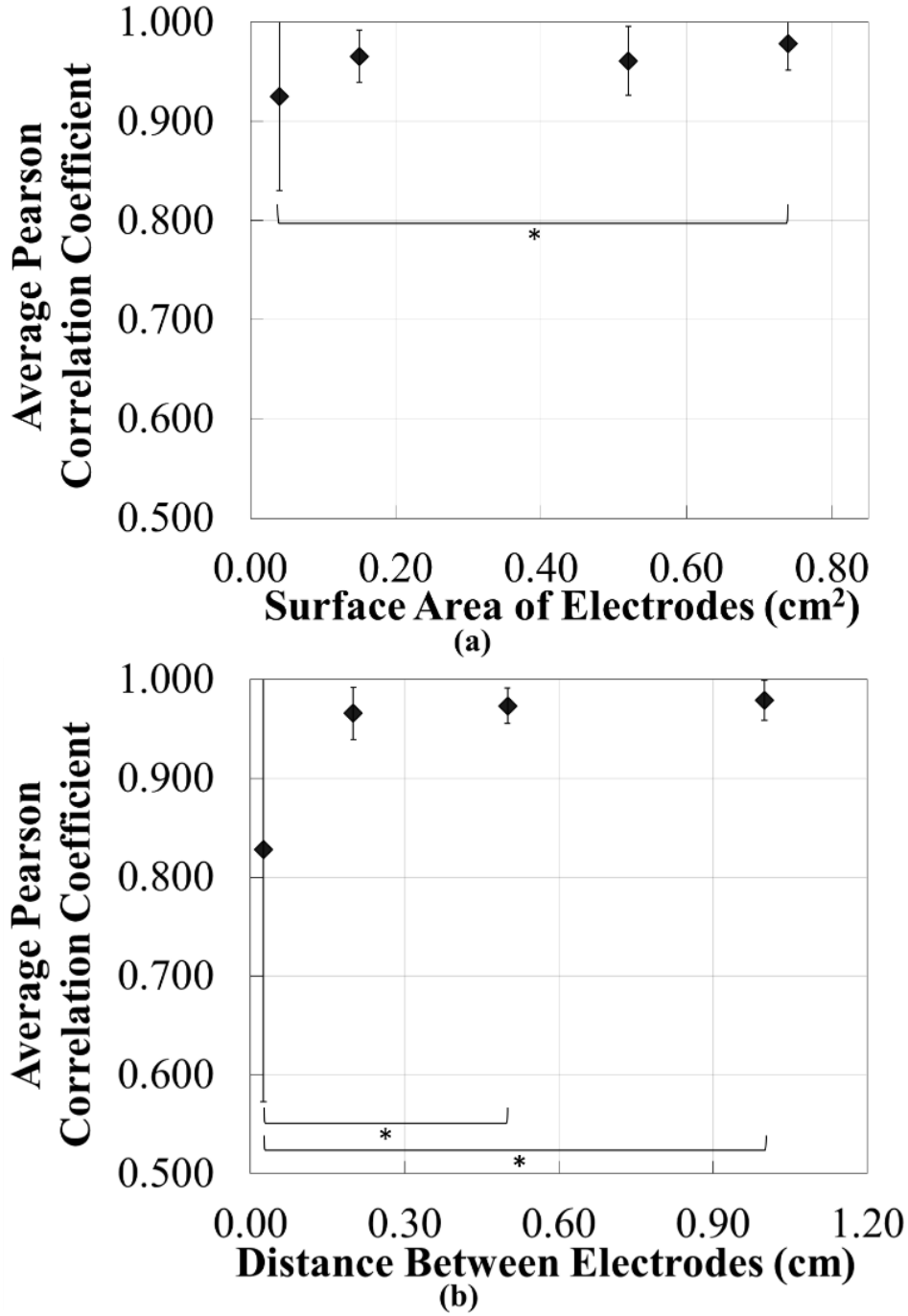

Figure 3.8 The average Pearson correlation coefficients for the comparison of the EDA stimulus response signals of the commercial rigid silver/silver chloride electrodes (1.50 cm distance, 1.00 cm^2 surface area) to the signals of the flexible silver/silver chloride electrodes of (a) 0.20 cm distance with surface areas of 0.04 cm^2, 0.15 cm^2, 0.52 cm^2 and 0.74 cm^2, as well as (b) 0.15 cm^2 surface area with distances of 0.025 cm, 0.20 cm, 0.50 cm and 1.00 cm. Standard deviations are shown and one-tailed t-test results with p-values<0.05 are indicated (*). For each value n=10 (© 2017 IEEE) [136].

The effect of geometry of the electrodes (rectangular, circular or serpentine) was also assessed by comparing the detected EDA stimulus response to the EDA signals recorded by the standard electrodes. The results are shown in Figure 3.9 and it was observed that while testing circular, rectangular and serpentine geometries of the electrodes, all with a surface area of 0.15 cm^2 and distance of 0.20 cm, the average Pearson correlation coefficients were 0.934±0.075, 0.966±0.027 and 0.979±0.015, respectively. The correlation coefficient of the serpentine electrodes (0.979±0.015) was statistically significantly greater than the correlation coefficient of the circular electrodes (0.934±0.075) with a p-value of 0.04. These results show that electrodes with greater coverage of sweat glands (as shown in the Figure 3.9 inset) have higher Pearson correlation coefficients, therefore are more accurate and precise. By changing the geometry of the flexible electrodes, the number of sweat glands between the two EDA electrodes varies, while the sweat glands under the electrodes are constant. Of note, the serpentine design for flexible electrodes increased the number of sweat glands between electrodes when compared to the circular design. This larger sweat gland coverage by the serpentine design is believed to reduce the total resistance, which is potentially related to the better detection of the EDA stimulus response observed.

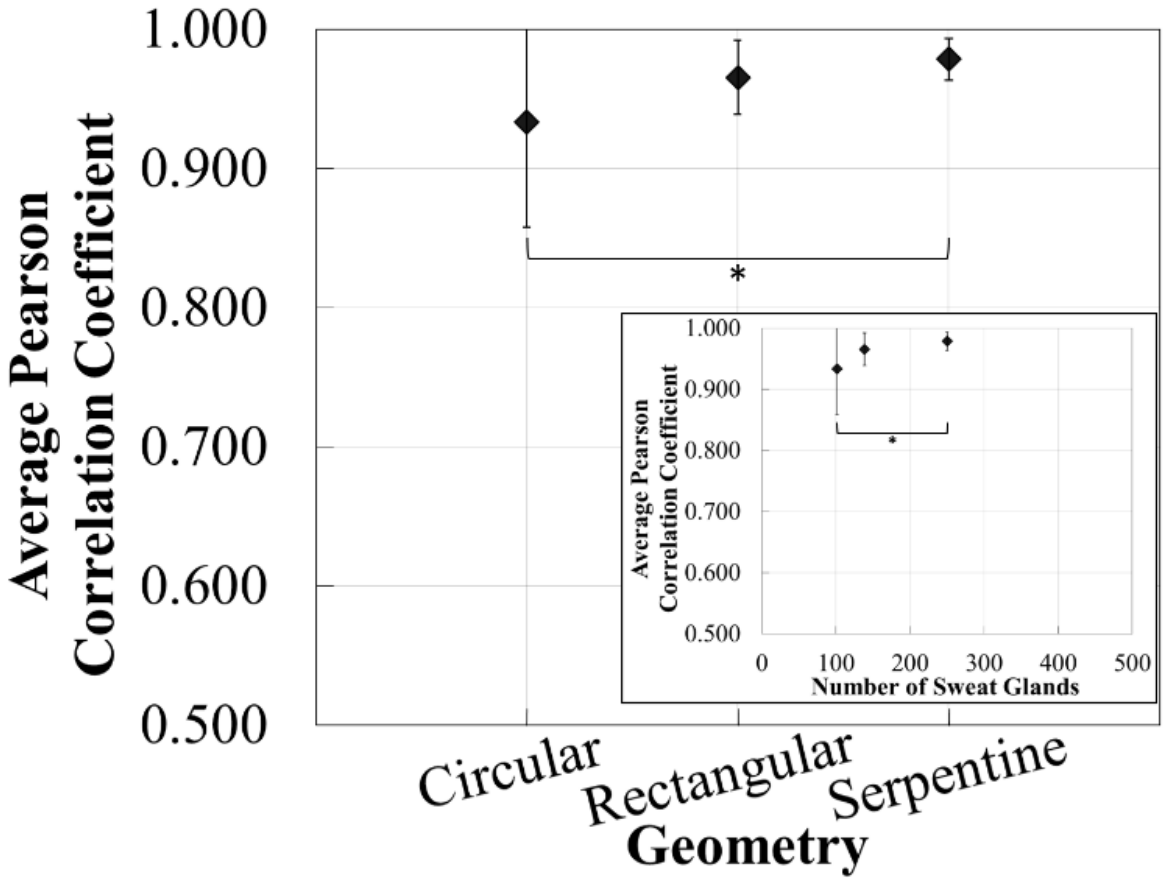

Figure 3.9 The average Pearson correlation coefficients for the comparison of the EDA stimulus response signals of the commercial silver/silver chloride electrodes (1.50 cm distance, 1.00 cm^2 surface area) to the signals of the flexible silver/silver chloride electrodes of 0.20 cm distance with a surface area of 0.15 cm^2 with circular, rectangular and serpentine geometries. Inset shows average Pearson correlation coefficients and associated number of sweat glands covered with electrode designs. Standard deviations are shown and one-tailed t-test results with p-values<0.05 are indicated (*). For each value n=10 (© 2017 IEEE) [136].

The results of the Pearson correlation coefficients are assessed in relation to the estimated total coverage of sweat glands (under and between electrodes) when modifying the surface area, distance between and geometry of electrodes, and can be observed in Figure 3.10. The possible reason for the increase in accuracy and precision of the larger surface areas and the larger distances between electrodes is that both scenarios increase the source of electrical conductivity, namely the sweat, which is illustrated in Figure 3.10. Also, the experimental

setting is not varying the bending conditions of the electrodes and should therefore not have a recognizable impact on the results, since the radius of curvature of all electrodes is the same during testing.

One can approximate a lower threshold limit of the minimum number of sweat glands required to be covered to enable the electrode designs to maintain accuracy and precision when compared to standard electrodes, and it is indicated as a red dashed line in Figure 3.10. This threshold is between an estimated 100 to 140 sweat glands. Based on the results, it is possible to maintain similar functionality to standard rigid electrodes with flexible electrodes, provided that an estimated 140, or more, sweat glands are covered by the design of flexible electrodes. Among all electrode designs tested, it can be observed that electrodes with a distance of 0.20 cm and with a surface area of 0.15 cm^2 in a serpentine geometry have the highest average Pearson correlation of 0.979 with the smallest standard deviation of 0.015 when compared to the standard electrodes. When considering all of the tested electrodes, the serpentine design is the most ideal for a wearable device, as it is one of the most reduced form factors that maintains high accuracy and precision of detectability of EDA stimulus responses.

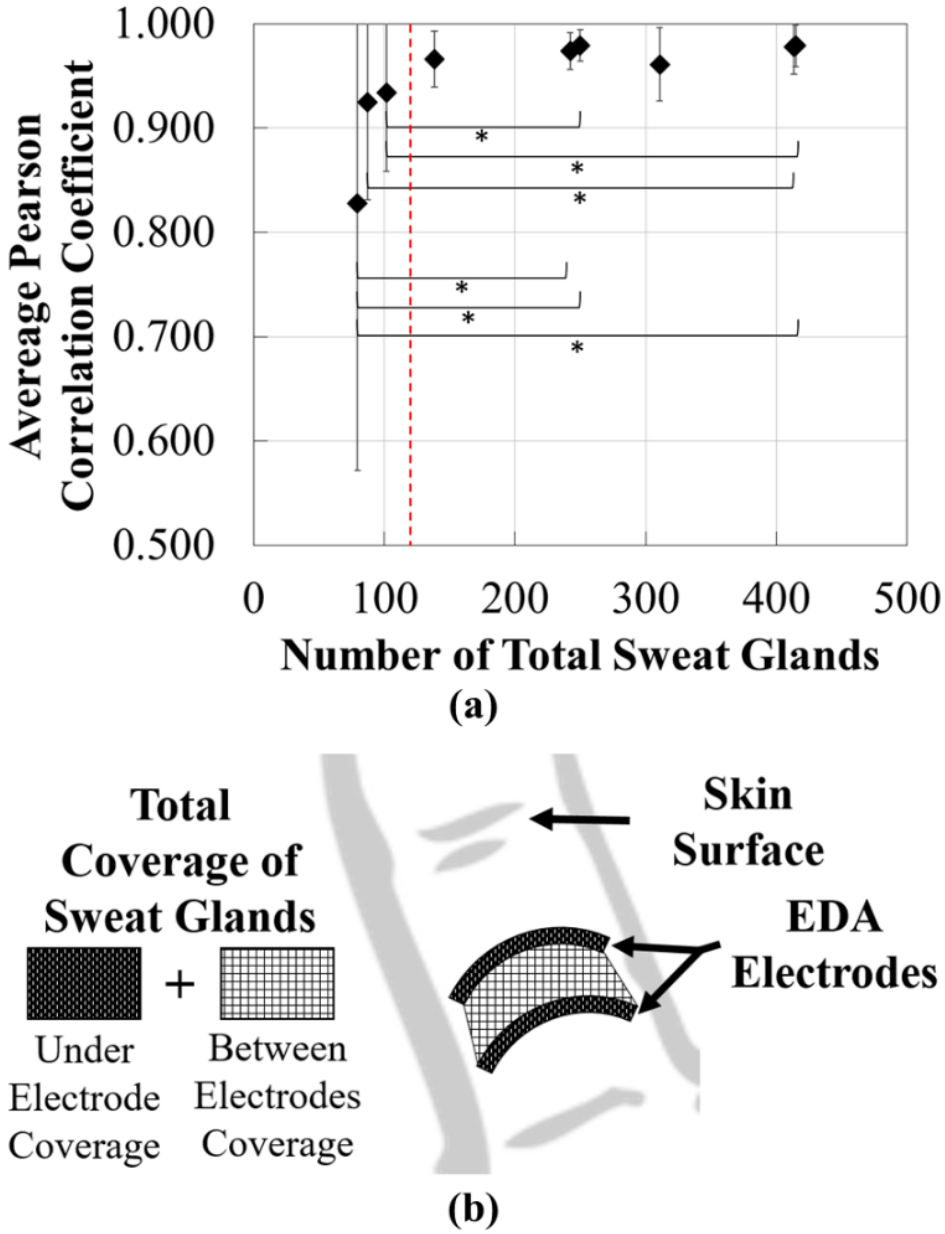

Figure 3.10 (a) The average Pearson correlation coefficients of all electrode designs versus total number of sweat glands covered under and between electrodes. Dashed red line indicates approximate lower limit threshold for accurate and precise EDA response detection. Standard deviations are shown and one-tailed t-test results with p-values<0.05 are indicated (*). For each value n=10. (b) Coverage evaluated when calculating number of sweat glands (© 2017 IEEE) [136].

3.3 Discussion

Through the modification of the surface area, distance between and geometry of flexible EDA electrodes, one can design dry flexible electrodes that are functionally similar to standard dry rigid electrodes. Specifically, this can be accomplished by maintaining the total number of sweat glands covered by the flexible electrodes to be 140 or more, as this was the experimental lower threshold limit established. This result can have significant implications when designing EDA monitoring devices for different locations of the body that have different distributions of sweat glands [144], [145] and varying ability to monitor EDA when standard electrodes are utilized [151]. Therefore, if an area of the body has a lower density of sweat glands, an electrode design that has a sufficiently large number of sweat glands covered is expected to be required in order to record an accurate and precise EDA response. This could be an important factor in optimizing sensors for monitoring EDA at different locations with comfort as the main focus. One could develop a device for monitoring EDA with multiple EDA sensors of different designs at various locations to provide spatial information in relation to the responses. The contribution of our study shows that one could potentially utilize dry and flexible electrodes, which would increase comfort, yet maintain functionality by modifying the electrode designs to cover the required number of sweat glands at each location.

The experiments demonstrate that the custom flexible Ag/AgCl electrodes with a distance of 0.20 cm and surface area of 0.15 cm^2 in a serpentine geometry have one of the highest average correlations to the standard solid Ag/AgCl electrodes with the most reduced form factor. This showcases the potential to optimize flexible electrodes that record quality EDA signals. This finding is in contrast to a previous study conducted in 1980 which assessed the effect of the surface area of electrodes on the EDA recording and reported no significant

differences between the electrodes with sizes of 0.017 to 0.786 cm^2 [152]. However, those results were obtained under different experimental settings; they only tested the standard circular solid Ag/AgCl electrodes and utilized conductive gels during the experiments [152]. The significant differences with the experiments conducted for our research include the assessment of dry electrodes, which do not utilize gels, as well as the impact of flexibility, geometry and distance between electrodes. In addition, current EDA recording devices have an advantage in that they have a higher sensitivity to the response.

There has been a significant amount of research into flexible and stretchable electrodes, specifically for health monitoring applications [153]. Many approaches for fabrication have been researched, with many methods utilizing photolithography, etching and transfer printing to create a patterned structure on a flexible substrate [66]. Researchers have also used a process which involves etching and thermal evaporation with patterned masks to form conductive electrodes on flexible substrates [94]. In addition, inkjet technology has been used to create flexible electrodes on plastic substrates [100]. For our study, we aimed to utilize a relatively efficient printing method to pattern electrodes for our systematic testing. Our method limits the number of steps required for flexible electrode fabrication and does not use custom masks or more specialized equipment.

The microstructures of the fabricated flexible Ag/AgCl electrodes could promote favorable results when comparing their recorded EDA signals to those from commercial electrodes. It is possible that these microscopic features could increase the overall effective electrolyte-skin surface area, where in this case sweat is the electrolyte, which is known to influence electrode-skin impedance [36]. Further research will be required to assess the durability of the layer of Ag/AgCl, as the degradation rate of the layer can impact the EDA

monitoring. The results of our study do allow for further efficient and effective research to be conducted on novel or unconventional materials that have yet to be evaluated for EDA monitoring by having established a better understanding of the effect of design parameters of electrodes (surface area, distance and geometry) on recording EDA stimulus responses.

The EDA physiological response has significant inter-subject variation and requires more complex data analysis in order to normalize results of multiple subjects [154]. Therefore, to reduce the number of variables in this study, a one-subject approach for assessing and characterizing the printed flexible electrodes was conducted to focus on the characterization of the developed flexible electrodes, various designs and optimization of EDA stimulus response monitoring. The conclusions of our study can be further tested with multiple subjects and is an appropriate next step to confirm the observations, in addition to assessing the potential impact of other parameters. The current study evaluated the phasic responses to assess the effects of the electrode design on monitoring the EDA response. The experiments outlined in our research support future work with long-term studies that consider the potential effect of electrode designs on tonic EDA signals.

The most common approach to monitoring EDA is the two electrode system [35], [36]. Our study utilized this method for potential comparison with other research. In addition, the Thought Technology system used to monitor EDA is used in the clinical setting and is capable of simultaneously monitoring EDA from two sets of electrodes. The dry electrodes were not compared with electrodes that utilize gels, as the active area would effectively be that which the gel covers, and it would not be controllable or easily quantified. The goal of this study was to form a better understanding of the effect of design of dry electrodes, as this information was to be used in the development of comfortable wearable devices for long-term monitoring. Gels

and adhesives currently being used for monitoring biological signals are uncomfortable and can cause skin irritations [35], [36].

There are existing electrical models that describe EDA on the skin in terms of resistive and capacitive elements, but the most appropriate model that could apply to our research is the simplified Montagu-Coles model of EDA [35], [143], [144]. There are still many complexities with the physiology of the skin that need further study. The results we are presenting can add more insight into the theoretical models from previous studies. By increasing the number of sweat glands covered, the total resistance is reduced, which could relate to the higher detectability of EDA responses. However, more experimentation with multiple subjects will be required to further develop the existing models and to understand all factors involved.

The research discussed in this chapter highlights the importance of design parameters including surface area, distance between and geometry of flexible dry electrodes on the EDA stimulus response detection. In addition, a repeatable fabrication process to develop Ag/AgCl electrodes of various designs has been established. The results obtained to date show promise for the potential to optimize electrode designs for the monitoring of EDA by modifying the distance between flexible electrodes, as well as the surface area and geometry, in order to increase the number of sweat glands covered to 140 or more, as shown experimentally. These conditions allow for accurate and precise detection of EDA stimulus responses when compared to the standard rigid electrodes currently being used commercially. In particular, the serpentine geometry with a surface area of 0.15 cm^2 and a distance between electrodes of 0.20 cm proved to be the ideal electrode design for a flexible and wearable EDA system. The results of the study in this chapter can also be utilized to understand how to effectively reduce the overall form factor of EDA sensors without compromising functionality and create a foundation for

novel and innovative approaches towards the development of wearable EDA sensors. The application of wearable EDA sensors has the potential to be used in laboratory, clinical and personal settings. Progress in the development of this type of device can also help in advancing a variety of other research endeavors.

Chapter 4: Flexible and Breathable Electronic Textile EDA Electrode Development

E-textiles have the potential to create a truly ubiquitous and unobtrusive method of monitoring individuals for a variety of healthcare applications [21]. In regards to EDA, there have been significant strides in the development of an e-textile (stainless steel conductor material) EDA monitoring glove, which has identified important electrical parameters and algorithms required to obtain reliable EDA data [23], [28], [31]. Other research has focused on utilizing silver as the conductive material when monitoring EDA [24], [26], [27], [33], [34]. A particular area not currently explored in the field of e-textiles in general, and also when considering EDA monitoring, is the fabrication of an Ag/AgCl e-textile that can be directly compared to Ag/AgCl solid electrodes, which are currently used in the clinical setting for monitoring human physiological signals. In addition, understanding the effect that different textile materials have on an EDA recording has not been discussed in the literature to date. Previous studies utilizing e-textiles for EDA monitoring have also indicated the need for a better understanding of the effect of e-textiles and textiles on EDA monitoring [23], [28], [34]. Resistance is an important parameter to consider when developing an Ag/AgCl e-textile and it should be significantly lower than the resistance of biological processes on the surface of the human skin, which is in the range of several thousand ohms [35]. The e-textile system should remain in contact with the skin during manipulation and should be biocompatible [155], [156].

Another area of interest in EDA research that still requires a significant amount of study is the concept of asymmetry of EDA on different sides of the human body [102]. This notion of multiple emotional substrates in the brain, which can lead to different innervations on each

side of the body, was introduced by Picard et al. in 2016 [102] and has promoted significant dialogue within the research community to ultimately develop a better understanding of EDA as a whole. Early research into understanding the underlying physiology associated with EDA began with animal models [157], [158]. In particular, the electrodermal response was shown to be attributed to 60% innervation by the ulnar nerve and 40% innervation by the median nerve in a feline model [157]. In a canine model, it was shown that the thoracic spinal root (T1), which is connected to the SNS, provides input to both the ulnar and median nerves, but the contribution is greater in the former [158].

In humans, the little finger is primarily innervated by the ulnar nerve, while the middle and index fingers are mainly innervated by the median nerve, with potential communication between the branches [77]. Also, on the palmar side of the hand, the distal phalanx of all fingers are known to have an increased EDA signal due to an increase in sweat gland density compared to the median and proximal phalanges [78], [79]. There is an opportunity to further explore whether there are differences in the EDA responses on the different fingers of the human hand, as there is limited information in previous literature. Therefore, it is believed that through fabrication and testing of e-textile electrodes, an understanding of the effect of materials and location of the electrodes on the EDA signal detection can be developed. Appendix B provides additional data figures and tables for this chapter.

4.1 Materials and Methods

4.1.1 Fabrication of E-textiles

Fabricating Ag/AgCl e-textiles began with acquiring 99% pure Ag coated nylon 6,6 2 ply yarn, where each ply has 17 filaments and a 117 linear density (dtex) (Shieldex by Statex,

Germany). The method to obtain the Ag/AgCl yarn in this work is adapted from a previous study that fabricated Ag/AgCl yarn in a static batch operation [114]. Our work develops a more dynamic roll-to-roll process to fabricate the Ag/AgCl yarn from the available Ag coated nylon yarn in which a custom electrochemical chamber was built, as shown in Figure 4.1. This roll-to-roll method to develop Ag/AgCl yarn has not been described in previous literature, to the best of our knowledge, and therefore the detailed experimental parameters are novel.

The roll-to-roll system contains a 250 mL beaker in which the electrochemical reaction occurs, a spring-loaded tension controller, as well as a non-conductive unplasticized polyvinyl chloride plate with integrated nylon plastic pulleys and screws to guide the yarn through the chamber on two sides of the plate (3.5 cm of yarn on each side of plate). The system also includes a conductive metal pulley and screw connected to the positive component of the Keithley 2400 SourceMeter (Keithley, United States), with which the yarn is in contact, thereby acting as the working electrode in the chamber. The negative component of the SourceMeter is connected to two platinum counter electrodes of 3.5 cm in length and 2 cm distance from the yarn on each side of the guide plate. In addition, a collecting yarn spool connected to a DC geared motor (12 V, 3.5 RPM, 37 Gear Boxes, Lee's Electronics, Canada) is used to control the rate of movement of the yarn on the delivery spool through the chamber by controlling the voltage supplied to the motor through a voltage power supply (LASCAR PSU 130, United States). The solution inside of the chamber is 0.9% sodium chloride (VWR International, United States) and is mixed with a magnetic stir bar at 1100 RPM. When the yarn exits the chamber, it is manually washed with deionized water. The voltage of the power supply for the motor is set at 4.00 V which results in a 1.00 RPM of the spool, a 0.08 cm/s movement of yarn and a total time of 89.17 s for a 7 cm section of yarn inside the

electrochemical chamber. The SourceMeter was set to function as a resistor with a potential limit of 2.00 V and the currents tested to optimize the functionality of the Ag/AgCl yarn were 0.5, 0.75, 1.00 and 1.25 mA.

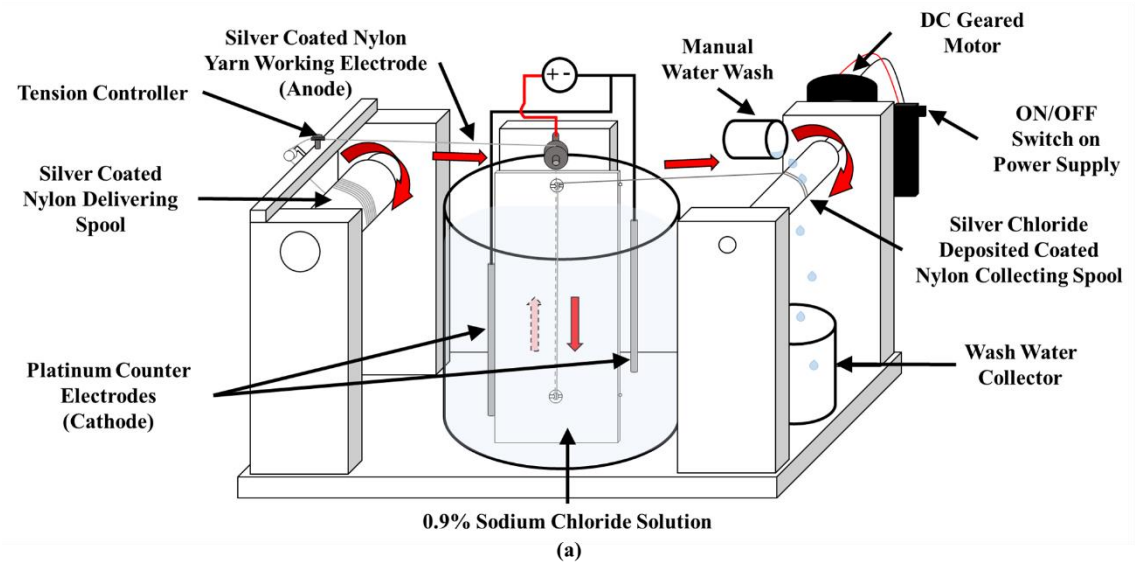

(a)

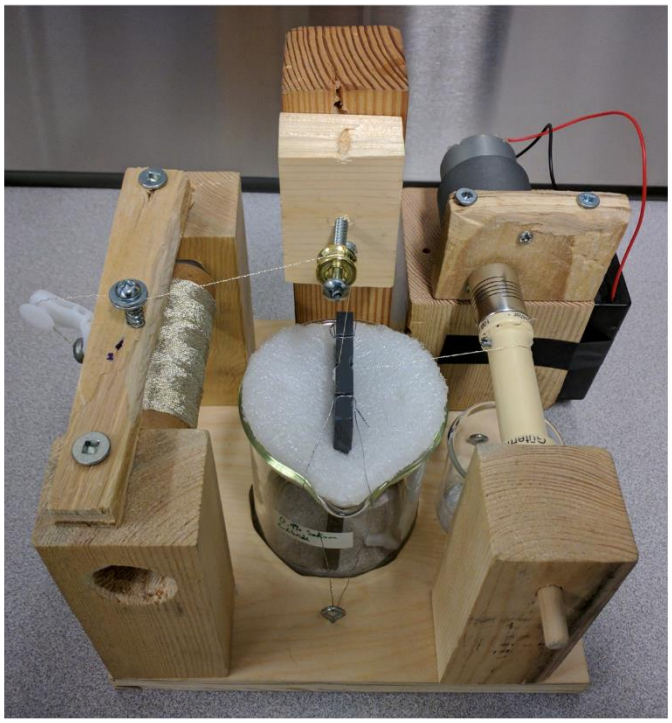

(b)

Figure 4.1 (a) Schematic of roll-to-roll system for silver/silver chloride yarn development and (b) actual image of roll-to-roll system.

4.1.2 Characterization of E-textile Electrodes and Textile Substrates

Resistances for 10 cm samples at each cm of the original Ag and Ag/AgCl coated nylon yarns fabricated with different applied currents were measured using a multimeter (Agilent U1232A, United States) to identify the yarn with an ideal resistance for an e-textile EDA electrode (n = 10). Also, the resistances at increasing increments of 1 cm, to a total length of 10 cm, were measured with a multimeter for the optimal fabricated Ag/AgCl yarn and original Ag yarn (n = 3). The contact resistances for these measurements were approximated by referring to a methodology previously studied [159]. To calculate the average contact resistances, the lengths of yarn in which average resistances were evaluated were of 1 and 2 cm, 2 and 4 cm, 3 and 6 cm, 4 and 8 cm, and 5 and 10 cm (n = 5). The equations utilized for contact resistance calculations are shown below, with the assumption that there is a linear relationship between increase in resistivity and length of the sample [159]:

$$\frac{R_2}{R_1} = \frac{L_2}{L_1} \tag{5}$$

Where R_1 and R_2 are the resistances in ohms measured at lengths L_1 and L_2 in cm, respectively.

$$R_1 + 2R_K = R_{T1} \tag{6}$$

$$R_2 + 2R_K = R_{T2} \tag{7}$$

Where R_K is the contact resistance, R_{T1} and R_{T2} are the total resistances of L_1 and L_2 of the yarns, respectively. Also, L_2 is twice the length of L_1. Through subtraction of (6),(7) and through rearrangement and modification, the following equations are used to calculate the actual resistances of R_1 and R_K:

$$R_1 = R_{T2} - R_{T1} \tag{8}$$

$$R_K = \frac{R_{T1} + R_1}{2} \tag{9}$$

To evaluate the replicability of the fabrication method of the optimal Ag/AgCl yarn, three separate development processes with identical optimal parameters were conducted and the resistances at every cm for each 10 cm sample prepared was measured (n = 3). In addition, optical images of the different yarns were obtained using a Leica S9i stereo microscope (Leica, Germany). An optimal Ag/AgCl coated nylon yarn was then selected based on resistance and visual coverage of the AgCl layer for further characterization and comparison to the original Ag coated nylon yarn. This included calculating the current density and mass of AgCl formed during the roll-to-roll electrochemical process.

The maximum load at break and tenacity of the original Ag and optimal Ag/AgCl coated nylon yarns were determined utilizing a dual column tabletop materials testing system (INSTRON 5969, United States) with a 2 kN static load cell, extension rate of 0.83 mm/s and yarn samples of 20 cm with 10 cm between grips (n = 3). The dtex used for the tenacity calculations was 234, which was from the manufacturer, for the original Ag coated nylon yarn. The dtex for the optimal Ag/AgCl coated nylon was estimated by calculating the weight of AgCl deposited on the original Ag yarn through the electrochemical process. X-ray diffraction (XRD) patterns of the surface of the fabricated Ag/AgCl e-textiles and the original Ag e-textiles were obtained using a D8-Advance X-ray diffractometer (Bruker, United States). For a cross-sectional analysis of the Ag and Ag/AgCl e-textiles, the yarn samples were secured in EpoFix Resin (25 parts by weight, Struers, Denmark) and EpoFix Hardner (3 parts by weight, Struers, Denmark), allowed to cure for 48 hours and then polished. To observe the morphology, thickness and diameters of the Ag and Ag/AgCl layers of the yarns, a scanning electron microscope (SEM) (Hitachi S-3000N, Japan) was used. The top surface of the Ag and

optimal Ag/AgCl yarns were evaluated with the SEM, which was also equipped with energy-dispersive x-ray spectroscopy (EDS).

The textile substrates selected to support and integrate the Ag/AgCl e-textile electrodes were 100% cotton, 100% nylon and 100% polyester, which are all woven fabrics with a plain weave structure (Fabricland, Canada). The threads in the warp and weft direction of each textile substrate were counted with the use of a Leica S9i stereo microscope and the thickness was measured with a Mitutoyo Digimatic micrometer (MDC-1″ SX, Japan). Each textile substrate was tested three times for breathability in terms of permeability by following a previous standard protocol by the American Society for Testing and Materials (ASTM) [160] (n = 3). Specifically, the water cup testing method was utilized for an eight-hour duration with data collected each hour. A cup (EZ-Cup Vapormeter, United States) that complies with the ASTM E96 standard was used. The cup, which can hold test samples up to 3 mm thick with a diameter of 63.5 mm, is sealed mechanically with rubber and Teflon. The cup itself has a depth of 19.05 mm and weight of 127.36 g. The chamber used to control airflow was an AirClean System (AC710C, United States), and a digital hygrometer/psychrometer (TPI 597, United States) monitored temperature and humidity. A weighing balance (Sartorius CPA225D, United States) was used to monitor the change of weight. The following equations were used to calculate permeability:

$$WVT = W/tA = (W/t)/SA \quad (10)$$

Where *WVT* is the rate of water vapor transmission in g/h·m^2, *W* is weight change in g, *t* is time in h and *SA* is the sample test area in m^2.

$$Permeance = WVT/\Delta p = WVT/S_p(RH_1 - RH_2) \quad (11)$$

Where permeance is in g/Pa·s·m^2, Δp is the vapor pressure difference in Pa, S_p is the saturation vapor pressure at test temperature in Pa calculated by the Arden Buck equation [161], [162] shown below, RH_1 is the relative humidity at the source expressed as a fraction (in the cup) and RH_2 is the relative humidity of the vapor sink expressed as a fraction.

$$S_p = 611.21 \exp\left(\left(18.678 - \frac{T}{234.5}\right)\left(\frac{T}{(257.14+T)}\right)\right), \text{ over liquid water, } T > 0\ °C \quad (12)$$

Where T is the temperature of the air in degrees Celsius (°C).

$$Average\ Permeability = Permeance\ x\ Thickness \quad (13)$$

Where *Average Permeability* is in g/Pa·s·m and *Thickness* is in m.

The wettability of cotton, nylon and polyester fabrics, as well as the surface of a solid Ag/AgCl standard electrode, were evaluated by determining the contact angle of a pendant deionized water droplet [163]. The 10 µL water droplet was formed with the use of a 25-gauge needle (305122, BD, United States) and a 1 mL syringe with tubing. The image to calculate the contact angle of the water droplet was obtained with the use of a high speed camera (X-PRI, High Speed Imaging, Canada) and a high intensity illuminator (Fiber-Lite MI-150, Dolan-Jenner Industries, United States). The contact angle of a water droplet was measured on the two sides of the droplet by using Image J software (Version 1.51, National Institutes of Health, United States) and then averaged. Each material was imaged three times (n = 3). The material was considered to be hydrophilic if the water droplet contact angle was less than 90° and hydrophobic if the contact angle was greater than 90°.

The bending moment versus curvature curves were plotted for the woven textile substrates and the bending rigidity and hysteresis (recoverability) were determined with a KES-FB2-S bending tester (Kato Tech, Japan) and associated software (KES-FB

Measurement Program, Version 8.07, Japan) with a sensitivity of 20 gram force·cm [140]. The bending tests were done on 5 cm wide cotton, nylon and polyester fabrics in the warp and weft directions (n = 3). Also, the bending displacement velocity was 0.5 cm^{-1}/s and the sample size in the bending direction was 1.00 cm.

4.1.3 Integration Technique for E-textile Electrodes with Textile Substrate

The integration of the Ag/AgCl e-textile with the textile substrates went through various iterations with the final design choice described in this work. Importantly, the straps with hand-stitched e-textile electrodes were designed to be adjustable for use on the distal phalanx of index, middle and little fingers. The final design for the EDA e-textile electrode straps, shown in Figure 4.2, was influenced by the requirement of the electrodes to cover 140 sweat glands to effectively detect EDA stimulus responses, which was outlined in previous work in chapter 3 [136]. The final size of the textile substrate was 6 cm long by 1 cm wide, which was specifically intended to be placed on the distal phalanx of the index, middle and little finger. The ends of the textile straps have Velcro hooks or pads for easy application or removal of the straps. The e-textile electrodes were hand-stitched with an adapted back stitch, as shown in Figure 4.3. The two e-textile electrodes exposed to the skin are 2.0 cm long (0.5 cm stitch length) and 0.4 cm apart, with an approximate surface area of 0.12 cm^2 covered by each electrode. The electrical connector was secured by first stitching it with the e-textile and then coating the conductive yarn on the connector with silver paint (TED PELLA, United States) and allowing it to dry for 20 minutes. To encapsulate the yarn and secure the connector, a coating of cyanoacrylate (LePage, Canada) was applied on the silver paint and allowed to dry for 20 minutes. Six sets of e-textile electrodes for each of the three textile substrates were

stitched by hand to assess the success rate of the integration process (n = 6). Also, the resistances from the solid electrical connector to the furthest end of a usable e-textile electrode were all measured (n = 18).

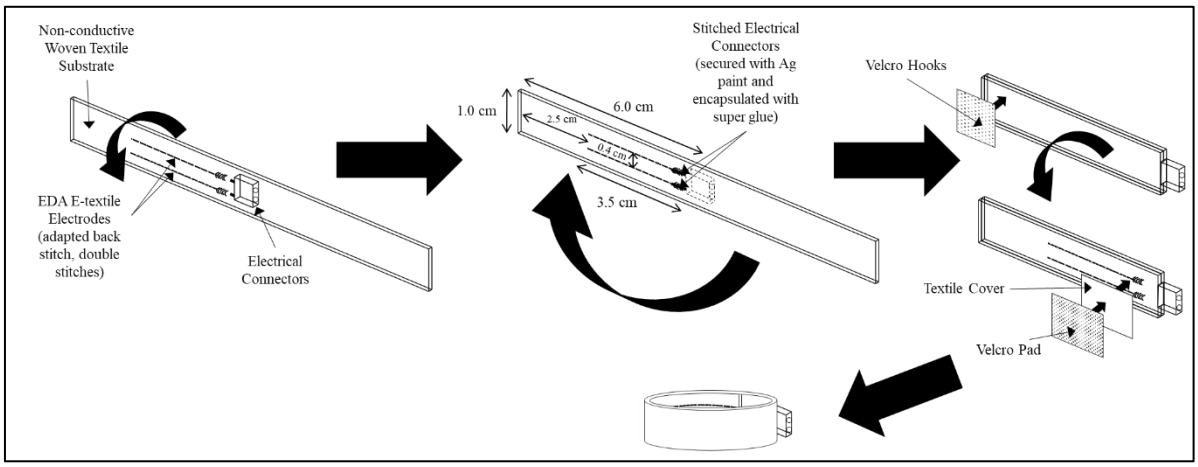

Figure 4.2 Final design of straps for e-textile EDA electrodes on woven substrates of cotton, nylon and polyester.

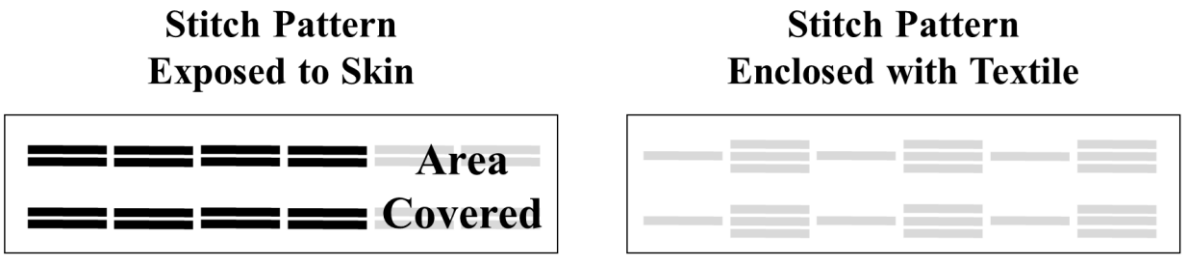

Figure 4.3 Stitch patterns for e-textile EDA electrodes where each e-textile electrode exposed to the surface of the skin covers 0.12 cm^2 of surface area.

4.1.4 EDA Monitoring Testing Protocols

The chosen method to monitor EDA has been previously described in chapter 3 [136]. Briefly, skin conductance and the EDA response were recorded by utilizing an adapted Stroop color test [141], [142]. The experiments assessed EDA for a 15 minute time period, which includes a 22.5 second time period to confirm that the electrodes are connected properly and then an initial rest period of 4 minutes. The Stroop test then begins and lasts for 5 seconds

followed by another 2 minute rest period. There are 3 cycles of a 5 second Stroop test and 2 minute resting period. After the 3 cycles, there is a final 4 minute rest period and another 22.5 seconds to observe and confirm that the electrodes are still recording data.

A 4-hour EDA monitoring experiment was also conducted in which the subject would remain as still as possible during the test. There were no controlled external stimuli provided to the subject and the temperature and humidity of the room were recorded at the beginning and end of the 4-hour test with a digital hygrometer/psychrometer.

4.1.5 Systematic Testing of E-textile and Textile Materials

The dry Ag/AgCl e-textile EDA electrodes integrated into the cotton, nylon and polyester substrates were each compared to the standard rigid, non-breathable and dry Ag/AgCl electrodes simultaneously. Three sets of e-textile electrodes integrated into one type of substrate were attached on the distal phalanx of the index, middle and little finger and secured with the use of Velcro, and compared against a set of commercially available standard sintered solid Ag/AgCl electrodes (Thought Technology, Canada) with approximately 1.00 cm^2 surface area. Straps were used to secure the standard solid Ag/AgCl electrodes, which were placed on the proximal and medial phalanges of the middle finger with a constant distance of 1.50 cm between. To measure the compressive force applied on the electrodes by a strap or tape, a 0.51 cm diameter force sensor (Pololu, United States) was placed at each sensor location shown in Figure 4.4, and an Arduino UNO R3 (Arduino, Italy) was utilized as the data collection system (n = 3).

To quantify the sweat gland density of the locations on the palm of the hand of the subject where EDA electrodes were placed, a 10% povidone-iodine topical solution (Betadine

Solution, Purdue Pharma, United States) with linen paper test was performed [164], [165]. The povidone-iodine topical solution was stamped on the location of interest on the palm of the hand of the subject with a 2 by 2 cm piece of linen paper, which was then allowed to dry for approximately 10 minutes. A clean piece of 2 by 2 cm linen paper was then pressed onto the location of interest for 20 seconds until small dots appeared on the paper, which indicate the presence of sweat gland ducts. A Leica S9i stereo microscope was used to image the dotted linen paper to count the number of sweat glands per cm^2 in the area of interest. The sweat gland density of the locations where EDA electrodes were placed were tested three times (n = 3).

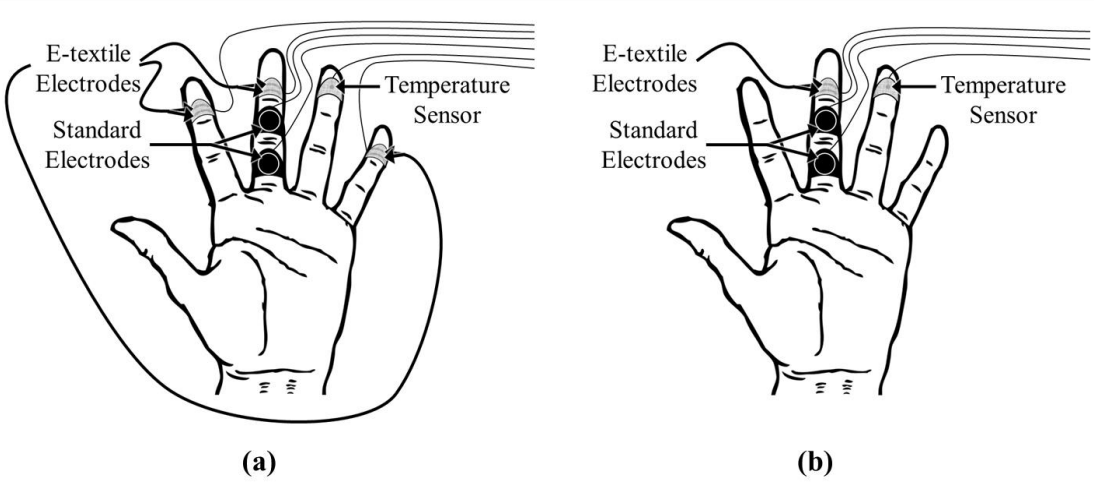

Figure 4.4 Schematics showing the location of sensors for (a) 15-minute and (b) 4-hour tests.

For EDA monitoring, the e-textile electrodes and standard electrodes were connected to the FlexComp Infiniti (Thought Technology, Canada), which uses DC and constant voltage with 0.01 µS sensitivity to measure skin conductance [34]. The experimental set-up for monitoring EDA is similar to that reported in previous work [136] and is most closely related to the simplified Montagu-Coles model of EDA [35], [143], [144]. The FlexComp Infiniti was then connected to a computer in which the EDA data would be collected with the use of the BioGraph Infiniti software at a sampling rate of 256 Hz for the 15-minute tests and at 32 Hz

for the 4-hour test. For the 15-minute tests, the EDA stimulus response was monitored with three e-textile electrodes of a specific textile substrate material (cotton, nylon or polyester) on the distal phalanx of the index, middle and little finger. The EDA stimulus response monitored with the e-textile electrodes was compared to that of the standard electrodes (located on the proximal and medial phalanges of the middle finger). EDA responses were measured three times for each finger location and substrate material, and at no time was a single e-textile strap was used twice in one location (n = 3). In previous work outlined in chapter 3 [136], the standard EDA electrodes were compared to another set of standard EDA electrodes to confirm the reliability of the test method (n = 1). The average minimum to maximum EDA signal percent change per sweat gland was evaluated to determine if there was a difference in the EDA waveforms recorded on the distal phalanx of the index, middle and little fingers, regardless of textile substrate used (n = 9).

For the 4-hour test, the EDA data recorded with a set of e-textile electrodes with a cotton textile substrate on the distal phalanx of the middle finger was compared to the EDA data collected by the standard electrodes on the proximal and medial phalanges of the middle finger (n =1). All tests were conducted on one subject. A temperature sensor (Thought Technology, Canada) was used to monitor skin surface temperature during all experiments.

4.1.6 Statistical Analysis

The statistical analysis for the comparison of EDA stimulus responses collected during the 15-minute tests was done similarly to a previous study [136], which was outlined in chapter 3. Briefly, the EDA signals evaluated were collected during the same experiment and the data utilized in the statistical analysis was selected by visual analysis of the three EDA responses

to the Stroop test stimuli. The data selected for further analysis was based on identifying one apparent EDA response with the standard electrodes, which was then sectioned 10 seconds before and 20 seconds after the stimulus. The EDA data of the e-textile electrodes was sectioned at the same time points and compared to the standard electrode data. This analysis approach allowed for the inclusion of important components of the signal response [35].

The Pearson correlation coefficient [146] was used to compare the EDA response signals recorded by e-textile and rigid electrodes, which has been previously done when comparing EDA signals [34], [136], [147]. A one-tailed paired t-test was completed to compare the averages and the standard deviations of the Pearson correlation coefficients of different textile substrate materials and locations on the hand that were tested. The significance level (p-value) is less than 0.05 or 0.10 and a correlation coefficient value of 1 means perfect positive correlation between the signals, while a value of -1 means perfect negative correlation. A one-tailed paired t-test, with a p-value of less than 0.05, was also done to assess significant differences between the resistances per cm of Ag and Ag/AgCl coated yarns, breathability and wettability results, sweat gland density and force test results for sensor locations, with standard deviations between tests stated. A one-tailed paired t-test, with a p-value of less than 0.05, was also done on the bending rigidity and hysteresis results of the fabric substrates. Another one-tailed paired t-test, with a p-value of less than 0.05, was done to assess significant differences between the contact resistances per cm for Ag and optimal Ag/AgCl coated yarns. A two-tailed paired t-test, with a p-value of less than 0.05, was done on the results of the maximum load at break tests and tenacity calculations of the Ag coated nylon yarn and the optimal Ag/AgCl coated nylon yarn, as well as when comparing different fabrication trials for the optimal Ag/AgCl yarn.

To further evaluate the effect of location of the e-textile electrodes on the EDA stimulus response waveform, the average percent change from the minimum to maximum conductance across all tests on a specific location was calculated and then divided by the sweat gland density of the location on the finger. A one-tailed paired t-test, with a p-value of less than 0.05 or 0.10, was conducted on the average minimum to maximum EDA signal percent change per sweat gland to evaluate if there was a difference in the EDA waveforms recorded on the distal phalanx of the index, middle and little fingers when corrected for sweat gland density.

The trends for the 4-hour EDA experiment were evaluated based on the signal percent difference of the skin surface temperature, standard electrode baseline EDA signal and e-textile baseline EDA signal from the beginning of the test and at each hour time point ± 10 minutes, depending on the time point of the baseline EDA signals. In addition, the Pearson correlation coefficient was calculated with the data for the entire 4-hour experiment to compare the EDA signals collected by the standard and e-textile electrodes, the EDA signal of the standard electrodes versus the skin surface temperature, as well as the EDA data recorded by the e-textile electrodes versus skin surface temperature.

4.2 Results

4.2.1 Characterization of E-textile Electrodes and Textile Substrates

The roll-to-roll electrochemical system for the development of Ag/AgCl coated nylon yarn from Ag coated nylon yarn went through a series of iterations, with the main goals being to reduce high tension points for the yarn, in addition to identifying the optimal parameters to obtain Ag/AgCl e-textile yarns appropriate for prototyping and EDA monitoring. The applied currents during the electrochemical process varied (0.5 mA, 0.75 mA, 1.00 mA and 1.25 mA),

while all other parameters were maintained constant, and the resulting optical images of the yarns are shown in Figure 4.5. The original Ag coated yarn has a resistance of 2.0±0.6 Ω/cm, while the Ag/AgCl yarns fabricated have resistances of 4.4±1.0 Ω/cm, 12.4±2.5 Ω/cm, 40.0±10.1 Ω/cm and > 1 MΩ/cm for the applied currents of 0.50 mA, 0.75 mA, 1.00 mA and 1.25 mA, respectively (n = 10 for each value). Larger average values of resistances per cm for each yarn are statistically significantly greater than all smaller average values of the other yarns (p-values<0.05) and Figure 4.5 shows these results.

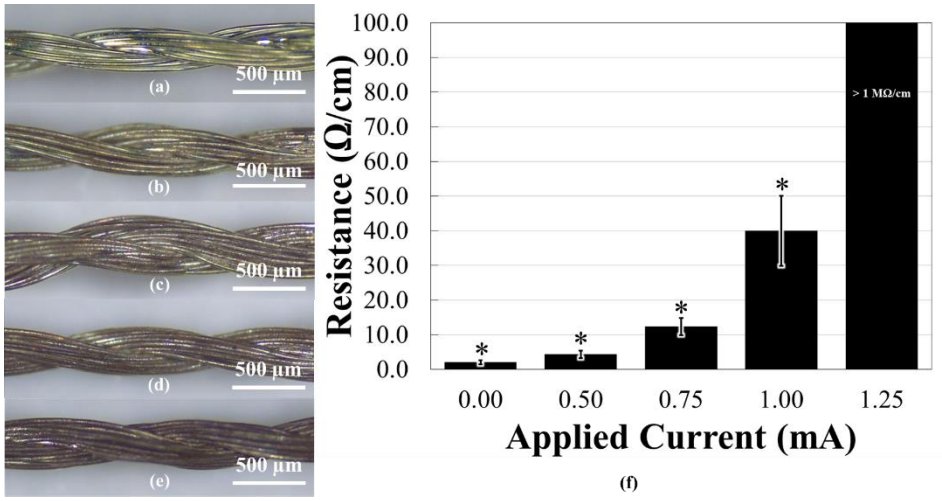

Figure 4.5 Optical images of (a) original silver coated nylon yarn and (b) silver/silver chloride coated nylon yarn fabricated with 0.50 mA, (c) 0.75 mA, (d) 1.00 mA and (e) 1.25 mA applied current. (f) A graph of applied current used to fabricate silver/silver chloride coated nylon yarn versus resistance (Ω/cm). Standard deviations are shown and one-tailed t-test results with p-values<0.05 are indicated (*). For each value n=10.

The optimal parameters for developing Ag/AgCl coated yarn were selected on the basis of having sufficient coverage of AgCl, determined through visual evaluation, and a resistance as low as possible. Utilizing 0.75 mA of applied current in the electrochemical roll-to-roll set-up developed optimal Ag/AgCl yarn with an average resistance of 11.0±1.8 Ω/cm when measuring the resistance per cm of yarn fabricated with three distinct experiments. When comparing the average resistances per cm between most trials for the applied current of 0.75

mA, there was no statistically significant difference between them as the p-values were greater than 0.05, demonstrating a relatively repeatable fabrication process. There was, however, a p-value of less than 0.05 when comparing trials 1 and 3. This indicates that further optimization and automation of the process is possible, and it is important to note that this method is still in the relatively early stages of development. The results of the resistances for the original Ag yarn and the optimal Ag/AgCl yarn at increasing lengths are shown in Figure 4.6 and demonstrate the linear relationship between resistance and length of yarn. The contact resistance with the optimal Ag/AgCl yarn (2.46±1.81 Ω) was shown to be statistically significantly greater than the contact resistance associated with the original Ag yarn (0.11±0.05 Ω) with a p-value of 0.02. The current density of the yarn, when using the optimal roll-to-roll parameters, was 1.82 mA/cm^2 when using a cylindrical approximation for the 7 cm of yarn with an estimated radius of 93.45 µm. The mass of AgCl formed on the Ag coated nylon yarns was calculated as described in previous literature [95] and is shown below for a 7 cm length of yarn, which is in the electrochemical chamber for 89.17 s:

$$q = \int_0^{89.17} I\, dt = 0.75\, mA \int_0^{89.17} e^{-3.42x10^{-7}t} dt = 0.07\, C \qquad (14)$$

Where q is the charge crossing the electrode-electrolyte interface during the electrochemical reaction in C, I is the applied current in mA and t is the time in s. The equation for the growth of AgCl was determined experimentally by measuring the current during the reaction, plotting current versus time, and then fitting an exponential trend line to the data.

$$N_{atoms} = \frac{0.07\, C}{1.6\, x\, 10^{-19} C/atom} = 4.38\, x\, 10^{17} atoms \qquad (15)$$

Where N_{atoms} is the number of atoms deposited, since one molecule of AgCl is deposited for each electron.

$$N_{moles} = \frac{4.38\ x\ 10^{17} atoms}{6.03\ x\ 10^{23} atoms/mol} = 7.26\ x\ 10^{-7} mol \quad (16)$$

Where N_{moles} is the number of moles, which is found by dividing by Avogadro's number.

$$m_{\frac{AgCl}{cm}} = \frac{MW_{AgCl}\ x\ N_{moles}}{l} = \frac{143.32 \frac{g}{mol} x\ 7.26\ x\ 10^{-7} mol}{7\ cm} = 1.49\ x\ 10^{-5}\ g/cm \quad (17)$$

Where $m_{AgCl/cm}$ is the mass of AgCl formed per cm of conductive yarn, l is the length of conductive yarn and MW_{AgCl} is the molecular weight of AgCl.

Therefore, for the optimal Ag/AgCl coated nylon yarn, there is approximately 1.49 x 10^{-5} g of AgCl per cm. Also, 30 minutes of fabrication time produced approximately 120 cm of usable Ag/AgCl yarn with the optimal parameters. The optimized Ag/AgCl coated nylon yarn was then further characterized and compared to the original Ag coated nylon yarn.

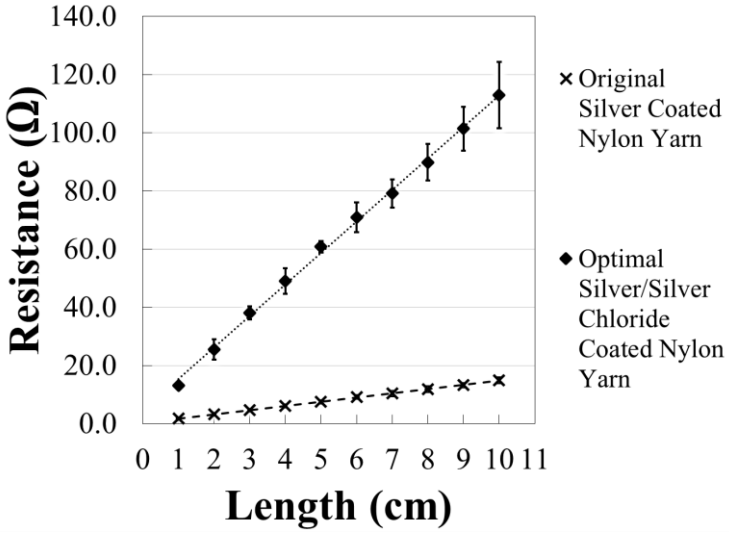

Figure 4.6 Measured resistance at different lengths for the original silver coated nylon yarn and the optimal silver/silver chloride coated nylon yarn.

The maximum load at the break of the Ag and optimal Ag/AgCl coated yarn was 12.19±0.75 N and 11.50±0.86 N, respectively. There was no statistically significant difference (p-value=0.48) between the maximum load at break values. The tenacity of the Ag and optimal Ag/AgCl yarns was calculated by utilizing the approximated dtex of 234 and 238, respectively.

The average tenacity of the Ag and optimal Ag/AgCl yarns are 0.52±0.03 N/tex and 0.48±0.04 N/tex, respectively. These results are shown in Figure 4.7 and again, there was no statistical difference between the tenacity values of the yarns (p-value=0.38). The XRD analysis for the Ag and Ag/AgCl yarns is shown in Figure 4.8 and confirms the elemental composition of the surface of the two yarns based on the peaks identified as Ag and AgCl, which follow the same diffraction pattern as what has been previously shown [148], [149]. The early signal peaks that are not identified in the XRD analysis of both yarns is potentially due to the nylon 6,6 core of the yarn sample, as the core was exposed when the yarn was cut and prepared. The cross-sectional SEM images presented in Figure 4.9 show the thickness of the coatings on the yarn, which were estimated to be approximately 150 nm with each of the 17 filaments having a diameter of 32.05 µm. The total cross-sectional area of each yarn is approximately 0.0003 cm^2. The Ag/AgCl coating on the nylon yarn has some thicker regions around the circumference of each filament when compared to the original Ag yarn coating.

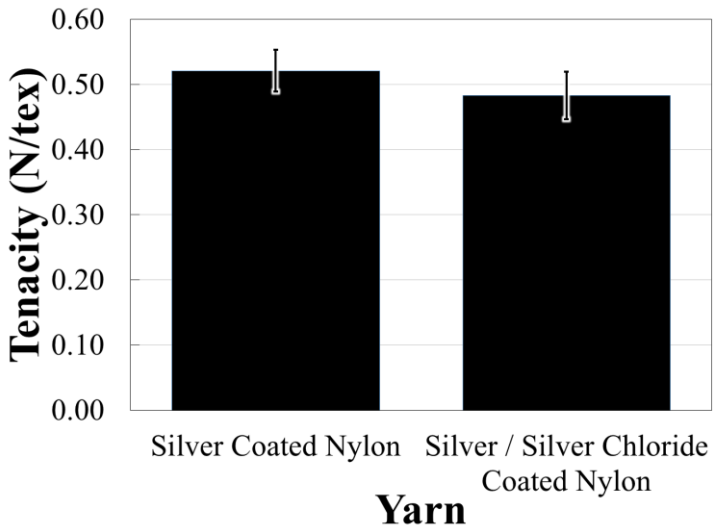

Figure 4.7 Average tenacity values from the maximum load at break tests for the silver and optimal silver/silver chloride coated nylon yarn. No significant differences between the yarns for maximum load at breaking with a two tailed t-test (p-value=0.38). Standard deviations are shown. For each value n=3.

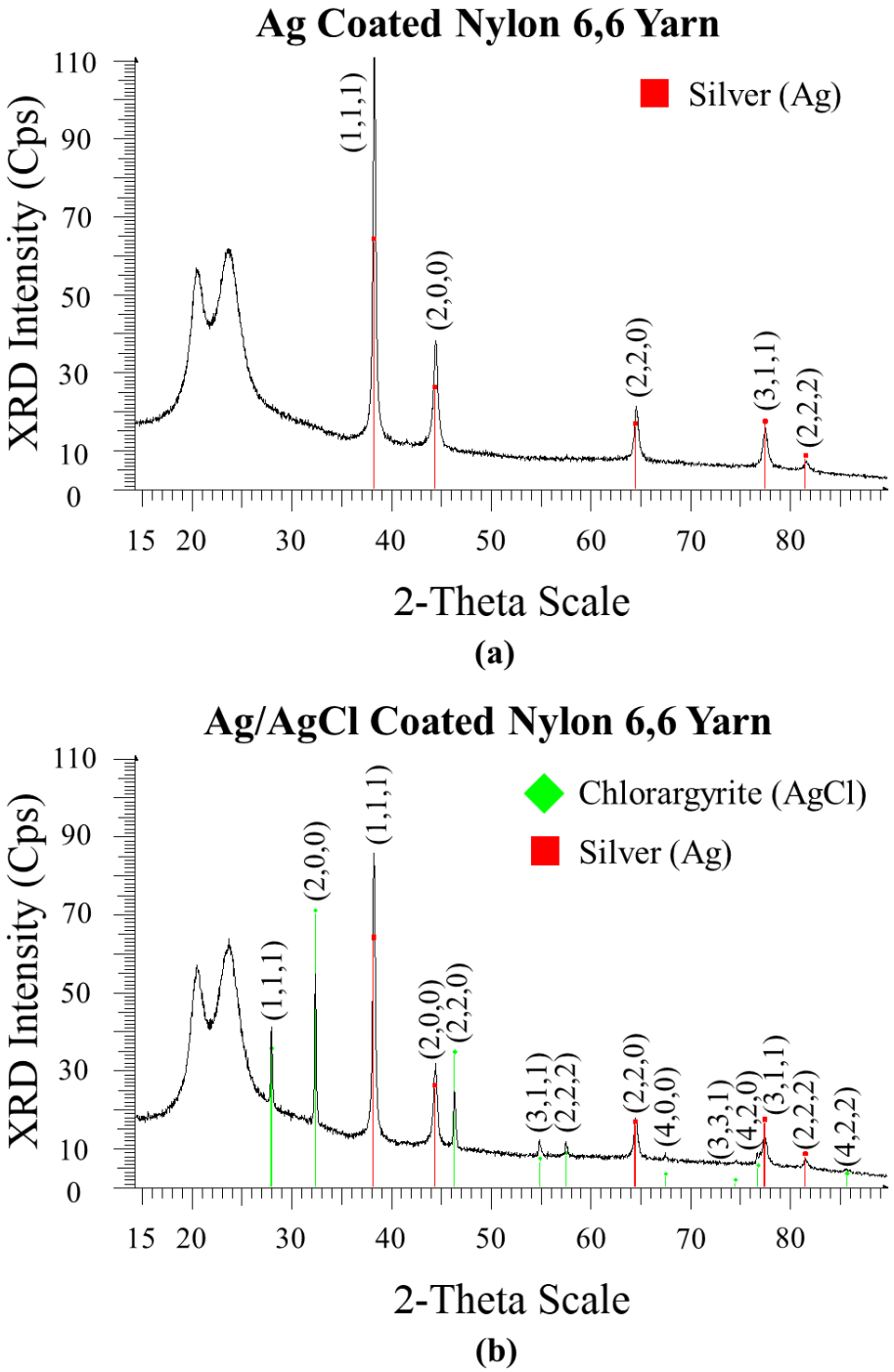

Figure 4.8 The XRD pattern of the surface of the (a) silver coated nylon yarn and (b) optimal silver/silver chloride coated nylon yarn with peaks corresponding to silver and silver/silver chloride.

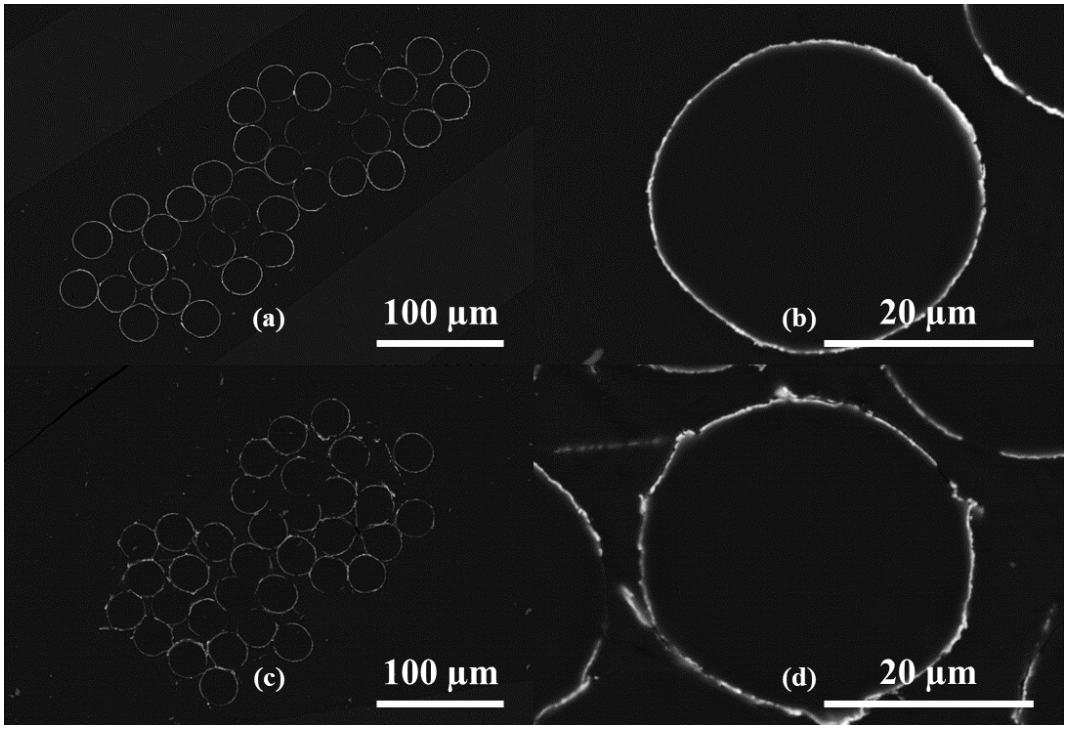

Figure 4.9 (a) Cross-sectional SEM micrographs of silver coated nylon yarn at 300 X and (b) 2.5 kX magnification. (c) Cross-sectional SEM micrographs of silver/silver chloride coated nylon yarn at 300 X and (d) 2.5 kX magnification.

SEM micrographs in Figure 4.10 of the Ag coated and Ag/AgCl yarns showed the surfaces of the e-textiles. Morphological differences on the top surface of the yarns were observed. To confirm the composition of the surface of the yarns, SEM micrographs were analyzed with the use of EDS map analysis and the results are presented in Figure 4.11 and Figure 4.12. The SEM micrographs showed quite uniform distribution of the AgCl layer on the Ag/AgCl yarn, which is important for the e-textile to function as a non-polarizable electrode. The EDS results show the distribution of Ag and Cl, as well as a relatively high Cl peak in the graphical representation for the Ag/AgCl e-textiles and no apparent Cl peak for the original Ag coated e-textiles.

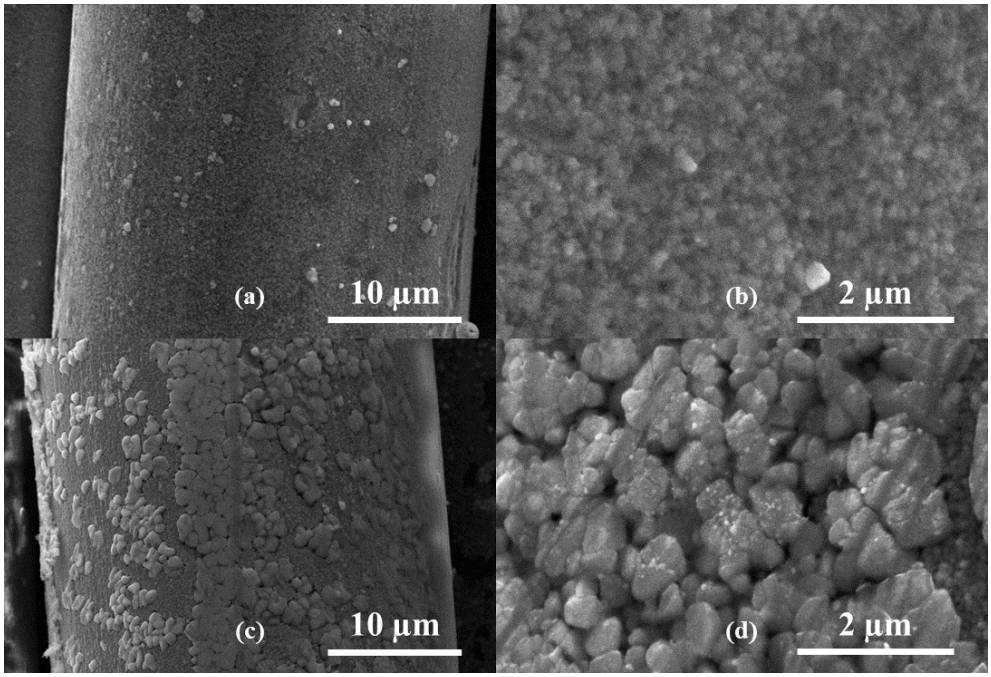

Figure 4.10 (a) Top surface SEM micrographs of silver coated nylon yarn at 3.5 kX and (b) 20 kX magnification. (c) Top surface SEM micrographs of silver/silver chloride coated nylon yarn at 3.5 kX and (d) 20 kX magnification.

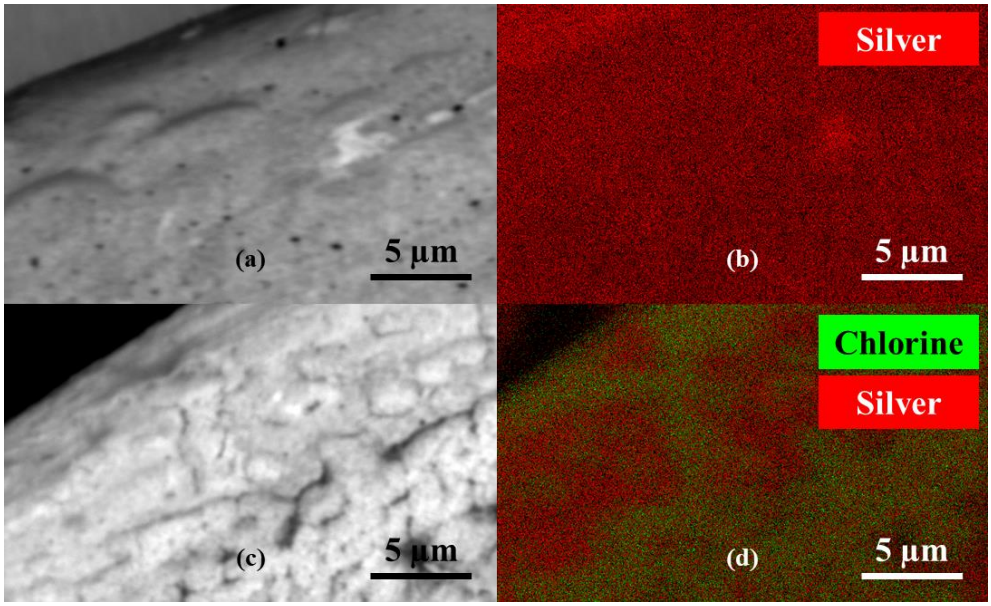

Figure 4.11 (a) SEM micrograph and (b) EDS map analysis at 5 kX magnification of the top surface of silver coated nylon yarns. (c) SEM micrograph and (d) EDS map analysis at 5 kX magnification of the top surface of silver/silver chloride coated nylon yarns.

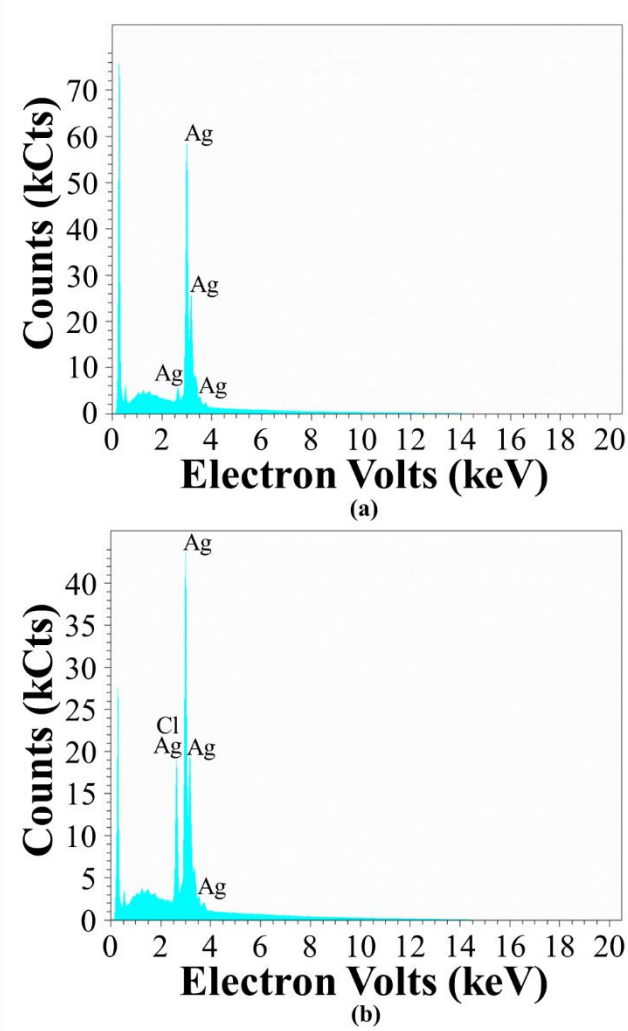

Figure 4.12 EDS map analysis graphical results for the (a) silver coated nylon yarn and (b) silver/silver chloride coated nylon yarn.

The threads in a 1 x 1 cm area in the warp and weft directions of the woven textile substrates of cotton, nylon and polyester were approximated at 40 x 50, 60 x 40 and 40 x 30, respectively (warp thread count per cm x weft thread count per cm). Optical images obtained of the substrates are shown in Figure 4.13. The thickness of the cotton, nylon and polyester substrates are 0.108, 0.097 and 0.065 mm, respectively, and represent important values when calculating the permeability of the textiles. In addition, the chamber temperature of all tests was 22.74±0.10 °C, the average relative humidity was 27.93±0.83% and the air flow was

maintained at an average of 0.97±0.00 feet per second (FPS). The permeability of each of the textile substrates is shown in Figure 4.14. Results indicate that cotton is statistically significantly more permeable than nylon and polyester (p-value<0.05), and nylon is significantly more permeable than polyester (p-value<0.05). Cotton, nylon and polyester have a permeability of 7.02 x 10^{-10}±2.69 x 10^{-11} g/Pa·s·m, 5.50 x 10^{-10}±1.85 x 10^{-11} g/Pa·s·m and 4.05 x 10^{-10}±1.18 x 10^{-11} g/Pa·s·m, respectively. It is also important to note that standard Ag/AgCl electrodes are solid materials and will therefore have a permeability many orders of magnitude less than textiles.

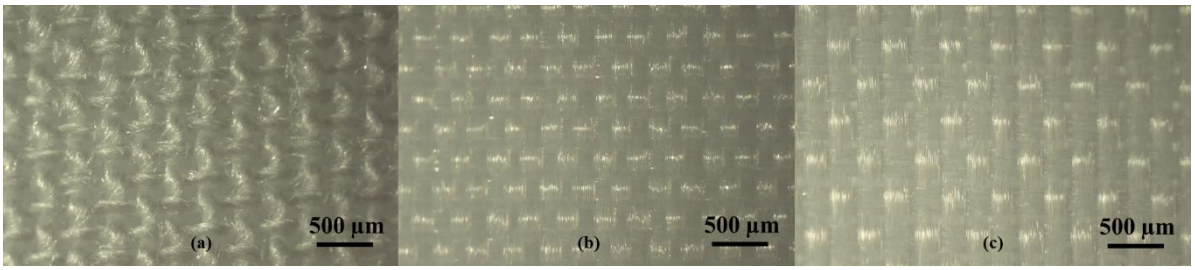

Figure 4.13 Optical images of textile substrates of (a) cotton, (b) nylon and (c) polyester used to estimate the warp and weft thread counts in a 1 cm by 1 cm area.

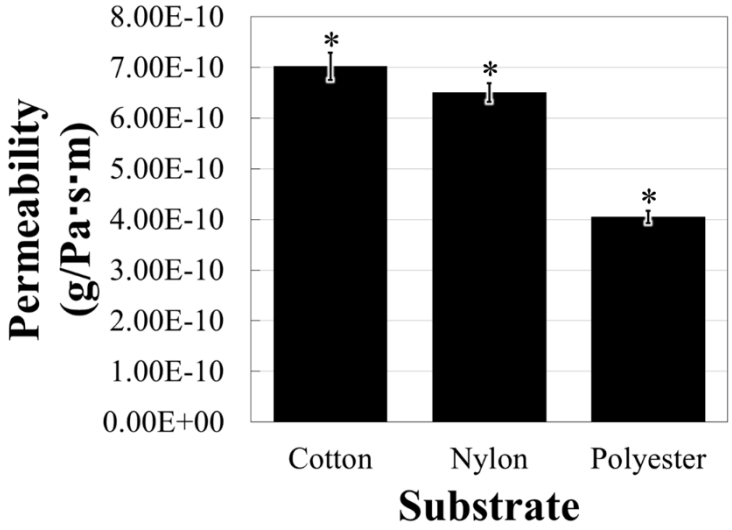

Figure 4.14 Permeability values for woven textile substrates of cotton, nylon and polyester. Standard deviations are shown and one-tailed t-test results with p-values<0.05 are indicated (*). For each value n=3.

The wettability results of solid Ag/AgCl and cotton, nylon and polyester textiles are presented in Figure 4.15. Ag/AgCl and cotton were found to have water droplet contact angles of 60±3° and 0°, respectively, demonstrating hydrophilic properties. Nylon and polyester have water droplet contact angles of 124±1° and 117±2°, respectively, confirming their hydrophobic characteristics. All smaller average values of the water droplet contact angle for materials are statistically significantly less than larger average values of the water droplet contact angles (p-values<0.05).

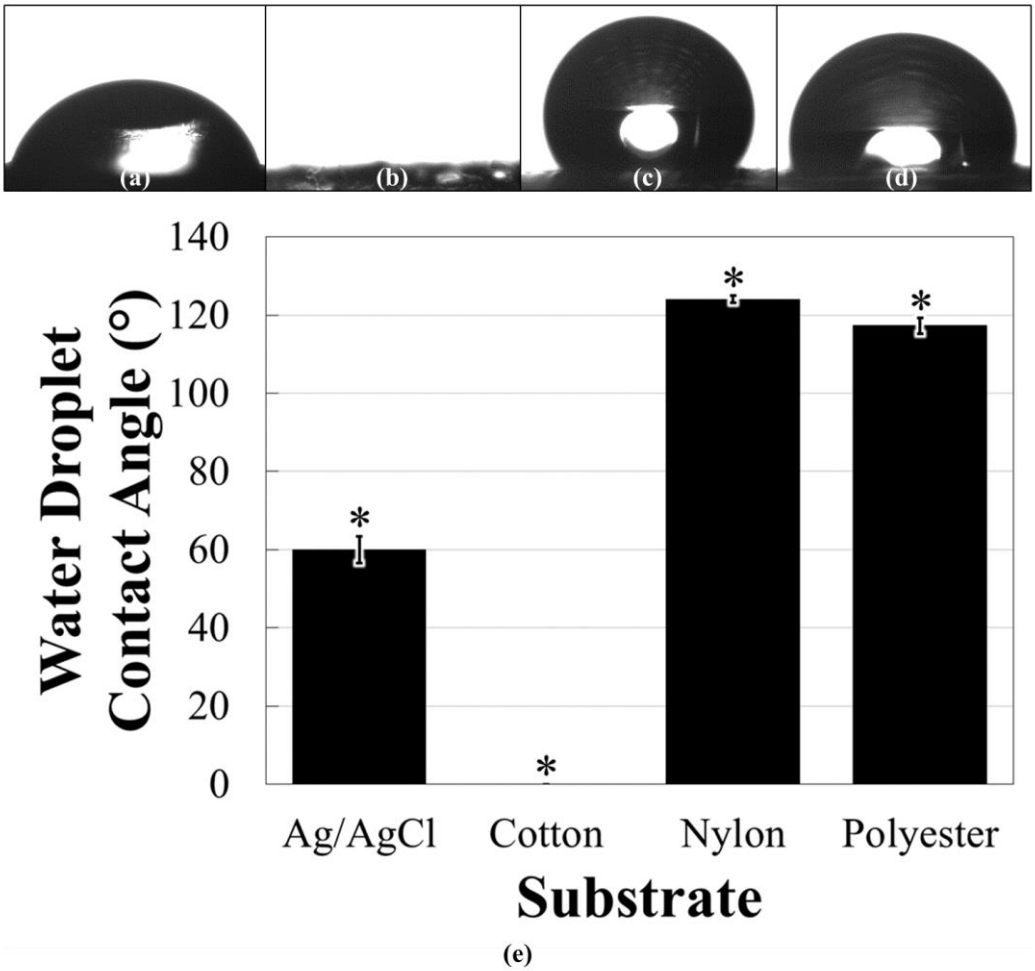

Figure 4.15 Optical images of water droplet on surfaces of (a) solid silver/silver chloride as well as (b) cotton, (c) nylon and (d) polyester textiles with (e) a graphical representation of the contact angle values of each material. Standard deviations are shown and one-tailed t-test results with p-values<0.05 are indicated (*). For each value n=3.

The average curves for the bending momentum per unit width versus the curvature, during a load and unload cycle, in the warp and weft directions for the cotton, nylon and polyester textile substrates are shown in Figure 4.16. The average bending rigidity results in the combined warp and weft directions of cotton, nylon and polyester fabrics, shown in Figure 4.17, were 0.03 x 10^{-4}±0.00 x 10^{-4} Nm/m, 0.08 x 10^{-4}±0.00 x 10^{-4} Nm/m and 0.10 x 10^{-4}±0.00 x 10^{-4} Nm/m, respectively. The smaller average bending rigidity values were statistically significantly less than the larger values (p-values<0.05). The average bending hysteresis results in the combined warp and weft directions for cotton, nylon and polyester, shown in Figure 4.17, were 0.03 x 10^{-2}±0.00 x 10^{-2} N/m, 0.05 x 10^{-2}±0.00 x 10^{-2} N/m and 0.01 x 10^{-2}±0.00 x 10^{-2} N/m, respectively. The smaller average bending hysteresis values were statistically significantly less than the larger values (p-values<0.05). Lower values for bending rigidity and bending hysteresis indicate that the material being tested is less rigid and has good recoverability, respectively [140]. Therefore, cotton was observed to be the least rigid, while polyester had the best recoverability. Notably, since the solid standard Ag/AgCl electrodes are rigid, they lack the ability to conform to the skin, reducing their potential to be worn comfortably [96].

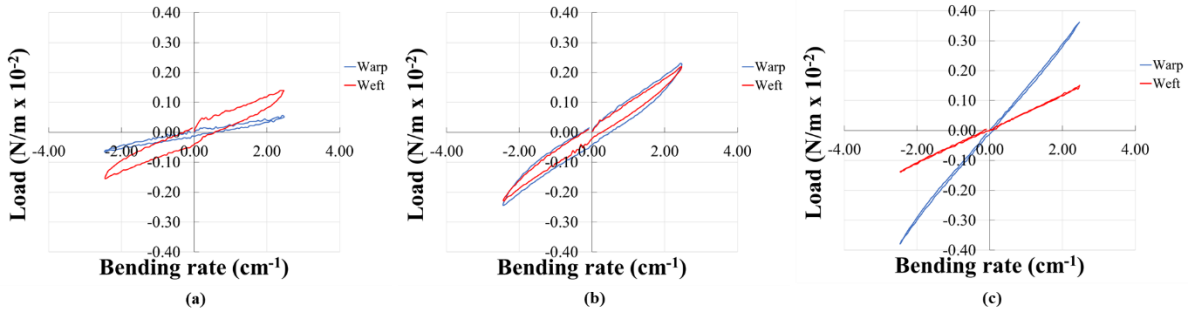

Figure 4.16 The average bending moment versus curvature curve in the warp and weft directions for the woven textile substrates of (a) cotton, (b) nylon and (c) polyester. Samples tested had a width of 5.00 cm (n=3).

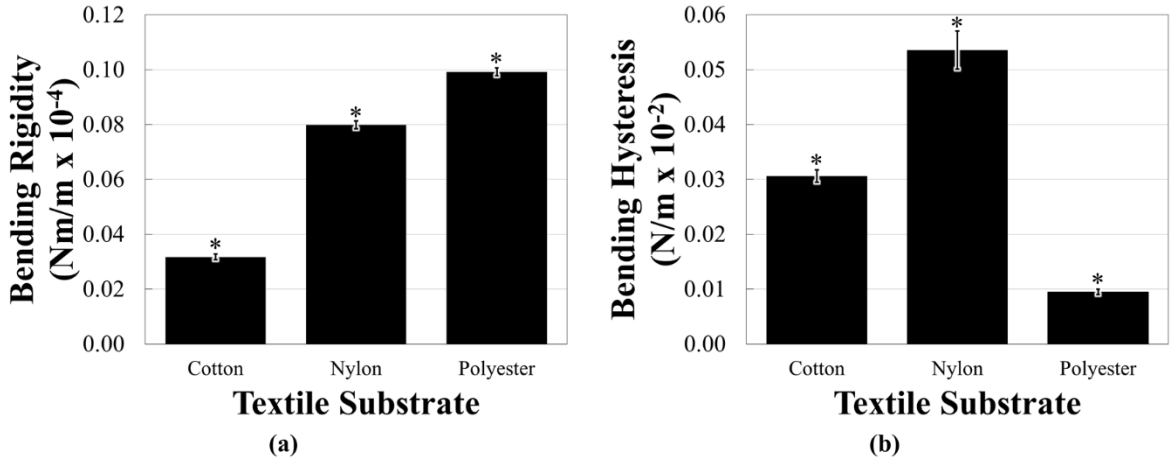

Figure 4.17 The average (a) bending rigidity and (b) bending hysteresis in the combined warp and weft directions for cotton, nylon and polyester fabrics. Standard deviations are shown and one-tailed t-test results with p-values<0.05 are indicated (*). For each value n=3.

4.2.2 Evaluation of Integration of E-textile Electrodes with Textile Substrates

The integration of Ag/AgCl e-textiles with the textile substrates of cotton, nylon and polyester proved to be a challenge and showed a success rate of approximately 50%. In particular, the interface between the solid electrical connection and the conductive yarn was one of the more difficult aspects to accomplish successfully. In addition, since the e-textile EDA electrode straps were developed by hand, the tension of the stitched yarn was difficult to maintain, resulting in a decent amount of variation in the resistance between the electrical connector and the furthermost end of an e-textile electrode, which was on average 80.96±26.53 Ω. The surface area covered under the e-textile electrodes, when added to the area in between e-textile electrodes, was approximately 1.04 cm^2 for each of the e-textile EDA monitoring straps. In comparison, the surface area covered under the standard electrodes, when added to the area in between the standard electrodes, was estimated to be 3.96 cm^2. Images of e-textile EDA electrode strap prototypes using cotton, nylon and polyester textile substrates are shown in Figure 4.18.

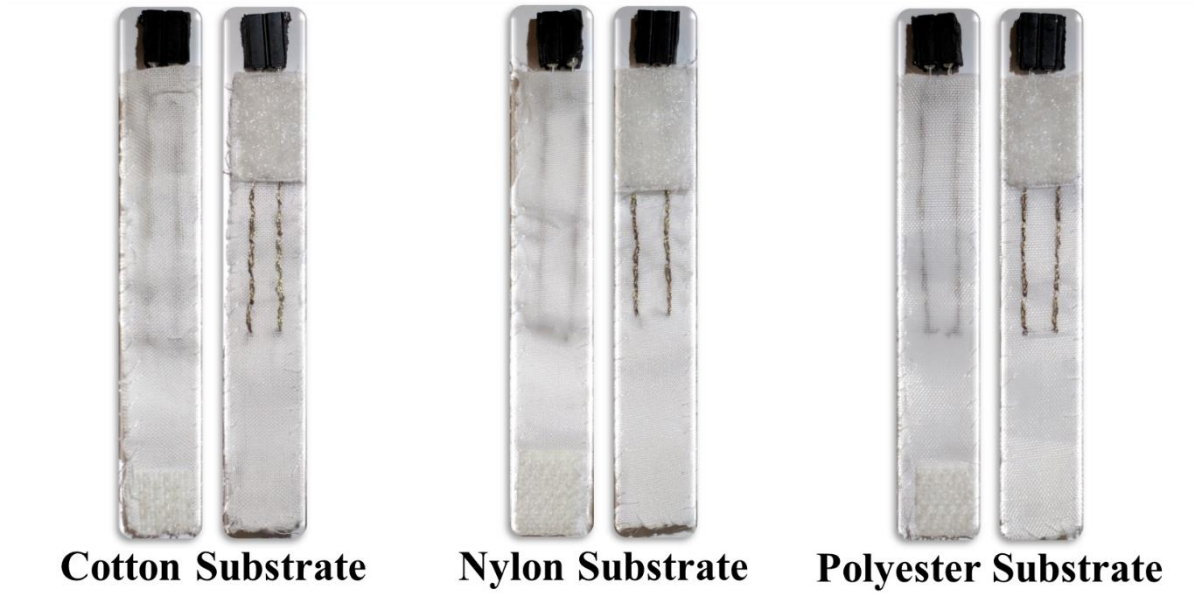

Figure 4.18 Images of e-textile EDA electrode strap prototypes using cotton, nylon and polyester textile substrates.

4.2.3 Analysis of EDA Stimulus Response Data for E-textile Electrodes

The results for the average compressive force tests with standard deviations between trials demonstrated that the e-textile EDA electrode straps at the distal phalanx of the index, middle and little finger exhibited 0.07±0.01 N, 0.07±0.00 N and 0.06±0.01 N, respectively. The average force at the distal phalanx of the ring finger with cloth tape for the temperature sensor was 0.07±0.01 N. The straps at the medial phalanx of the middle finger exhibited 0.13±0.02 N of force and at the proximal phalanx of the same finger it was 0.15±0.01 N. Overall, the standard electrode straps were observed to have a statistically significant (p-values<0.05) larger average force on the sensors than the e-textile electrode straps and cloth tape, which is shown in Figure 4.19. The sweat gland density of the different locations on the palmar region of the hand in which EDA electrodes were applied is shown in Figure 4.20 and represent important values when considering the effects that sweat gland coverage has on the

accuracy and precision of EDA stimulus response detection outlined in chapter 3 [136]. The e-textile EDA electrode straps cover 336±11, 366±3 and 442±9 sweat glands for the distal phalanx of the index, middle and little finger, respectively. The standard electrodes cover approximately 966±78 sweat glands for the medial and proximal phalanges of the middle finger.

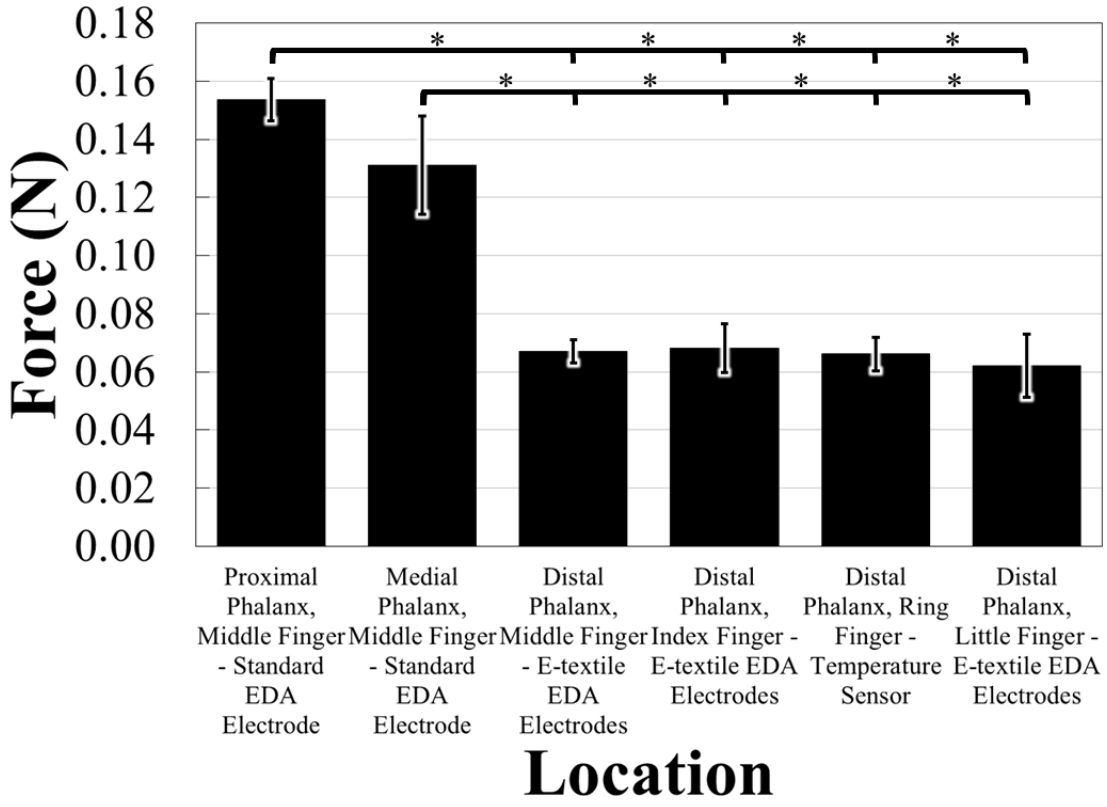

Figure 4.19 The compressive force test results for the different attachment methods and locations of sensors. Standard deviations are shown and one-tailed t-test results with p-values<0.05 are indicated (*). For each value n=3.

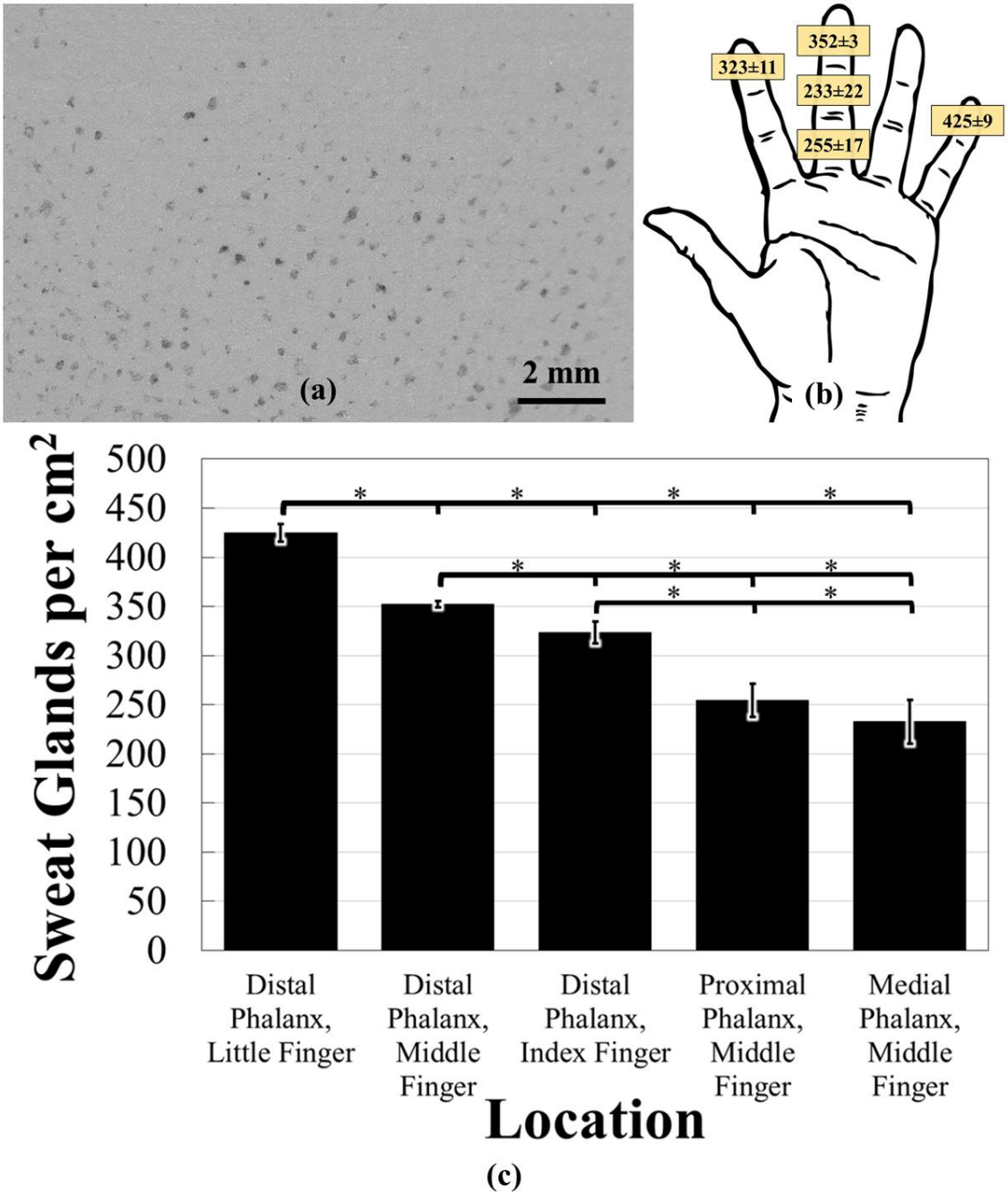

Figure 4.20 (a) Example of image used to count sweat glands per cm^2. (b) Values of sweat glands per cm^2 counted on specific locations of the hand. (c) Sweat gland density results for the locations of EDA electrodes. Standard deviations are shown and one-tailed t-test results with p-values<0.05 are indicated (*). For each value n=3.

The 15-minute EDA stimulus response detection tests were done at room temperature (approximately 25 °C) and the average skin surface temperature recorded with a standard deviation between the EDA monitoring trials was 22.76±0.70 °C. An example of an EDA stimulus response detected with e-textile electrodes on a cotton substrate at different locations on the palm of the hand is presented in Figure 4.21. The EDA stimulus responses detected by e-textile electrodes were compared to those recorded by standard solid electrodes in order to observe differences between the materials used, as well as the locations of the e-textile electrodes on the palm of the hand. The Pearson correlation coefficients for the comparison of EDA stimulus response signals are shown in Figure 4.22. In addition, two sets of standard electrodes were tested to confirm the reliability of the testing method previously described in chapter 3, which resulted in a Pearson correlation of 0.998 [136].

The cotton textile substrate on the distal phalanx of the middle finger was found to have the highest average Pearson correlation coefficient (0.913±0.041), when evaluating all of the e-textile EDA electrode straps and locations. The average correlation coefficient when utilizing the e-textile EDA electrodes integrated into the cotton textile substrate on the distal phalanx of the index finger (0.909±0.044) was statistically significantly greater than the correlation coefficient of the e-textile EDA electrodes integrated into the polyester textile substrate at the same location (0.807±0.089), with a p-value of 0.03. Also, the correlation coefficient from e-textile EDA electrodes integrated into the cotton textile substrate on the distal phalanx on the index finger (0.909±0.044) was statistically significantly greater than the correlation coefficient of the e-textile EDA electrodes integrated into the nylon textile substrate at the same location (0.828±0.087) with a p-value of 0.08. The e-textile EDA electrodes incorporated with the cotton textile substrate on the distal phalanx of the middle finger had a

Pearson correlation coefficient (0.913±0.041) statistically significantly greater than both the e-textile EDA electrodes stitched into the nylon (0.817±0.115) and polyester (0.799±0.097) textile substrates on the same finger, with p-values of 0.08 and 0.06, respectively. With this analysis, there were no statistically significant differences observed with the different textile substrate materials on the little finger or between different finger locations of e-textile EDA electrodes. The most notable result is that the cotton textile substrate with integrated Ag/AgCl e-textile EDA electrodes is the most accurate and precise e-textile strap tested when comparing the EDA stimulus response signal to that of the standard solid Ag/AgCl electrodes. In addition, with the cotton textile substrate, there appears to be a significant improvement in the repeatability between trials with Ag/AgCl e-textile electrodes, as the standard deviations on each finger are less than when nylon and polyester textile substrates are used.

To further analyze whether location of the e-textile EDA electrodes has an effect on the EDA stimulus response, the average minimum to maximum EDA signal change was evaluated when the electrodes were on the distal phalanx of the index, middle and little fingers, regardless of which textile substrate was used. The percent change was then corrected by the sweat gland density of the location of the e-textile EDA electrodes in order to observe if there was a potential for other factors to influence a difference in EDA stimulus response waveforms. As shown in Figure 4.23, the average EDA signal percent change per sweat gland on the distal phalanx of the little finger (0.055±0.022% per sweat gland) was statistically significantly greater than on the distal phalanx middle finger (0.048±0.015% per sweat gland), with a p-value of 0.03. In addition, the average EDA signal percent change per sweat gland on the distal phalanx of the little finger (0.055±0.022% per sweat gland) was also statistically significantly greater than that on the distal phalanx index finger (0.049±0.015% per sweat

gland), with a p-value of 0.06. These results indicate that there may be underlying factors that affect the EDA waveform other than the sweat gland density of the specific location being monitored. Longer-term experiments were then conducted on the e-textile EDA electrodes integrated into the cotton textile substrate, as these straps were shown to detect the most accurate and precise EDA stimulus response. The location for further EDA testing of the e-textile EDA electrodes was chosen to be the distal phalanx of the middle finger, as the standard EDA electrodes were also located on the middle finger. Choosing this experimental set-up eliminated the potential effects that the location of electrodes could have on the EDA signal.

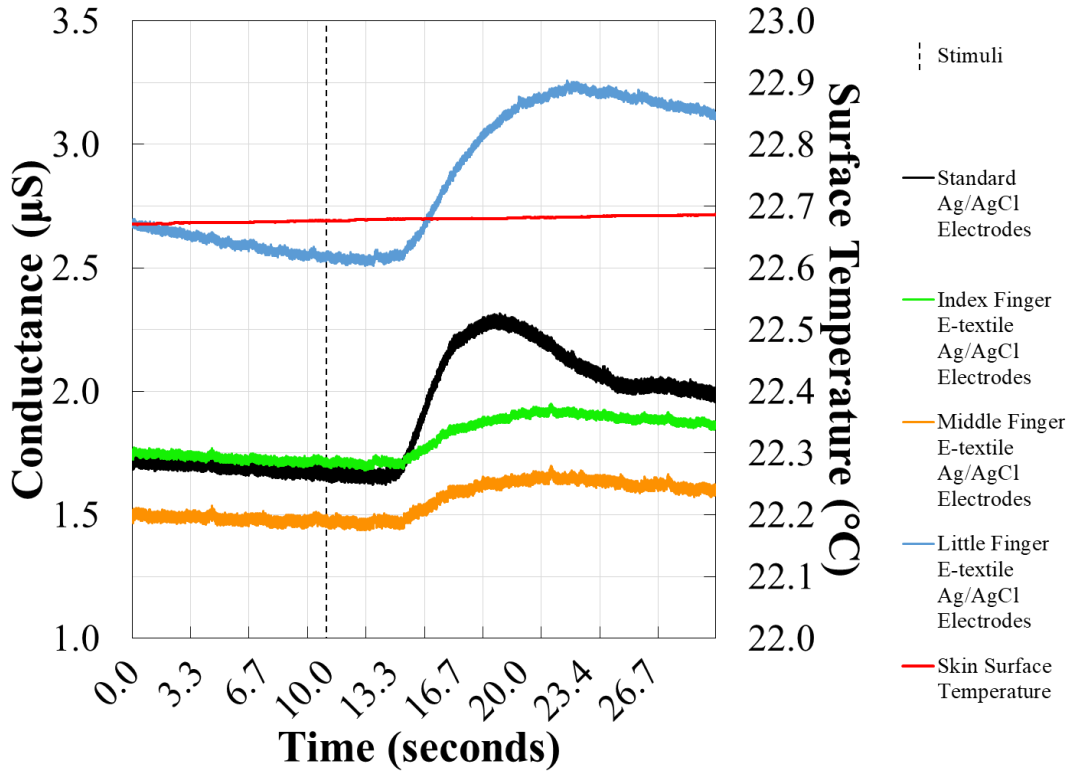

Figure 4.21 Example EDA stimulus response shown by conductance (primary y-axis) for dry e-textile electrodes (0.12 cm^2 surface area, 0.40 cm distance) at the distal phalanx of the index, middle and little fingers compared to dry commercial electrodes (1.00 cm^2 surface area, 1.50 cm distance) on the proximal and medial phalanges of the middle finger. Skin surface temperature is also shown (secondary y-axis) with time in seconds (x-axis).

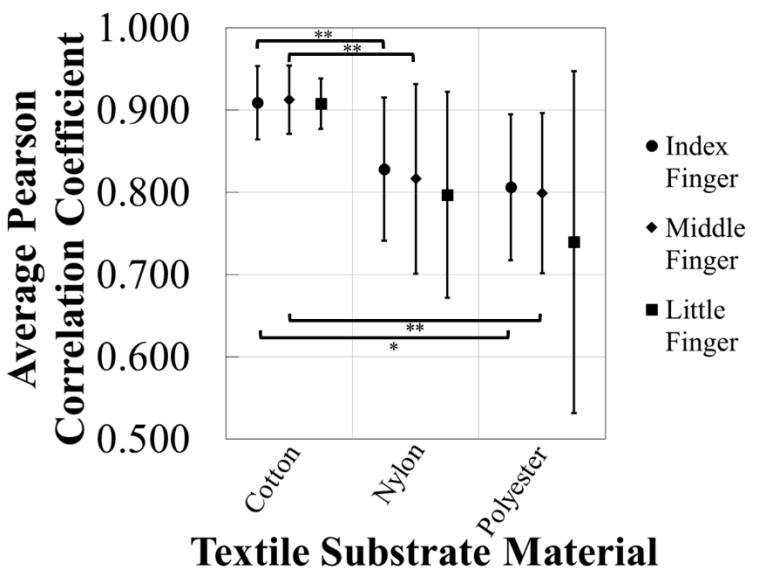

Figure 4.22 The average Pearson correlation coefficients for the comparison of the EDA stimulus response signals of the commercial rigid electrodes (1.50 cm distance, 1.00 cm^2 surface area) to the signals of the e-textile electrodes of 0.12 cm^2 surface area with distances of 0.40 cm integrated into cotton, nylon and polyester textile substrates on the distal phalanx of the index, middle and little finger on the palm of the hand. Standard deviations are shown and one-tailed t-test results with p-values<0.05 (*) and p-value<0.10 (**) are indicated. For each value n=3.

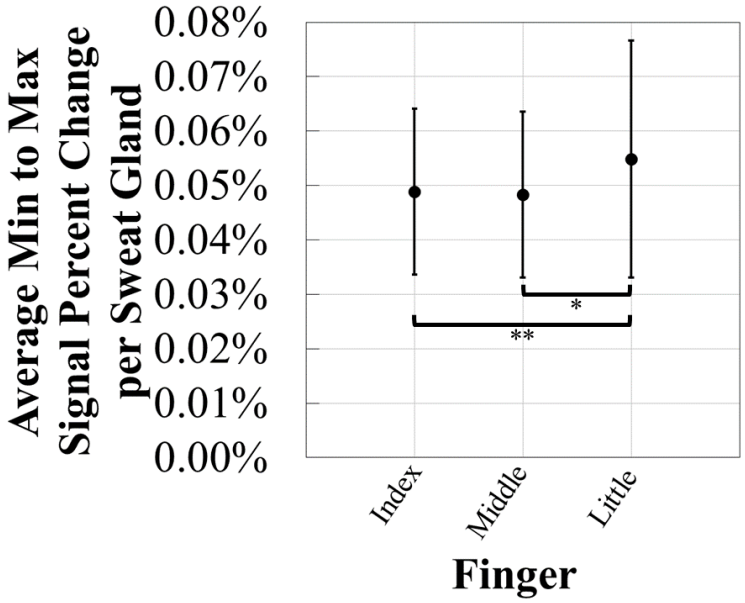

Figure 4.23 The average minimum to maximum EDA signal percent change per sweat gland for comparison of EDA waveforms monitored on the distal phalanx of the index, middle and little finger on the palm of the hand. Standard deviations are shown and one-tailed t-test results with p-values<0.05 (*) and p-value<0.10 (**) are indicated. For each value n=9.

4.2.4 Analysis of 4-hour EDA Data for E-textile Electrodes

The EDA data recorded over 4 hours with dry Ag/AgCl e-textile EDA electrodes integrated into a cotton textile substrate was compared to the EDA signal collected by dry standard solid Ag/AgCl electrodes. In addition, the EDA signals of both sets of electrodes were compared against the changing skin surface temperature. Figure 4.24 shows the EDA and temperature signals collected during the 4-hour test. Importantly, the change in all signals was evaluated across the 4-hour test to determine if there were observable trends with the data collected. The room, which had an open window, had a temperature and relative humidity at the beginning of the test to the end of approximately 23 °C and 26% to 30 °C and 17%, respectively. The signal percent difference of the skin surface temperature, standard electrode baseline EDA signal and e-textile baseline EDA signal from the beginning of the test and at each hour time point ± 10 minutes is presented in Figure 4.25. The trends observed indicate that the baseline EDA signal of the standard non-breathable and non-flexible electrodes is affected by the change in temperature more than the baseline EDA signal of the e-textile electrodes. Specifically, at the 4-hour time point, it is observed that the skin surface temperature has increased by 60%, the baseline EDA of the standard electrodes has increased by 61%, while the baseline EDA e-textile electrodes increased by 28%. Similar results are also observed at the other time points.

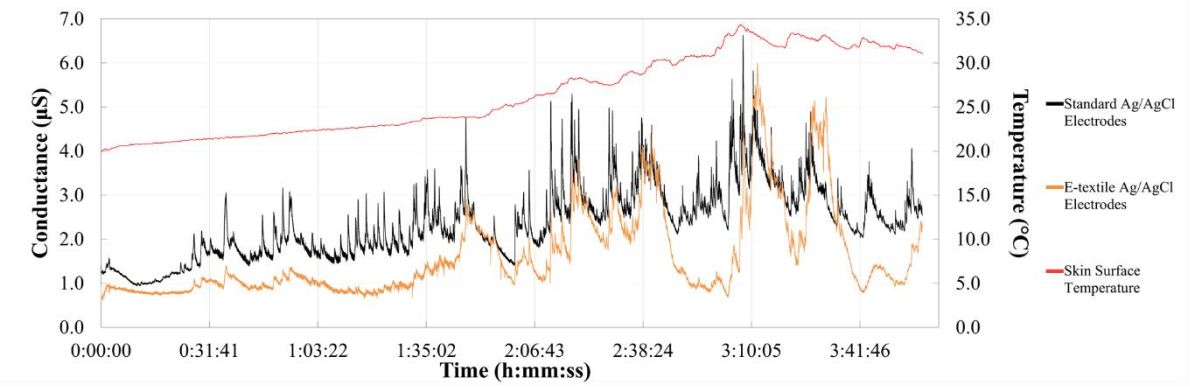

Figure 4.24 4-hour EDA data shown by conductance (primary y-axis) for dry e-textile electrodes (0.12 cm^2 surface area, 0.40 cm distance) on the distal phalanx of the middle finger compared to dry commercial electrodes (1.00 cm^2 surface area, 1.50 cm distance) on the proximal and medial phalanges of the middle finger. Skin surface temperature is also shown (secondary y-axis) with time in seconds (x-axis).

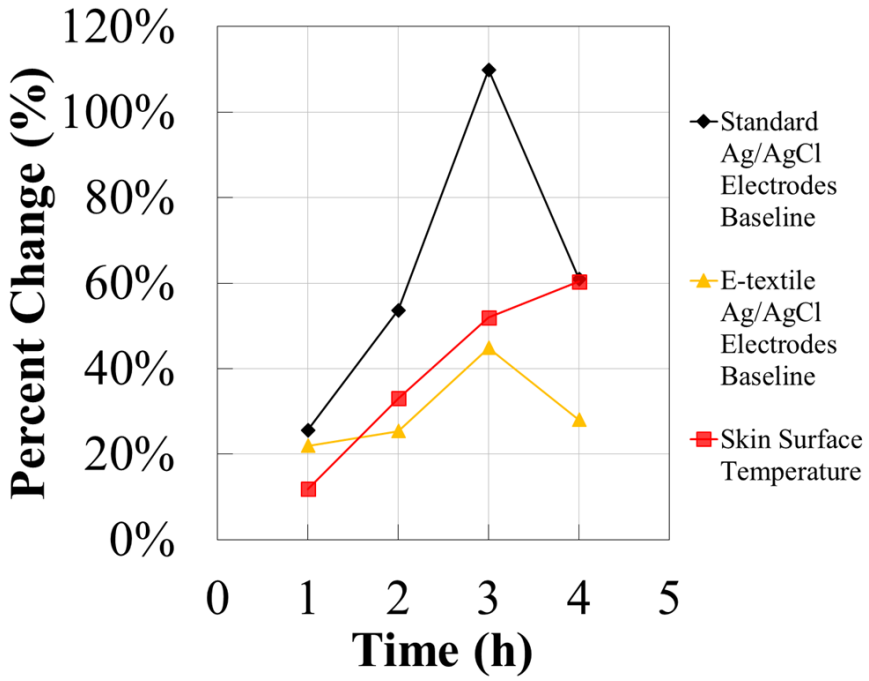

Figure 4.25 The signal percent difference of the skin surface temperature, standard electrode baseline EDA signal and e-textile baseline EDA signal from the beginning of the test and at each hour time point ± 10 minutes.

The Pearson correlation coefficients of the complete 4-hour test were calculated to compare the EDA signals collected by the standard and e-textile electrodes, the EDA signal of the standard electrodes versus the skin surface temperature, as well as the EDA data recorded by the e-textile electrodes versus skin surface temperature. The correlation coefficients are shown in Figure 4.26. The EDA signals collected by the standard and e-textile electrodes showed a relatively high correlation coefficient of 0.746, considering the length of the test. The EDA data recorded by the standard electrodes also showed a relatively high correlation coefficient of 0.746 when compared to the skin surface temperature signal. A lower correlation coefficient of 0.569 was obtained when comparing the EDA signal measured by the e-textile electrodes and the skin surface temperature data. These results demonstrate a trend that the EDA signal recorded by standard electrodes are more correlated to the skin surface temperature signal than that of e-textile electrodes.

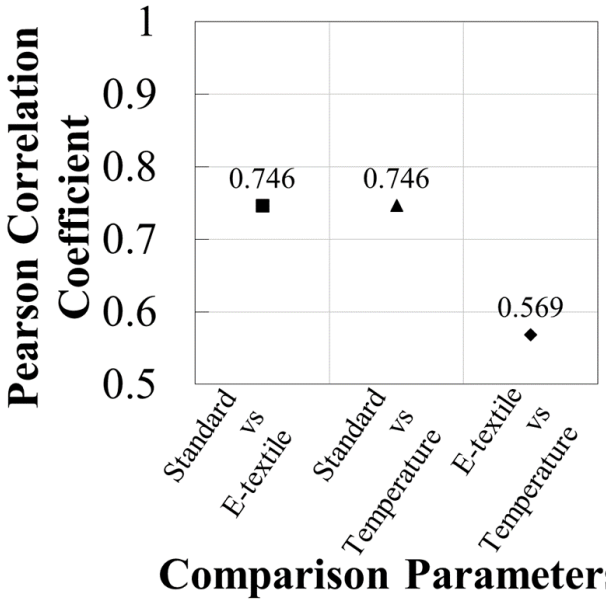

Figure 4.26 The Pearson correlation coefficients for the comparison of the EDA signals of the commercial rigid electrodes (1.50 cm distance, 1.00 cm^2 surface area), the EDA signals of the e-textile electrodes of 0.12 cm^2 surface area with distances of 0.40 cm integrated into cotton on the distal phalanx of the middle finger on the palm of the hand and the skin surface temperature data. For each value n=1.

4.3 Discussion

The development of functional Ag/AgCl e-textile EDA electrodes was detailed and the effect of textile substrate materials on monitoring EDA when compared to using non-breathable and non-flexible standard electrodes was discussed. After establishing a practical design for e-textile EDA electrode straps, it was observed that the optimal tested woven textile substrate material to accurately and precisely detect an EDA stimulus response, comparable to signals recorded by standard solid EDA electrodes, is cotton. It was also shown that the EDA waveforms recorded on the distal phalanx of the little finger are different when compared to those recorded on the distal phalanx of the index and middle finger when correcting for sweat gland density at each location. This provides additional discussion points to further the conversation regarding EDA asymmetry in the literature [102], as well as the effect of nerve innervations on EDA [157], [158]. In addition, for a 4-hour EDA monitoring experiment, a trend indicated that the EDA signal of standard electrodes seem to be more affected by changes in skin surface temperature than the EDA data collected by e-textile electrodes. Each of these conclusions can impact the development approach of future e-textile systems for monitoring EDA. This work identifies important e-textile design criteria for accurate and precise EDA recording, which has the potential to lead to the creation of fully wearable and comfortable long-term e-textile EDA monitoring devices.

Ag/AgCl coated yarns have been minimally tested in previous literature [114], [115] when comparing standard solid Ag/AgCl electrodes for the detection of physiological signals on the surface of the skin. The conductive materials for e-textiles that have been used to detect EDA signals include steel [23], [28], [31], [85], [88] and silver [24], [26], [27], [33], [34], but no study exists in the EDA monitoring research that compares Ag/AgCl coated e-textiles with

the standard Ag/AgCl electrodes used clinically. There are challenges associated with the fabrication of Ag/AgCl e-textiles in regards to maintaining conductivity, which is why it is believed that the most recent e-textile fabrication methods focus on highly conductive silver coatings through dip-coating [110]–[112] and electroless plating [166], [167]. Also, these fabrication methods generally do not require specialized or expensive equipment [155]. Furthermore, it is important to note that when monitoring biological signals on the surface of the skin, non-polarizable Ag/AgCl electrodes are the current clinical standard due to having low electrode-skin impedance, low noise and low motion artifact when compared to polarizable electrodes such as those made of stainless steel [168]. However, Ag/AgCl electrode materials are known to degrade over time, especially when in contact with sweat [35], [36], [168]. One of the main justifications for utilizing Ag/AgCl e-textile electrodes in this work is specifically because a comparable material to the standard solid Ag/AgCl electrodes was required in order to more reasonably conclude that the results observed were not due to the use of different conductive materials, but rather to the different properties of e-textiles, textiles and solid materials. Hence, developing a controllable roll-to-roll electrochemical system to produce Ag/AgCl yarn not only detailed novel parameters for effective fabrication, but also provided a means to create practical prototypes of e-textile EDA monitoring straps for further experimentation.

Effective EDA stimulus response detection was obtained with e-textile electrodes and as previously described, the cotton textile substrate was identified as the best material to use for the e-textile integrated EDA electrodes when compared to nylon and polyester textile substrates. Particular differences between the cotton, nylon and polyester textiles, which could be attributed to the differences observed when monitoring EDA stimulus responses, included

wettability and breathability. Also, cotton was shown to be the least rigid of the fabrics, potentially allowing this textile substrate to better conform to the surface of the skin. In order to determine an appropriate target flexibility of the e-textile electrodes, it will be important to consider the desired application and the curvature of the location in which the electrodes are placed. A major difference between the textile substrates is that cotton is hydrophilic and absorbs water, while nylon and polyester are specifically hydrophobic. Importantly, solid Ag/AgCl material was shown to be hydrophilic, but without fully absorbing water. The skin-electrode interface is a critical component in accurately detecting an EDA stimulus response [35], [36]. In particular, if there is a disturbance of the electrolytes near the solid-liquid electrode interface, artifacts in the signal can occur [35], [36]. The cotton textile substrate is able to maintain a relatively more stable solid-liquid interface, due to being hydrophilic and absorbing sweat, when compared to nylon and polyester. This property of the Ag/AgCl e-textiles with the cotton textile substrate is believed to enable accurate and precise detection of the EDA stimulus response, comparable to the EDA signal recorded by solid Ag/AgCl electrodes, which are also hydrophilic.

The slight but statistically significant difference in the EDA waveform monitored on the distal phalanx of the little finger, when compared to the distal phalanges of the middle and index fingers, was observed irrespective of the different sweat gland density at each location. Previous literature showed the amplitude of EDA stimulus responses measured between the distal phalanx of the thumb and the medial phalanx of the little finger to be approximately 1.53 times larger than the EDA responses measured between the distal phalanx of the index and middle fingers [169]. Ranogajec and Geršak in 2014 compared different locations on the hand for EDA monitoring and utilized solid Ag/AgCl electrodes with isotonic gels to highlight the

differences in amplitude of skin conductance at these different locations [169]. Importantly, the work presented in this chapter identifies a previously unknown difference between EDA stimulus response waveforms recorded exclusively on the little finger when compared to the middle and index fingers. Other studies related to observing skin conductance values at different locations on the body were concerned with identifying areas on the surface of the skin that had high correlation to the most common placement of electrodes on the distal or medial phalanx of the index and middle fingers [151], [170]. Previous work showed that solid electrodes on the inner side of the foot over the abductor hallucis muscle detect the most correlated EDA signal when compared to the EDA signal obtained from the common location of the middle and index fingers [151], [170]. Our study shows a high correlation of the EDA stimulus response signal collected by our dry Ag/AgCl e-textile electrodes to the clinical grade dry and solid Ag/AgCl electrodes, which encourages research in this field to look towards utilizing e-textiles to increase comfort and wearability of EDA monitoring systems. In addition, the results detailed in this work could be helpful in identifying underlying nerve innervation injuries, as electrical properties of the skin are known to be affected [76], [171]. Specifically, nerve injuries related to the ulnar and median nerve, as well as spinal cord injuries, can be further understood through monitoring EDA, as these types of injuries are known to be related to EDA signals [157], [158]. Also, the concept of asymmetry of the EDA response across the body [102] has potentially an added complexity to it, in regards to the contribution that the ulnar and median nerve have on the EDA stimulus response. Further testing on multiple subjects to explore the difference of EDA signals on the different fingers of the hand is justified and required in order to make more inferences on the underlying

physiology associated with EDA, as there are known variations between individuals in regards to communication branches in the nerves located in the hand [77].

There has been a significant amount of previous research on the effect of ambient and skin surface temperature when monitoring EDA [172]–[175], however none of these studies tested the use of e-textile EDA electrodes. The 4-hour experiment assessing e-textile electrodes with the cotton textile substrate developed in our work was conducted in order to identify trends with the EDA data over an extended time. In particular, the EDA signals of the Ag/AgCl e-textile electrodes and the standard solid Ag/AgCl electrodes were evaluated against the skin surface temperature. The trend observed was that the EDA baseline signal from the standard solid electrodes was more affected by the increase in skin surface temperature than the baseline signal from the breathable and flexible e-textile electrodes. In addition, the EDA signal of the standard electrodes was more closely correlated to the skin surface temperature data than that of the e-textile electrodes. It is believed that the breathability of the cotton substrate allowed the sweat on the surface of the skin to evaporate more freely than that of non-breathable standard electrodes, reducing the drift in the EDA baseline signal, which is known to occur with increasing moisture on the skin under the EDA electrodes, most commonly caused by additional electrolyte cream [35], [36]. The drift in baseline EDA was also seen in this study when utilizing dry solid electrodes, with the electrolyte solution being the sweat generated by the subject. Also, it is important to note that by not using an electrolyte cream, the recording conditions could become more uncontrollable [35], [36]. However, by using a textile cotton substrate that is permeable to water and sweat, there is a potential to be able to record a more biologically accurate EDA signal, as the surface of the skin would be able to function more naturally than if covered with non-permeable materials, electrolyte gels and skin irritating

adhesives. Previous work on monitoring EDA with e-textiles showed a higher EDA baseline signal after physical exertion that was attributed to the terrycloth textile substrate used, which absorbs sweat more readily [34]. In our experiments, the subject was at rest for the 4 hours and therefore minimal sweat was generated, which is a very different experimental approach than having the subject do physical exercise. In addition, even though the cotton textile substrate used for our research absorbed water, it was also quite permeable to water vapor, which could have reduced the effect on the EDA baseline signal when recording with e-textile electrodes. Future work can explore different states of user activity and the effects on EDA baseline signals when using e-textile electrodes.

Previous research on evaluating skin resistance levels and temperature demonstrated that as skin surface temperatures increase, skin resistance levels decrease when using solid Ag/AgCl electrodes [172], [176], which is consistent with the results observed with the rigid Ag/AgCl electrodes in our work. Environmental temperature was also shown to affect EDA baseline levels in previous studies [173], [174], and therefore should be considered as an important parameter to be recorded in addition to skin surface temperature. Utilizing e-textile and textile materials could help in explain interactions between electrodes, electrolytes and skin, which are beginning to be observed and analyzed in this current study. Furthermore, polarization at the boundaries of the electrode and skin interface due to the applied DC may influence the EDA signal [35], [36], which is why a non-polarizing material of Ag/AgCl for the standard and developed e-textile electrodes was used for this work.

When developing electrodes for biological signal monitoring, it is critical to evaluate alternative e-textile electrode materials to Ag/AgCl and to assess materials that record signals other than EDA on the surface of the skin [155]. An example of an effective alternative

material developed and used for long-term recordings for electrocardiograms, which is an important field of research for utilizing e-textiles, includes an e-textile with a silver/titanium coating [177]. Some of the key aspects identified for monitoring bio-signals long-term include: biocompatibility, no cytotoxicity, good signal quality and low impedance, as well as long-term durability, potential for reutilization, washing ability and no need for initial skin preparation [177]. A moisturized layer of water vapor is still required for the use of the developed silver/titanium coating [177], but this type of exploratory research is important and required in order to identify optimal e-textile materials for physiological signal monitoring. Ag/AgCl materials are known to be effective in recording EDA on the human skin long-term, however, a surface layer of Ag/AgCl is vulnerable and known to deteriorate over time if proper care of the material is not taken, in addition to irritating the skin if gels and adhesives are used [35], [36], [96], [178]. Therefore, a more practical future research initiative is the development of comfortable, low-cost and disposable designs of Ag/AgCl e-textile electrodes for use in the clinical setting. In regards to cost of materials used for this research, a standard Ag/AgCl electrode (Thought Technology, Canada) is $3.13 CAD per unit, and the original Ag conductive yarn (Shieldex by Statex, Germany) is $0.04 CAD per meter, or $1.55 CAD per gram. Approximately 15 cm of yarn is used per e-textile electrode, resulting in a cost of $0.01 CAD for each. The e-textile is more economical than solid Ag/AgCl electrodes when considering these material costs. However, calculation of the total resources required to fabricate and integrate the Ag/AgCl e-textile yarn into a textile substrate has not been accounted for and is beyond the scope of this work.

A significant challenge in the use of dry e-textile electrodes for bio-signal monitoring, including EDA, is the elimination of motion artifacts in the signal. The focus of this study was

on the development, characterization and evaluation of e-textile electrodes on the EDA signal, while motion noise was outside the scope of this study. Other research has focused on addressing the challenge of motion artifacts with e-textiles by increasing pressure on the electrodes on the skin [179], skin preparation [180], or through signal processing algorithms specifically for EDA [181]. In particular, it was shown that reduction of motion noise was seen with padding the e-textile electrodes, which exerted 15 mmHg and 20 mmHg of pressure [179] and a system that can distinguish EDA response waveforms from artifacts with an accuracy of 74% [181]. Further evaluation of effective interconnections between e-textiles and electronic components, a major challenge in e-textile integration [182], is also important for future work. The integration process for the Ag/AgCl e-textiles into textile substrates showed a relatively low prototype success rate due to it all being done by hand, therefore further research on automating the procedure could create more effective integration methods. However, it should be noted that the developed process to integrate the e-textiles into textile substrates, when successful, created functional prototypes that effectively detected EDA signals. Also, work on evaluating the compatibility of e-textile yarns and textile substrates in terms of mechanical and physical properties could provide a better understanding of effective e-textile integration techniques. In particular, further research on the fatigue and cyclic behaviours of the e-textile electrodes and textile substrates can be explored. Our work on the selection of optimal materials and designs for detection of EDA can be incorporated with research focused on developing effective and robust designs for interconnects for e-textiles [183] to outline a more practical manufacturing approach for future e-textile wearable systems.

Similar to previous work outlined in chapter 3 [136], a one-subject approach was used for evaluating the e-textile electrodes and textile substrates for EDA monitoring in order to

reduce the inter-subject variation associated with a multi-subject experimental design [154]. The goal was to focus on the development, design and functionality of e-textile electrodes, and the current results of our research justify additional studies on multiple subjects, especially when developing a further understanding of the physiological aspects associated with EDA signals and on the asymmetrical responses across the body. Further research that is focused on the electrical specifications for EDA, similar to work outlined by Greco et al. in 2016 [23], is necessary to advance alternative monitoring methods for EDA other than the most common two electrode system with DC and constant voltage [35], [36]. Our study used the most common method for monitoring EDA with a clinical grade Thought Technology system, as the focus of our work was on comparing our developed e-textile EDA electrode strap prototypes to current clinical standards.

Ag/AgCl coated nylon yarn was fabricated through a roll-to-roll system with novel optimized parameters identified, which have the potential to be scaled-up. The Ag/AgCl e-textiles and textile substrates used to prototype e-textile EDA electrode straps were characterized and a practical final design for the prototypes was established. The dry e-textile EDA electrodes were stitched into woven cotton, nylon and polyester textile substrates, where hydrophilic cotton was shown to be the most accurate and precise substrate used to detect EDA stimulus responses when comparing to EDA signals recorded simultaneously by dry standard solid Ag/AgCl electrodes. In addition, the EDA waveform recorded by e-textile EDA electrodes on the distal phalanx of the little finger was shown to be different from the EDA waveforms detected on the distal phalanx of the index and middle fingers, potentially a result of different nerve innervations on the human hand. 4-hour EDA monitoring tests were also conducted and demonstrated a trend indicating that the EDA signal recorded by solid standard

Ag/AgCl electrodes EDA is more affected by changes in skin surface temperature than Ag/AgCl e-textile EDA electrodes. The development of breathable and flexible Ag/AgCl e-textiles that can monitor EDA comparably to standard solid non-breathable Ag/AgCl electrodes represents an important technological step. The identified effective design criteria for e-textile EDA electrode straps detailed in this work can help advance the comfort and wearability of long-term EDA monitoring systems to help advance our knowledge of the human neurological system. This further understanding could have a direct positive impact on individuals with autism [127], Parkinson's disease [129] and epilepsy [29].

Chapter 5: Conclusions

There have been significant advances in the field of wearable systems for biological health monitoring, specifically in the development of integrated sensors [1]–[5], [21]. The work detailed here builds upon previously published research by exploring novel approaches to designing and developing flexible and breathable electrodes, specifically optimized for electrodermal activity monitoring. EDA is a result of the sympathetic nervous system being stimulated and causes a change in electrical properties on the surface of the skin due to sweat secretion, which can be quantitatively monitored [35], [36]. The ability to quantify neurological responses has the potential to further our understanding of human physiology and multiple pathologies [35], [36]. Current wearable EDA monitoring systems are rigid and lack the ability to conform well to the surface of the skin. In addition, many of these systems require irritating skin preparations, as well as utilize gels and adhesives, which are uncomfortable for individuals who are required to wear the electrodes long-term [35], [36]. The work described in this dissertation aims to address current technical challenges associated with the development of flexible and breathable electrodes and identifies previously undocumented design criteria that are important for recording accurate and precise EDA signals.

The flexible EDA electrodes based on a polymer substrate were fabricated with various surface areas, geometries and distances between electrodes. The electrodes were also characterized to evaluate the fabrication process, which was shown to be an effective and repeatable method for the design and development of flexible EDA electrodes. The effect of dry flexible Ag/AgCl EDA electrode designs on the detection of EDA stimulus responses was assessed by comparing the EDA signals to data collected by standard rigid Ag/AgCl electrodes. Surface area, distance between and geometry of electrodes are shown to affect the

detectability of the EDA response and the minimum number of sweat glands to be covered by the electrodes has been estimated at 140, or more, in order to maintain functionality. The optimal flexible EDA electrode is of serpentine design with a 0.15 cm^2 surface area and a 0.20 cm distance, with an average Pearson correlation coefficient of 0.979±0.015. Utilizing the protocols and results from this work on flexible EDA electrodes, an approach for electronic textile-based electrode research was developed.

Breathable and flexible e-textile EDA Ag/AgCl electrodes were developed by using a base material of Ag coated nylon 6,6 yarn. A roll-to-roll system was created and novel processing parameters associated with developing Ag/AgCl coated yarn were detailed. The developed e-textile was characterized and then integrated into cotton, nylon and polyester textile substrates, utilizing designs based on practicality for further testing of EDA signal monitoring. Short-term EDA stimulus responses and longer 4-hour tests were conducted to compare and evaluate the accuracy and precision of the EDA signals recorded by dry Ag/AgCl e-textile EDA electrodes and dry standard non-breathable Ag/AgCl electrodes. In addition, e-textile electrodes were secured to various locations on the palmar region of the hand to assess differences in the EDA waveforms recorded.

The cotton textile substrate with stitched e-textile electrodes, with a 0.12 cm^2 surface area and a 0.40 cm distance between, was shown to be the most effective at detecting accurate and precise EDA stimulus responses at the distal phalanx of the middle finger, with a Pearson correlation coefficient of 0.913±0.041. These ideal results can potentially be attributed to the hydrophilicity of cotton. EDA stimulus response waveforms were shown to be different when recorded on the distal phalanx of the little finger when compared to the EDA signals detected on the distal phalanx of the middle and index fingers separately. These findings can possibly

be caused by the differences in nerve innervations on the human hand. Also, the 4-hour tests showed a trend of standard non-breathable and rigid Ag/AgCl electrodes being more affected by and correlated to changes in skin surface temperature than breathable e-textile Ag/AgCl electrodes.

5.1 Objectives and Contributions

The objectives that were previously outlined for this research on EDA are shown below for convenience and to provide structure to the following sections of this dissertation, which will discuss the answers to the questions stated:

1. Flexible Polymer Objectives:
    a. How can we fabricate flexible macroscale silver/silver chloride (Ag/AgCl) electrodes with varying surface areas, geometries and distances between electrodes?
    b. How does surface area of the electrode affect the EDA recording?
    c. How does distance between electrodes affect the EDA recording?
    d. How does the geometry of the electrode affect the EDA recording?
2. Flexible and Breathable Electronic Textile Objectives:
    a. How can we fabricate flexible and breathable Ag/AgCl e-textile electrodes?
    b. How can we prototype functional flexible and breathable EDA electrodes?
    c. How does the material of textile substrates affect the EDA recording in terms of breathability, wettability and bendability?
    d. How does the location of electrodes on the hand affect the EDA recording?

The following sections are organized based on these objectives in order to more effectively summarize the contributions of the work conducted for this dissertation to the existing literature in the field.

5.1.1 Fabrication of Flexible Ag/AgCl Electrodes with Varying Designs

There have been many approaches previously researched to fabricate electrodes on flexible substrates, which include photolithography [66], thermal evaporation [94] and specialized inkjet technology [100]. Our work on developing flexible Ag/AgCl electrodes of varying designs focused on minimizing the number of steps required, as well as removing the need for custom mask fabrication and more specialized equipment. The process developed was adapted from previous research [137]–[139] and proved to be a repeatable and efficient printing method to pattern electrodes for further testing of their abilities to monitor EDA signals. The success rate of the flexible electrodes was approximately 94% and they showed a relatively uniform distribution of the Ag/AgCl on the top layer. This study for this dissertation further built upon the existing literature by detailing additional parameters required for effective fabrication of flexible Ag/AgCl electrodes that can be easily and appropriately designed for a specific application.

5.1.2 Effect of Electrode Design on EDA Stimulus Response Detection

The goal of this part of the dissertation was to evaluate the effect of surface area, geometry and distances between electrodes on the detection of EDA stimulus responses. A common method called the Stroop color test [141], [142] was adapted for this research to prompt an EDA response by the subject. A clinical grade EDA monitoring system was utilized

to simultaneously record EDA stimulus responses from flexible Ag/AgCl electrodes of various designs and standard rigid Ag/AgCl electrodes. The EDA signals from both were compared and evaluated to identify flexible electrode designs that detect EDA stimulus responses that are accurate and precise. There are existing standards outlined in detail for the requirements of electrical systems for EDA monitoring [35], [36], but there has been minimal research on the effect of electrode designs on EDA stimuli response detection.

Previous work on the effect of electrode design and EDA focused on evaluating standard circular solid Ag/AgCl electrodes and utilized conductive gels during the experiments [152]. Our work in this dissertation differed, as our assessment concentrated on dry flexible electrodes in addition to identifying effects on EDA stimulus detection by modifying the surface area, geometry and distance between electrodes. The experimentation identified a minimum coverage of approximately 140 sweat glands by the area under and between the flexible electrodes, in order to detect EDA stimulus responses with comparable functionality to standard rigid electrodes. This important criterion can be utilized for future wearable systems that record EDA on different locations on the body, which are known to have varying distributions of sweat glands [144], [145]. In addition, the flexibility of the fabricated electrodes provides a more practical approach to monitoring a larger variety of locations on the skin than standard rigid electrodes, as electrode-skin contact is critical for monitoring skin conductance [35], [36].

5.1.3 Fabrication and Integration of Ag/AgCl E-textile

Most research on e-textiles and EDA monitoring has been done using silver as the conductive material [24], [26], [27], [33], [34], in addition to extensive work evaluating

stainless steel-based e-textiles [23], [28], [31]. There has not been any work in relation to EDA monitoring that has explored the effectiveness of Ag/AgCl e-textiles on the detection of EDA stimulus responses, which is the same material used with solid clinical grade electrodes. The more recent e-textile fabrication approaches are interested in highly conductive silver coatings through dip-coating [110]–[112] and electroless plating [166], [167] as these processes generally do not require specialized or expensive equipment [155]. A previous protocol for the development of Ag/AgCl yarn in a static batch environment [114] was referred to when creating our novel electrochemical roll-to-roll system to fabricate Ag/AgCl coated nylon 6,6 yarn. Effective roll-to-roll parameters identified include an applied current of 0.75 mA, with the Ag coated nylon yarn having an approximate current density of 1.82 mA/cm^2 and a voltage limit of 2.00 V while in the electrochemical chamber. In addition, the yarn had a uniform movement of 0.08 cm/s which meant that 7 cm of yarn was in the chamber for approximately 89.17 s. Also, in about 30 minutes, 120 cm of usable Ag/AgCl yarn was fabricated with the established parameters. The fabrication process was relatively repeatable, as the average resistance of the optimal Ag/AgCl coated yarn was 11.0±1.8 Ω/cm, showing a low standard deviation between different fabrication processes.

The integration of the fabricated Ag/AgCl yarns with textile substrates of cotton, nylon and polyester was accomplished by referring to the threshold of 140 sweat glands to be covered for effective EDA stimulus response detection identified in previous work [136]. More specifically, the two e-textile electrodes in contact with the surface of the skin are 2 cm long (0.5 cm stitch length) and 0.40 cm apart, with a surface area of approximately 0.12 cm^2 each. The sweat gland density determined on the distal phalanx of the index, middle and little fingers, which were the chosen locations for the EDA e-textile electrodes, resulted in 300 sweat glands

or more being covered under and between the e-textile electrodes. The e-textile EDA electrode straps were handmade with a practical approach, allowing them to be easily secured and removed during testing. When measuring the resistance from the electrical connector on the prototypes to the end of an e-textile electrode, it was determined to be on average 80.96±26.53 Ω, which is significantly below the approximate magnitude of the resistance of biological processes of 1000 Ω [35]. In addition, the e-textile electrodes were shown to be effective at detecting EDA signals when compared to the clinical standard solid Ag/AgCl electrodes. The Ag/AgCl e-textile EDA electrode straps developed for this work are the first e-textile electrodes that use Ag/AgCl as the surface layer in contact with the skin for EDA monitoring. The fabrication of these e-textiles provides a means to compare the functionality of dry Ag/AgCl e-textile electrodes to standard rigid Ag/AgCl electrodes. Hence, by having the same conductive material, it allows the differences observed when monitoring EDA to be a result of the different properties of e-textiles, textiles and solid materials.

5.1.4 Effect of Materials on EDA Signal Recording

Previous research on utilizing e-textiles has discussed a need to further understand the effects of different textile materials on EDA monitoring [23], [28], [34]. In particular, this work explored the effects of using cotton, nylon and polyester textile substrates with stitched Ag/AgCl e-textile electrodes on the EDA stimulus response detection when compared to standard rigid Ag/AgCl electrodes. Among the three textile substrates tested, it was observed that the cotton textile substrate performed the best, as this prototype detected EDA stimulus responses the most accurately and precisely. The skin-electrode interface is known to be an important component in monitoring EDA [35], [36]. Therefore, cotton is believed to be the

optimal textile material of the EDA monitoring straps tested because the flexible cotton textile is hydrophilic and absorbs the sweat on the surface of the skin, which can decrease the skin-electrode impedance and provide a more stable environment to record EDA. Nylon and polyester textiles are hydrophobic and do not absorb the sweat, which can create a more unpredictable skin-electrode interface that can significantly alter the accuracy and precision of the EDA recording. These conclusions can have significant implications on the future designs of wearable EDA monitoring systems that are integrating e-textiles and textile materials. In addition, this work provides a better understanding on how the selection of textile materials can affect the detection of the EDA stimulus response.

A 4-hour test was also conducted to evaluate the ability of Ag/AgCl e-textile electrodes to monitor EDA when compared to standard rigid Ag/AgCl electrodes. Since the experiments were using a clinical EDA monitoring system that utilizes DC and constant voltage to monitor EDA, having the non-polarizing Ag/AgCl e-textile material is important in order to reduce the potential signal drift over time [35], [36]. In addition, dry materials for electrodes were tested, as electrolyte creams can cause unwanted EDA baseline level drifts over time due to moistening of the skin [35], [36]. Previous literature regarding the effect of skin temperature on EDA reported that as skin temperature increased, skin resistance levels decreased [172], [176], which was also observed with our work when using solid Ag/AgCl electrodes. The interesting trend observed with the breathable dry e-textile Ag/AgCl electrodes is that they were shown to be less affected by and less correlated to the skin surface temperature changes than standard dry solid Ag/AgCl electrodes. This result, not observed in previous research, suggests that electrode material could play an important role in regards to the effect that skin surface temperature has on the EDA signal.

5.1.5 Effect of Location of Electrodes on EDA Stimulus Response Waveform

Understanding the underlying physiology associated with EDA is still a work in progress within the field. An interesting and more recent concept of asymmetry of the EDA signal on different sides of the human body [102] is a topic that requires further research. In our work, an experimental approach was formulated that would enable us to compare the EDA stimulus responses recorded by dry e-textile Ag/AgCl electrodes on the different fingers of the hand. Specifically, the distal phalanx of the little, middle and index fingers were the locations of interest due to the different nerve innervations associated with these areas [76], [77]. In terms of EDA, the ulnar nerve was shown to primarily innervate the little finger, while the median nerve was observed to mainly innervate the index and middle fingers [76]. Also, an important aspect to note is that the most common locations to place the two electrodes to record EDA are on the distal phalanx of the index and middle fingers [35], [36], [78], [79]. The results of our approach identified a difference in the EDA waveform recorded by the e-textile electrodes exclusively on the distal phalanx of the little finger when compared to the EDA waveforms monitored by e-textile electrodes on the distal phalanx of the middle and index fingers separately. These results were also corrected for the varying sweat gland densities at the different locations. These observations add further complexity to the concept of EDA asymmetry and provide justification to explore more physiological aspects associated with EDA, in order to better understand the implications that such information would have on designing wearable EDA systems.

5.2 Overall Conclusions

The research conducted for this dissertation aims to solve specific limitations of the current rigid and non-breathable Ag/AgCl electrodes, which are used as the clinical standard for EDA monitoring. These conventional solid electrodes limit the comfort and wearability potential of EDA recording systems, and the current long-term monitoring methods are cumbersome and can irritate the skin due to the potential need to use gels and adhesives. Detailed methodologies to fabricate both flexible dry polymer-based Ag/AgCl electrodes, as well as breathable dry e-textile Ag/AgCl electrodes, were described in this research. The polymer-based and e-textile electrodes were designed and developed specifically to evaluate their ability to accurately and precisely monitor EDA on the surface of human skin when compared to standard rigid and non-breathable Ag/AgCl electrodes. By testing various designs of flexible polymer-based Ag/AgCl electrodes, the understanding of surface area, geometry and distance between electrodes and their effects on the detection of EDA stimulus response was established in relation to estimated sweat gland coverage of the electrode designs. The Ag/AgCl e-textiles developed were integrated into cotton, nylon and polyester textile substrates and the effect of textile material properties on EDA stimulus response detection was observed. In addition, longer term experiments demonstrated the potential limited influence of skin surface temperature on EDA signals monitored by e-textile electrodes. Different locations on the palm of the hand where the e-textile electrodes were secured detected EDA stimulus responses with different waveforms, which can be related to nerve innervation differences.

Overall, the work and results from this dissertation can have a significant impact on future research of EDA monitoring and wearable systems. Specifically, novel design criteria for flexible and breathable EDA electrodes were identified, in addition to a further

understanding of the underlying physiological aspects associated with EDA. The results outlined in this dissertation create a foundation of knowledge for the future development of wearable systems for long-term EDA monitoring. Furthermore, by advancing the technology used for recording EDA, a variety of clinical applications can benefit from being able to unobtrusively and effectively quantify human neurological responses.

5.3 Recommendations and Future Work

The work discussed throughout this dissertation can impact future EDA research in addition to promoting further studies in regards to flexible and breathable electrode designs for monitoring other biological signals. As specific fabrication approaches for Ag/AgCl electrodes based on flexible film and breathable textiles have been described, one can utilize these methods to design sensors optimized to monitor a particular bio-signal. Also, further analysis on the cost associated with the development of flexible and breathable EDA electrodes can be conducted to assess scaling-up of the fabrication processes. This would contribute to the evaluation of whether to develop washable and re-usable or disposable electrodes. It is important to note that Ag/AgCl materials are susceptible to damage if not carefully maintained, therefore durability and washability are limited. It is believed that future research with flexible and breathable Ag/AgCl electrodes should explore low-cost methods of fabrication for disposable use.

A particular approach in regards to continued experimentation with the protocols outlined in this dissertation includes testing on multiple subjects. Specifically, recording EDA during neurological disorder treatment protocols could help identify EDA as a possible biomarker, which can be used to further optimize the care and quality of life of patients. This

monitoring could also promote further understanding of the underlying biological aspects associated with EDA.

In terms of the electrical aspects of EDA signal recording, more exploratory work could be done on utilizing different methods other than DC to monitor EDA with flexible and breathable electrodes. For example, a four-point electrode set-up could be used in addition to employing an AC method for EDA monitoring now that the novel e-textile EDA electrodes developed have been shown to be comparable to the existing standards. Also, miniaturization of the EDA circuitry is another interesting area of future work, whereby one can assess the form factor of the complete system, which can affect the overall wearability of the device. Power supply and consumption would be key parameters involved in the work in reducing the size of the EDA electrical components.

Additional research can also be done on characterizing the e-textile and textile materials in regards to their integration ability, packing density and structures. Specifically, by assessing the stress and strain of the e-textile yarn and textile substrates, one can evaluate their mechanical compatibility, as well as further explore the use of woven and knitted textile structures. Finally, one of the principal next steps most appropriate for this work is to design and develop an EDA wearable system with an array of multiple sensors. Utilizing the important and effective design criteria for flexible and breathable EDA electrodes discussed throughout this dissertation, an EDA monitoring system can have electrodes strategically designed and located across various locations of the body. A multiple electrode EDA monitoring system can not only further our understanding of the spatial component of the biological signal, but can also provide a means to more effectively monitor EDA.

Bibliography

[1] A. Bonfiglio and D. De Rossi, Eds., *Wearable Monitoring Systems*, 1st ed. Boston, MA: Springer US, 2011.

[2] G. Appelboom *et al.*, "Smart wearable body sensors for patient self-assessment and monitoring," *Arch. Public Health*, vol. 72, no. 1, p. 28, Jan. 2014.

[3] Y. L. Zheng *et al.*, "Unobtrusive sensing and wearable devices for health informatics," *IEEE Trans. Biomed. Eng.*, vol. 61, no. 5, pp. 1538–1554, May 2014.

[4] M. Marschollek, M. Gietzelt, M. Schulze, M. Kohlmann, B. Song, and K. Wolf, "Wearable sensors in healthcare and sensor-enhanced health information systems: all our tomorrows?," *Healthc. Inform. Res.*, vol. 18, no. 2, pp. 97–104, Jun. 2012.

[5] M. M. Baig, H. Gholam Hosseini, A. A. Moqeem, F. Mirza, and M. Lindén, "A systematic review of wearable patient monitoring systems – Current challenges and opportunities for clinical adoption," *J. Med. Syst.*, vol. 41, no. 7, p. 115, Jul. 2017.

[6] E. Topol, "Wireless sensors," in *The Creative Destruction of Medicine: How the Digital Revolution Will Create Better Health Care*, 1st ed., New York, NY: Basic Books, 2011, pp. 59–76.

[7] Y. Rajeshwari and T. Srilatha, "A real-time continuous monitoring of health using wearable biosensors," *Int. J. Emerg. Technol. Adv. Eng.*, vol. 3, no. 9, pp. 557–560, 2013.

[8] A. Pantelopoulos and N. G. Bourbakis, "A survey on wearable sensor-based systems for health monitoring and prognosis," *IEEE Trans. Syst. Man Cybern. Part C Appl. Rev.*, vol. 40, no. 1, pp. 1–12, Jan. 2010.

[9] R. Fensli, P. E. Pedersen, T. Gundersen, and O. Hejlesen, "Sensor acceptance model –

Measuring patient acceptance of wearable sensors," *Methods Inf. Med.*, pp. 89–95, 2008.

[10] M. Chan, D. Estève, J. Fourniols, C. Escriba, and E. Campo, "Smart wearable systems: current status and future challenges," *Artif. Intell. Med.*, vol. 56, no. 3, pp. 137–56, Nov. 2012.

[11] P. Bonato, "Clinical applications of wearable technology," in *2009 Annual International Conference of the IEEE Engineering in Medicine and Biology Society*, 2009, vol. 2009, pp. 6580–6583.

[12] P. Shyamkumar, P. Rai, S. Oh, M. Ramasamy, R. Harbaugh, and V. Varadan, "Wearable wireless cardiovascular monitoring using textile-based nanosensor and nanomaterial systems," *Electronics*, vol. 3, no. 3, pp. 504–520, Aug. 2014.

[13] P. Rai, S. Oh, P. Shyamkumar, M. Ramasamy, R. E. Harbaugh, and V. K. Varadan, "Nanotextile bio-sensors with mobile wireless wearable health monitoring of neurological and cardiovascular disorders," *J. Inst. Smart Struct. Syst.*, vol. 3, no. 1, pp. 28–77, Dec. 2014.

[14] C. R. Merritt, H. T. Nagle, and E. Grant, "Textile-based capacitive sensors for respiration monitoring," *IEEE Sens. J.*, vol. 9, no. 1, pp. 71–78, Jan. 2009.

[15] N. F. Butte, U. Ekelund, and K. R. Westerterp, "Assessing physical activity using wearable monitors: measures of physical activity," *Med. Sci. Sports Exerc.*, vol. 44, no. 1, pp. S5-12, Jan. 2012.

[16] W. Zeng, L. Shu, Q. Li, S. Chen, F. Wang, and X.-M. Tao, "Fiber-based wearable electronics: A review of materials, fabrication, devices, and applications," *Adv. Mater.*, vol. 26, no. 31, pp. 5310–5336, Aug. 2014.

[17] M. Stoppa and A. Chiolerio, “Wearable electronics and smart textiles: a critical review,” *Sensors*, vol. 14, no. 7, pp. 11957–11992, Jul. 2014.

[18] L. M. Castano and A. B. Flatau, “Smart fabric sensors and e-textile technologies: a review,” *Smart Mater. Struct.*, vol. 23, no. 5, p. 053001, May 2014.

[19] E. Ethridge and D. Urban, “Electrotextiles,” *Int. J. High Speed Electron. Syst.*, vol. 12, no. 2, pp. 365–369, Jun. 2002.

[20] X. Tao, Ed., *Wearable electronics and photonics*, 1st ed. Cambridge: Woodhead Publishing Ltd., 2005.

[21] C. Gonçalves, A. Ferreira da Silva, J. Gomes, and R. Simoes, “Wearable e-textile technologies: a review on sensors, actuators and control elements,” *Inventions*, vol. 3, no. 1, p. 14, Mar. 2018.

[22] H. Carvalho, A. P. Catarino, A. Rocha, and O. Postolache, “Health monitoring using textile sensors and electrodes: an overview and integration of technologies,” in *2014 IEEE International Symposium on Medical Measurements and Applications (MeMeA)*, 2014, pp. 1–6.

[23] A. Greco, A. Lanata, L. Citi, N. Vanello, G. Valenza, and E. Scilingo, “Skin admittance measurement for emotion recognition: a study over frequency sweep,” *Electronics*, vol. 5, no. 4, p. 46, Aug. 2016.

[24] F. Seoane *et al.*, “Wearable biomedical measurement systems for assessment of mental stress of combatants in real time,” *Sensors*, vol. 14, no. 4, pp. 7120–7141, 2014.

[25] Jeehoon Kim, Sungjun Kwon, Sangwon Seo, and Kwangsuk Park, “Highly wearable galvanic skin response sensor using flexible and conductive polymer foam,” in *2014 36th Annual International Conference of the IEEE Engineering in Medicine and*

Biology Society, 2014, pp. 6631–6634.

[26] O. Postolache, V. Viegas, J. M. Dias Pereira, D. Vinhas, P. S. Girao, and G. Postolache, "Toward developing a smart wheelchair for user physiological stress and physical activity monitoring," in *2014 IEEE International Symposium on Medical Measurements and Applications (MeMeA)*, 2014, pp. 1–6.

[27] F. Seoane *et al.*, "Sensorized garments and textrode-enabled measurement instrumentation for ambulatory assessment of the autonomic nervous system response in the ATREC project," *Sensors*, vol. 13, no. 7, pp. 8997–9015, Jan. 2013.

[28] A. Lanatà, G. Valenza, and E. P. Scilingo, "A novel EDA glove based on textile-integrated electrodes for affective computing," *Med. Biol. Eng. Comput.*, vol. 50, no. 11, pp. 1163–1172, Nov. 2012.

[29] M. Poh *et al.*, "Convulsive seizure detection using a wrist-worn electrodermal activity and accelerometry biosensor," *Epilepsia*, vol. 53, no. 5, pp. e93-7, May 2012.

[30] J. Healey, "GSR sock: a new e-textile sensor prototype," in *2011 15th Annual International Symposium on Wearable Computers*, 2011, pp. 113–114.

[31] G. Valenza, A. Lanatà, E. P. Scilingo, and D. De Rossi, "Towards a smart glove: arousal recognition based on textile electrodermal response," in *2010 Annual International Conference of the IEEE Engineering in Medicine and Biology*, 2010, pp. 3598–3601.

[32] Ming-Zher Poh, T. Loddenkemper, N. C. Swenson, S. Goyal, J. R. Madsen, and R. W. Picard, "Continuous monitoring of electrodermal activity during epileptic seizures using a wearable sensor," in *2010 Annual International Conference of the IEEE Engineering in Medicine and Biology*, 2010, pp. 4415–4418.

[33] R. R. Fletcher *et al.*, "iCalm: wearable sensor and network architecture for wirelessly

communicating and logging autonomic activity," *IEEE Trans. Inf. Technol. Biomed.*, vol. 14, no. 2, pp. 215–23, Mar. 2010.

[34] M. Poh, N. C. Swenson, and R. W. Picard, "A wearable sensor for unobtrusive, long-term assessment of electrodermal activity," *IEEE Trans. Biomed. Eng.*, vol. 57, no. 5, pp. 1243–52, May 2010.

[35] W. Boucsein, *Electrodermal Activity*, 2nd ed. Boston, MA: Springer US, 2012.

[36] W. Boucsein *et al.*, "Publication recommendations for electrodermal measurements," *Psychophysiology*, vol. 49, no. 8, pp. 1017–1034, Aug. 2012.

[37] H. Kim, "Exploring the user requirements for wearable healthcare systems," in *2011 IEEE 13th International Conference on e-Health Networking, Applications and Services*, 2011, pp. 74–77.

[38] S. Coyle, V. F. Curto, F. Benito-Lopez, L. Florea, and D. Diamond, "Wearable bio and chemical sensors," in *Wearable Sensors*, 1st ed., E. Sazonov and M. R. Neuman, Eds. San Diego, CA: Elsevier, 2014, pp. 65–83.

[39] M. R. Mahfouz, M. J. Kuhn, and G. To, "Wireless medical devices: a review of current research and commercial systems," in *2013 IEEE Topical Conference on Biomedical Wireless Technologies, Networks, and Sensing Systems*, 2013, pp. 16–18.

[40] J. R. Windmiller and J. Wang, "Wearable electrochemical sensors and biosensors: a review," *Electroanalysis*, vol. 25, no. 1, pp. 29–46, Jan. 2013.

[41] W. D. van Marken Lichtenbelt *et al.*, "Evaluation of wireless determination of skin temperature using iButtons," *Physiol. Behav.*, vol. 88, no. 4–5, pp. 489–97, Jul. 2006.

[42] J. Goodwin, M. Bilous, S. Winship, P. Finn, and S. C. Jones, "Validation of the Oscar 2 oscillometric 24-h ambulatory blood pressure monitor according to the British

Hypertension Society protocol," *Blood Press. Monit.*, vol. 12, no. 2, pp. 113–117, 2007.

[43] R. Villar, T. Beltrame, and R. L. Hughson, "Validation of the Hexoskin wearable vest during lying, sitting, standing, and walking activities," *Appl. Physiol. Nutr. Metab.*, vol. 40, no. 10, pp. 1019–1024, 2015.

[44] I. Ayoola, S. B. Oetomo, and L. Feijs, "Non-invasive blood oxygen saturation monitoring for neonates using reflectance pulse oximeter," in *2010 Design, Automation & Test in Europe Conference & Exhibition*, 2010, pp. 1530–1535.

[45] A. Salameh, R. a Gebauer, O. Grollmuss, P. Vít, O. Reich, and J. Janousek, "Normal limits for heart rate as established using 24-hour ambulatory electrocardiography in children and adolescents," *Cardiol. Young*, vol. 18, no. 5, pp. 467–72, 2008.

[46] M. Duvinage, T. Castermans, M. Petieau, T. Hoellinger, G. Cheron, and T. Dutoit, "Performance of the Emotiv Epoc headset for P300-based applications," *Biomed. Eng. Online*, vol. 12, p. 56, 2013.

[47] M. Georgi, C. Amma, and T. Schultz, "Recognizing hand and finger gestures with IMU based motion and EMG based muscle activity sensing," in *Proceedings of the International Conference on Bio-inspired Systems and Signal Processing*, 2015, pp. 99–108.

[48] S. Liang *et al.*, "Development of an EOG-based automatic sleep-monitoring eye mask," *IEEE Trans. Instrum. Meas.*, vol. 64, no. 11, pp. 2977–2985, Nov. 2015.

[49] J. Takacs, C. L. Pollock, J. R. Guenther, M. Bahar, C. Napier, and M. a. Hunt, "Validation of the Fitbit One activity monitor device during treadmill walking," *J. Sci. Med. Sport*, vol. 17, no. 5, pp. 496–500, Sep. 2014.

[50] J. Torniainen, B. Cowley, A. Henelius, K. Lukander, and S. Pakarinen, "Feasibility of

an electrodermal activity ring prototype as a research tool," in *2015 37th Annual International Conference of the IEEE Engineering in Medicine and Biology Society (EMBC)*, 2015, pp. 6433–6436.

[51] A. Sa-ngasoongsong, J. Kunthong, V. Sarangan, X. Cai, and S. T. S. Bukkapatnam, "A low-cost, portable, high-throughput wireless sensor system for phonocardiography applications," *Sensors*, vol. 12, no. 12, pp. 10851–10870, Aug. 2012.

[52] S. D. Milne *et al.*, "A wearable wound moisture sensor as an indicator for wound dressing change: an observational study of wound moisture and status," *Int. Wound J.*, pp. 1–6, Nov. 2015.

[53] M. Fasih and S. Saleem, "Wearable biosensors in terms of energy consumption, placement and communication level: a survey," *Int. J. Enhanc. Res. Sci. Technol. Eng.*, vol. 3, no. 1, pp. 259–265, 2014.

[54] D. Fred, "Perceived usefulness, perceived ease of use, and user acceptance of information technology," *MIS Q.*, vol. 13, no. 3, pp. 319–340, 1989.

[55] V. Venkatesh, M. G. Morris, G. B. Davis, and F. D. Davis, "User acceptance of information technology: toward a unified view," *Manag. Inf. Syst. Res. Cent.*, vol. 27, no. 3, pp. 425–478, 2003.

[56] C. Huang, M. Chan, C. Chen, and B. Lin, "Novel wearable and wireless ring-type pulse oximeter with multi-detectors," *Sensors*, vol. 14, no. 9, pp. 17586–99, Jan. 2014.

[57] C. Shen, T. Kao, C. Huang, and J. Lee, "Wearable band using a fabric-based sensor for exercise ECG monitoring," in *2006 10th IEEE International Symposium on Wearable Computers*, 2006, pp. 143–144.

[58] T. Yamada *et al.*, "A stretchable carbon nanotube strain sensor for human-motion

detection," *Nat. Nanotechnol.*, vol. 6, no. 5, pp. 296–301, May 2011.

[59] Y. Zhang, C. C. Y. Poon, C. Chan, M. W. W. Tsang, and K. Wu, "A health-shirt using e-textile materials for the continuous and cuffless monitoring of arterial blood pressure," in *2006 3rd IEEE/EMBS International Summer School on Medical Devices and Biosensors*, 2006, pp. 86–89.

[60] Y.-D. Lee and W.-Y. Chung, "Wireless sensor network based wearable smart shirt for ubiquitous health and activity monitoring," *Sensors Actuators B Chem.*, vol. 140, no. 2, pp. 390–395, Jul. 2009.

[61] Z. Zhang, Y. Shen, W. Wang, and B. Wang, "Design and implementation of sensing shirt for ambulatory cardiopulmonary monitoring," *J. Med. Biol. Eng.*, vol. 31, no. 3, pp. 207–216, 2010.

[62] C. Gopalsamy, S. Park, R. Rajamanickam, and S. Jayaraman, "The wearable motherboard: the first generation of adaptive and responsive textile structures (ARTS) for medical applications," *Virtual Real.*, vol. 4, no. 3, pp. 152–168, Sep. 1999.

[63] Y. M. Chi, S. R. Deiss, and G. Cauwenberghs, "Non-contact low power EEG/ECG electrode for high density wearable biopotential sensor networks," *2009 Sixth Int. Work. Wearable Implant. Body Sens. Networks*, pp. 246–250, Jun. 2009.

[64] Z. Deng and J. Liu, "Effect of fixing material on skin-contact temperature measurement by wearable sensor," in *2008 5th International Summer School and Symposium on Medical Devices and Biosensors*, 2008, pp. 137–140.

[65] R. Yousefi, M. Nourani, and I. Panahi, "Adaptive cancellation of motion artifact in wearable biosensors," in *2012 Annual International Conference of the IEEE Engineering in Medicine and Biology Society*, 2012, pp. 2004–2008.

[66] D.-H. Kim *et al.*, “Epidermal electronics,” *Science.*, vol. 333, no. 6044, pp. 838–843, Aug. 2011.

[67] J. Jung and J. Lee, “ZigBee device access control and reliable data transmission in ZigBee based health monitoring system,” in *2008 10th International Conference on Advanced Communication Technology*, 2008, pp. 795–797.

[68] G. Gargiulo, P. Bifulco, M. Cesarelli, C. Jin, A. McEwan, and A. van Schaik, “Wearable dry sensors with Bluetooth connection for use in remote patient monitoring systems,” *Stud. Health Technol. Inform.*, vol. 161, no. December, pp. 57–65, 2010.

[69] A. J. Jara, D. Fernandez, P. Lopez, M. A. Zamora, and A. F. Skarmeta, “Evaluation of Bluetooth low energy capabilities for tele-mobile monitoring in home-care,” *J. Univers. Comput. Sci.*, vol. 19, no. 9, pp. 1219–1241, 2013.

[70] E. Shahhaidar, “Decreasing power consumption of a medical e-textile,” *World Acad. Sci. Eng. Technol.*, vol. 2, no. 8, pp. 329–333, 2008.

[71] CDC, “Chronic disease prevention and health promotion,” Atlanta, GA, 2013.

[72] R. Vigouroux, “Sur le rôle de la résistance électrique des tissues dans l’électrodiagnostic,” *Comptes rendus des société Biol.*, vol. 31, pp. 336–339, 1879.

[73] C. Féré, “Note on changes in electrical resistance under the effect of sensory stimulation and emotion,” *Comptes Rendus des Seances la Soc. Biol. (Series 9)*, vol. 5, no. October, pp. 217–219, 1888.

[74] L. C. Johnson and A. Lubin, “Spontaneous electrodermal activity during waking and sleeping,” *Psychophysiology*, vol. 3, no. 1, pp. 8–17, Jul. 1966.

[75] C. C. Brown, “A proposed standard nomenclature for psychophysiological measures,” *Psychophysiology*, vol. 4, no. 2, pp. 260–264, Oct. 1967.

[76] B. Egyed, A. Eory, T. Veres, and J. Manninger, “Measurement of electrical resistance after nerve injuries of the hand,” *Hand*, vol. 12, no. 3, pp. 275–281, Oct. 1980.

[77] M. Loukas *et al.*, “The surgical anatomy of ulnar and median nerve communications in the palmar surface of the hand,” *J. Neurosurg.*, vol. 106, no. 5, pp. 887–893, May 2007.

[78] A. S. Scerbo, L. W. Freedman, A. Raine, M. E. Dawson, and P. H. Venables, “A major effect of recording site on measurement of electrodermal activity,” *Psychophysiology*, vol. 29, no. 2, pp. 241–246, Mar. 1992.

[79] L. W. Freedman, A. S. Scerbo, M. E. Dawson, A. Raine, W. O. Mcclure, and P. H. Venables, “The relationship of sweat gland count to electrodermal activity,” *Psychophysiology*, vol. 31, no. 2, pp. 196–200, Mar. 1994.

[80] K. Seppi *et al.*, “The movement disorder society evidence-based medicine review update: treatments for the non-motor symptoms of Parkinson’s disease,” *Mov. Disord.*, vol. 26, no. S3, pp. S42–S80, Oct. 2011.

[81] B. E. Hubert, B. Wicker, E. Monfardini, and C. Deruelle, “Electrodermal reactivity to emotion processing in adults with autistic spectrum disorders,” *Autism*, vol. 13, no. 1, pp. 9–19, Jan. 2009.

[82] O. Pabst, C. Tronstad, S. Grimnes, D. Fowles, and Ø. G. Martinsen, “Comparison between the AC and DC measurement of electrodermal activity,” *Psychophysiology*, vol. 54, no. 3, pp. 374–385, Mar. 2017.

[83] M. Schmidt, D. Penner, A. Burkl, R. Stojanovic, T. Schümann, and P. Beckerle, “Implementation and evaluation of a low-cost and compact electrodermal activity measurement system,” *Measurement*, vol. 92, pp. 96–102, Oct. 2016.

[84] G. Baysal, F. Neşe Kök, L. Trabzon, H. Kizil, İ. Gocek, and B. K. Kayaoğlu,

"Microfluidic nonwoven-based device as a potential biosensor for sweat analysis," *Appl. Mech. Mater.*, vol. 490–491, pp. 274–279, Apr. 2014.

[85] T. Pereira, P. Silva, H. Carvalho, and M. Carvalho, "Textile moisture sensor matrix for monitoring of disabled and bed-rest patients," in *2011 IEEE EUROCON - International Conference on Computer as a Tool*, 2011, pp. 1–4.

[86] P. Salvo, F. Di Francesco, D. Costanzo, C. Ferrari, M. G. Trivella, and D. De Rossi, "A wearable sensor for measuring sweat rate," *IEEE Sens. J.*, vol. 10, no. 10, pp. 1557–1558, Oct. 2010.

[87] D. Morris, S. Coyle, Y. Wu, K. T. Lau, G. Wallace, and D. Diamond, "Bio-sensing textile based patch with integrated optical detection system for sweat monitoring," *Sensors Actuators B Chem.*, vol. 139, no. 1, pp. 231–236, May 2009.

[88] M. Cheng, L. Chen, Y. Hung, and C. Chen, "A vital wearing system with wireless capability," in *2008 Second International Conference on Pervasive Computing Technologies for Healthcare*, 2008, no. 27, pp. 268–271.

[89] M. V. Villarejo, B. G. Zapirain, and A. M. Zorrilla, "A stress sensor based on galvanic skin response (GSR) controlled by ZigBee," *Sensors (Basel).*, vol. 12, no. 5, pp. 6075–101, Jan. 2012.

[90] L. K. Lam and A. J. Szypula, "Wearable emotion sensor on flexible substrate for mobile health applications," in *2018 IEEE Sensors Applications Symposium (SAS)*, 2018, no. 11, pp. 1–5.

[91] Y. Ayzenberg and R. W. Picard, "FEEL: a system for frequent event and electrodermal activity labeling," *IEEE J. Biomed. Heal. Informatics*, vol. 18, no. 1, pp. 266–277, Jan. 2014.

[92] P. Cao, S. Jia, X. Wang, and J. Zhou, “Wearable and wireless multi-electrophysiological system,” in *2006 3rd IEEE/EMBS International Summer School on Medical Devices and Biosensors*, 2006, pp. 83–85.

[93] Jongyoon Choi and R. Gutierrez-Osuna, “Estimating mental stress using a wearable cardio-respiratory sensor,” in *2010 IEEE Sensors*, 2010, pp. 150–154.

[94] S. Yoon, J. K. Sim, and Y.-H. Cho, “A flexible and wearable human stress monitoring patch,” *Sci. Rep.*, vol. 6, no. 1, p. 23468, Sep. 2016.

[95] C. W. J. John *et al.*, *Medical Instrumentation: Application and Design*, 4th ed. Hoboken, New Jersey, USA: John Wiley & Sons, Inc., 2009.

[96] Y. M. Chi, T. Jung, and G. Cauwenberghs, “Dry-contact and noncontact biopotential electrodes: methodological review,” *IEEE Rev. Biomed. Eng.*, vol. 3, pp. 106–119, 2010.

[97] CRC, *CRC Handbook of Chemistry and Physics*, 98th ed. Boca Raton, FL: CRC Press/Taylor & Francis Group, 2018.

[98] L. A. Geddes and R. Roeder, “Measurement of the direct-current (Faradic) resistance of the electrode-electrolyte interface for commonly used electrode materials,” *Ann. Biomed. Eng.*, vol. 29, no. 2, pp. 181–186, Feb. 2001.

[99] M. W. Shinwari, D. Zhitomirsky, I. A. Deen, P. R. Selvaganapathy, M. J. Deen, and D. Landheer, “Microfabricated reference electrodes and their biosensing applications,” *Sensors*, vol. 10, no. 3, pp. 1679–1715, Mar. 2010.

[100] E. T. S. G. da Silva, S. Miserere, L. T. Kubota, and A. Merkoçi, “Simple on-plastic/paper inkjet-printed solid-state Ag/AgCl pseudoreference electrode,” *Anal. Chem.*, vol. 86, no. 21, pp. 10531–10534, Nov. 2014.

[101] C. Pang, C. Lee, and K. Y. Suh, “Recent advances in flexible sensors for wearable and implantable devices,” *J. Appl. Polym. Sci.*, vol. 130, no. 3, pp. 1429–1441, Nov. 2013.

[102] R. W. Picard, S. Fedor, and Y. Ayzenberg, “Multiple arousal theory and daily-life electrodermal activity asymmetry,” *Emot. Rev.*, vol. 8, no. 1, pp. 62–75, Jan. 2016.

[103] Empatica, “Empatica,” 2018. [Online]. Available: www.empatica.com. [Accessed: 19-May-2018].

[104] Moodmetric, “Moodmetric,” 2018. [Online]. Available: www.moodmetric.com. [Accessed: 19-May-2018].

[105] Movisens, “edaMove,” 2018. [Online]. Available: www.movisens.com/en/products/eda-sensor/. [Accessed: 19-May-2018].

[106] A. Luzio, E. V. Canesi, C. Bertarelli, and M. Caironi, “Electrospun polymer fibers for electronic applications,” *Materials (Basel).*, vol. 7, no. 2, pp. 906–947, 2014.

[107] T. I. Oh, T. E. Kim, S. Yoon, K. J. Kim, E. J. Woo, and R. J. Sadleir, “Flexible electrode belt for EIT using nanofiber web dry electrodes,” *Physiol. Meas.*, vol. 33, no. 10, pp. 1603–1616, Oct. 2012.

[108] F. Xu and Y. Zhu, “Highly conductive and stretchable silver nanowire conductors,” *Adv. Mater.*, vol. 24, no. 37, pp. 5117–5122, 2012.

[109] Z. Cui, F. R. Poblete, G. Cheng, S. Yao, X. Jiang, and Y. Zhu, “Design and operation of silver nanowire based flexible and stretchable touch sensors,” *J. Mater. Res.*, vol. 30, no. 01, pp. 79–85, 2014.

[110] Y. Atwa, N. Maheshwari, and I. A. Goldthorpe, “Silver nanowire coated threads for electrically conductive textiles,” *J. Mater. Chem. C*, vol. 3, no. 16, pp. 3908–3912, 2015.

[111] A. C. Myers, H. Huang, and Y. Zhu, “Wearable silver nanowire dry electrodes for

electrophysiological sensing," *RSC Adv.*, vol. 5, no. 15, pp. 11627–11632, 2015.

[112] H.-W. Cui, K. Suganuma, and H. Uchida, "Highly stretchable, electrically conductive textiles fabricated from silver nanowires and cupro fabrics using a simple dipping-drying method," *Nano Res.*, vol. 8, no. 5, pp. 1604–1614, May 2015.

[113] E. P. Scilingo, A. Gemignani, R. Paradiso, N. Taccini, B. Ghelarducci, and D. DeRossi, "Performance evaluation of sensing fabrics for monitoring physiological and biomechanical variables," *IEEE Trans. Inf. Technol. Biomed.*, vol. 9, no. 3, pp. 345–352, Sep. 2005.

[114] P. J. Xu, H. Liu, H. Zhang, X. M. Tao, and S. Y. Wang, "Electrochemical modification of silver coated multifilament for wearable ECG monitoring electrodes," *Adv. Mater. Res.*, vol. 332–334, pp. 1019–1023, Sep. 2011.

[115] H. Zhang, W. Li, X. Tao, P. Xu, and H. Liu, "Textile-structured human body surface biopotential signal acquisition electrode," in *2011 4th International Congress on Image and Signal Processing*, 2011, vol. 5, pp. 2792–2797.

[116] S. Bouwstra, W. Chen, L. Feijs, and S. B. Oetomo, "Smart jacket design for neonatal monitoring with wearable sensors," in *2009 Sixth International Workshop on Wearable and Implantable Body Sensor Networks*, 2009, pp. 162–167.

[117] W. Chen, S. T. Nguyen, R. Coops, S. B. Oetomo, and L. Feijs, "Wireless transmission design for health monitoring at neonatal intensive care units," in *2009 2nd International Symposium on Applied Sciences in Biomedical and Communication Technologies*, 2009, pp. 1–6.

[118] W. Chen, S. Bouwstra, S. Oetomo, and L. Feijs, "Intelligent design for neonatal monitoring with wearable sensors," in *Intelligent and Biosensors*, 1st ed., no. January,

V. S. Somerset, Ed. Croatia: InTech, 2010, pp. 1–25.

[119] S. Patel, H. Park, P. Bonato, L. Chan, and M. Rodgers, “A review of wearable sensors and systems with application in rehabilitation,” *J. Neuroeng. Rehabil.*, vol. 9, no. 1, p. 21, Jan. 2012.

[120] S. Patel *et al.*, “Monitoring motor fluctuations in patients with Parkinson’s disease using wearable sensors,” *IEEE Trans. Inf. Technol. Biomed.*, vol. 13, no. 6, pp. 864–873, Nov. 2009.

[121] D. M. Sherrill *et al.*, “Advanced analysis of wearable sensor data to adjust medication intake in patients with Parkinson’s disease,” in *Conference Proceedings. 2nd International IEEE EMBS Conference on Neural Engineering, 2005.*, 2005, pp. 202–205.

[122] S. Patel *et al.*, “Home monitoring of patients with Parkinson’s disease via wearable technology and a web-based application,” in *2010 Annual International Conference of the IEEE Engineering in Medicine and Biology*, 2010, vol. 2010, pp. 4411–4414.

[123] W. Maetzler, J. Domingos, K. Srulijes, J. J. Ferreira, and B. R. Bloem, “Quantitative wearable sensors for objective assessment of Parkinson’s disease,” *Mov. Disord.*, vol. 28, no. 12, pp. 1628–1637, Oct. 2013.

[124] J. Westerink, M. Ouwerkerk, G.-J. de Vries, S. de Waele, J. van den Eerenbeemd, and M. van Boven, “Emotion measurement platform for daily life situations,” in *2009 3rd International Conference on Affective Computing and Intelligent Interaction and Workshops*, 2009, pp. 1–6.

[125] H. J. Pijeira-Díaz, H. Drachsler, S. Järvelä, and P. A. Kirschner, “Investigating collaborative learning success with physiological coupling indices based on

electrodermal activity," in *Proceedings of the Sixth International Conference on Learning Analytics & Knowledge - LAK '16*, 2016, pp. 64–73.

[126] B. M. Schupak, R. K. Parasher, and G. P. Zipp, "Reliability of electrodermal activity: quantifying sensory processing in children with autism," *Am. J. Occup. Ther.*, vol. 70, no. 6, p. 7006220030p1, Sep. 2016.

[127] E. B. Prince *et al.*, "The relationship between autism symptoms and arousal level in toddlers with autism spectrum disorder, as measured by electrodermal activity," *Autism*, vol. 21, no. 4, pp. 504–508, May 2017.

[128] N. Ruiz-Robledillo and L. Moya-Albiol, "Lower electrodermal activity to acute stress in caregivers of people with autism spectrum disorder: an adaptive habituation to stress," *J. Autism Dev. Disord.*, vol. 45, no. 2, pp. 576–588, Feb. 2015.

[129] F. Esen, G. Çelebi, C. Ertekin, and Z. Çolakoglu, "Electrodermal activity in patients with Parkinson's disease," *Clin. Auton. Res.*, vol. 7, no. 1, pp. 35–40, Feb. 1997.

[130] R. Padilla and A. Domina, "Effectiveness of sensory stimulation to improve arousal and alertness of people in a coma or persistent vegetative state after traumatic brain injury: a systematic review," *Am. J. Occup. Ther.*, vol. 70, no. 3, p. 7003180030p1, Apr. 2016.

[131] P. Koldrack, R. Henkel, F. Krueger, S. Teipel, and T. Kirste, "Supporting situation awareness of dementia patients in outdoor environments," in *Proceedings of the 9th International Conference on Pervasive Computing Technologies for Healthcare*, 2015, pp. 245–248.

[132] Y. Treusch *et al.*, "Emotional reaction in nursing home residents with dementia-associated apathy: a pilot study," *Geriatr. Ment. Heal. Care*, vol. 3, no. 1, pp. 1–6, Aug. 2015.

[133] A.-A. Dubé, M. Duquette, M. Roy, F. Lepore, G. Duncan, and P. Rainville, “Brain activity associated with the electrodermal reactivity to acute heat pain,” *Neuroimage*, vol. 45, no. 1, pp. 169–180, Mar. 2009.

[134] J. Munsters, L. Wallström, J. Ågren, T. Norsted, and R. Sindelar, “Skin conductance measurements as pain assessment in newborn infants born at 22-27weeks gestational age at different postnatal age,” *Early Hum. Dev.*, vol. 88, no. 1, pp. 21–26, 2012.

[135] A. Sano, R. W. Picard, and R. Stickgold, “Quantitative analysis of wrist electrodermal activity during sleep,” *Int. J. Psychophysiol.*, vol. 94, no. 3, pp. 382–389, Dec. 2014.

[136] © 2017 IEEE. Reprinted, with permission, from, P. A. Haddad, A. Servati, S. Soltanian, F. Ko, and P. Servati, “Effects of flexible dry electrode design on electrodermal activity stimulus response detection,” *IEEE Trans. Biomed. Eng.*, vol. 64, no. 12, pp. 2979–2987, Dec. 2017.

[137] A. Liu *et al.*, “A composite additive used for an excellent new cyanide-free silver plating bath,” *New J. Chem.*, vol. 39, no. 4, pp. 2409–2412, 2015.

[138] A. Liu *et al.*, “A composite additive used for an excellent new cyanide-free silver plating bath [Supplementary],” *New J. Chem.*, vol. 39, no. 4, pp. 2409–2412, 2015.

[139] A. Liu *et al.*, “A combined theoretical and experimental study for silver electroplating,” *Sci. Rep.*, vol. 4, p. 3837, Jan. 2014.

[140] E. de Bilbao, D. Soulat, G. Hivet, and A. Gasser, “Experimental study of bending behaviour of reinforcements,” *Exp. Mech.*, vol. 50, no. 3, pp. 333–351, Mar. 2010.

[141] J. R. R. Stroop, “Studies of interference in serial verbal reactions,” *J. Exp. Psychol.*, vol. 18, no. 6, pp. 643–662, 1935.

[142] M. Svetlak, P. Bob, M. Cernik, and M. Kukleta, “Electrodermal complexity during the

Stroop colour word test," *Auton. Neurosci.*, vol. 152, no. 1–2, pp. 101–107, Jan. 2010.

[143] W. Boucsein, R. Baltissen, and M. Euler, "Dependence of skin conductance reactions and skin resistance reactions upon previous level," *Psychophysiology*, vol. 21, no. 2, pp. 212–218, Mar. 1984.

[144] J. D. Montagu and E. M. Coles, "Mechanism and measurement of the galvanic skin response," *Psychol. Bull.*, vol. 65, no. 5, pp. 261–279, 1966.

[145] P. F. Millington and R. Wilkinson, *Skin*. Cambridge: Cambridge University Press, 1983.

[146] K. Pearson, "Mathematical contributions to the theory of evolution – Regression, heredity, and panmixia," *Philos. Trans. R. Soc. A Math. Phys. Eng. Sci.*, vol. 187, no. 1400, pp. 253–318, Jan. 1896.

[147] H. F. Posada-Quintero, R. Rood, Y. Noh, K. Burnham, J. Pennace, and K. H. Chon, "Novel dry electrodes for recording electrodermal activity," in *2016 38th Annual International Conference of the IEEE Engineering in Medicine and Biology Society (EMBC)*, 2016, pp. 5701–5704.

[148] H. E. Swanson and E. Tatge, "Standard X-ray diffraction powder patterns," *National Bureau of Standards*, vol. I, no. 539. Washington, D.C., p. 23, 1953.

[149] S. Hull and D. A. Keen, "Pressure-induced phase transitions in AgCl, AgBr, and AgI," *Phys. Rev. B*, vol. 59, no. 2, pp. 750–761, Jan. 1999.

[150] H. E. Swanson and E. Tatge, "Standard X-ray diffraction powder patterns," *National Bureau of Standards*, vol. I, no. 539. Washington, D.C., p. 15, 1953.

[151] M. van Dooren, J. J. G. de Vries, and J. H. Janssen, "Emotional sweating across the body: comparing 16 different skin conductance measurement locations," *Physiol. Behav.*, vol. 106, no. 2, pp. 298–304, May 2012.

[152] D. A. Mitchell and P. H. Venables, “The relationship of EDA to electrode size,” *Psychophysiology*, vol. 17, no. 4, pp. 408–412, Jul. 1980.

[153] X. Wang, Z. Liu, and T. Zhang, “Flexible sensing electronics for wearable/attachable health monitoring,” *Small*, vol. 13, no. 25, p. 1602790, Jul. 2017.

[154] D. Giakoumis, D. Tzovaras, and G. Hassapis, “Subject-dependent biosignal features for increased accuracy in psychological stress detection,” *Int. J. Hum. Comput. Stud.*, vol. 71, no. 4, pp. 425–439, Apr. 2013.

[155] L. Allison, S. Hoxie, and T. L. Andrew, “Towards seamlessly-integrated textile electronics: methods to coat fabrics and fibers with conducting polymers for electronic applications,” *Chem. Commun.*, vol. 53, no. 53, pp. 7182–7193, 2017.

[156] L. Beckmann *et al.*, “Characterization of textile electrodes and conductors using standardized measurement setups,” *Physiol. Meas.*, vol. 31, no. 2, pp. 233–247, Feb. 2010.

[157] M. C. Koss and M. A. Davison, “Characteristics of the electrodermal response,” *Naunyn. Schmiedebergs. Arch. Pharmacol.*, vol. 295, no. 2, pp. 153–158, Nov. 1976.

[158] J. W. Sharp, C. S. Bailey, R. D. Johson, and R. L. Kitchell, “Spinal nerve root origin of the median, ulnar and musculocutaneous nerves and their muscle nerve branches to the canine forelimb,” *Anat. Histol. Embryol. J. Vet. Med. Ser. C*, vol. 19, no. 4, pp. 359–368, Dec. 1990.

[159] V. Safarova, L. Hes, and J. Militky, “An approach to electrical resistance measurement eliminating contact resistance problem,” in *2014 International Conference on Applied Electronics*, 2014, no. January, pp. 259–262.

[160] ASTM International, “ASTM E96 / E96M-16, Standard test methods for water vapor

transmission of materials," West Conshohocken, PA, 2016.

[161] A. L. Buck, "New equations for computing vapor pressure and enhancement factor," *J. Appl. Meteorol.*, vol. 20, no. 12, pp. 1527–1532, Dec. 1981.

[162] Buck Research Instruments, "Buck Research Instruments Manual, Appendix 1," Boulder, CO, 1996.

[163] G. Bracco and B. Holst, *Surface Science Techniques*, vol. 51, no. 1. Berlin, Heidelberg: Springer Berlin Heidelberg, 2013.

[164] W. C. Randall, "Quantitation and regional distribution of sweat glands in man," *J. Clin. Invest.*, vol. 25, no. 5, pp. 761–767, Sep. 1946.

[165] W. C. Randall, "Sweat gland activity and changing patterns of sweat secretion on the skin surface," *Am. J. Physiol. Content*, vol. 147, no. 2, pp. 391–398, Oct. 1946.

[166] H. Chen, F. Liao, Z. Yuan, X. Han, and C. Xu, "Simple and fast fabrication of conductive silver coatings on carbon fabrics via an electroless plating technique," *Mater. Lett.*, vol. 196, pp. 205–208, Jun. 2017.

[167] D. Yu, S. Mu, L. Liu, and W. Wang, "Preparation of electroless silver plating on aramid fiber with good conductivity and adhesion strength," *Colloids Surfaces A Physicochem. Eng. Asp.*, vol. 483, pp. 53–59, 2015.

[168] A. Albulbul, "Evaluating major electrode types for idle biological signal measurements for modern medical technology," *Bioengineering*, vol. 3, no. 3, p. 20, Aug. 2016.

[169] S. Ranogajec and G. Geršak, "Measuring site dependency when measuring skin conductance," in *Proceedings of the Twenty-third International Electrotechnical and Computer Science Conference*, 2014, pp. 155–158.

[170] A. F. H. Payne, A. M. Schell, and M. E. Dawson, "Lapses in skin conductance

responding across anatomical sites: comparison of fingers, feet, forehead, and wrist," *Psychophysiology*, vol. 53, no. 7, pp. 1084–1092, Jul. 2016.

[171] G. Wilson, "A simple device for the objective evaluation of peripheral nerve injuries," *J. Hand Surg. Br. Eur. Vol.*, vol. 10, no. 3, pp. 324–330, Oct. 1985.

[172] R. L. Maulsby and R. Edelberg, "The interrelationship between the galvanic skin response, basal resistance, and temperature," *J. Comp. Physiol. Psychol.*, vol. 53, no. 5, pp. 475–479, 1960.

[173] T. Lobstein and J. Cort, "The relationship between skin temperature and skin conductance activity: indications of genetic and fitness determinants," *Biol. Psychol.*, vol. 7, no. 1–2, pp. 139–143, Sep. 1978.

[174] G. Turpin, P. Shine, and M. Lader, "Ambulatory electrodermal monitoring: effects of ambient temperature, general activity, electrolyte media, and length of recording," *Psychophysiology*, vol. 20, no. 2, pp. 219–224, Mar. 1983.

[175] T. Deltombe, P. Hanson, J. Jamart, and M. Clérin, "The influence of skin temperature on latency and amplitude of the sympathetic skin response in normal subjects," *Muscle Nerve*, vol. 21, no. 1, pp. 34–39, Jan. 1998.

[176] W. W. Grings, "Recording of electrodermal phenomena," in *Methods in physiological psychology*, 1st ed., R. F. Thompson and M. M. Patterson, Eds. New York: Academic Press, 1974, pp. 273–296.

[177] M. Weder *et al.*, "Embroidered electrode with silver/titanium coating for long-term ECG monitoring," *Sensors*, vol. 15, no. 1, pp. 1750–1759, Jan. 2015.

[178] R. D. Miller, "Silver-silver chloride electrodermal electrodes," *Psychophysiology*, vol. 5, no. 1, pp. 92–96, Jul. 1968.

[179] A. Cömert, M. Honkala, and J. Hyttinen, “Effect of pressure and padding on motion artifact of textile electrodes,” *Biomed. Eng. Online*, vol. 12, no. 1, p. 26, 2013.

[180] H. Tam and J. G. Webster, “Minimizing electrode motion artifact by skin abrasion,” *IEEE Trans. Biomed. Eng.*, vol. BME-24, no. 2, pp. 134–139, Mar. 1977.

[181] M. Kelsey *et al.*, “Applications of sparse recovery and dictionary learning to enhance analysis of ambulatory electrodermal activity data,” *Biomed. Signal Process. Control*, vol. 40, pp. 58–70, Feb. 2018.

[182] T. Agcayazi, K. Chatterjee, A. Bozkurt, and T. K. Ghosh, “Flexible interconnects for electronic textiles,” *Adv. Mater. Technol.*, vol. 1700277, p. 1700277, Jan. 2018.

[183] J.-S. Roh, “All-fabric interconnection and one-stop production process for electronic textile sensors,” *Text. Res. J.*, vol. 87, no. 12, pp. 1445–1456, Jul. 2017.

Appendices

Appendix A - Additional Figures and Tables for Flexible EDA Electrode Development Based on Polymer Substrate Research

Table A.1 Success rate for fabrication of flexible EDA electrodes

Electrodes	Success Rate (%)	Overall Success Rate (%)
Rectangular, SA: 0.15 cm^2, D: 0.0025 cm	83.3% (10/12)	94%
Rectangular, SA: 0.15 cm^2, D: 0.20 cm	91.7% (11/12)	
Rectangular, SA: 0.15 cm^2, D: 0.50 cm	91.7% (11/12)	
Rectangular, SA:0.15 cm^2, D: 1.00 cm	100% (12/12)	
Rectangular, SA: 0.04 cm^2, D: 0.20 cm	83.3% (10/12)	
Rectangular, SA: 0.52 cm^2, D: 0.20 cm	91.7% (11/12)	
Rectangular, SA: 0.74 cm^2, D: 0.20 cm	100% (12/12)	
Circular, SA: 0.15 cm^2, D: 0.20 cm	100% (12/12)	
Serpentine, SA: 0.15 cm^2, D: 0.20 cm	100% (12/12)	

Table A.2 Bending rigidity and hysteresis values for flexible silver/silver chloride electrodes on Cu coated polyimide film

	Bending Rigidity Average ($N \cdot m/m \times 10^{-4}$)	Bending Hysteresis (Recoverability) Average ($N/m \times 10^{-2}$)
Trial 1	1.33	1.14
Trial 2	1.32	1.10
Trial 3	1.31	1.13
Overall Average	**1.32**	**1.12**
Standard Deviation Between Trials	**0.01**	**0.02**

Table A.3 Compressive force test results for sensors at different locations

Location	Average Force (N)	Standard Deviation Between (±N)
Proximal Phalanx, Middle Finger - Standard EDA Electrode	0.15	0.01
Medial Phalanx, Middle Finger - Standard EDA Electrode	0.13	0.02
Proximal Phalanx, Index Finger - Flexible EDA Electrodes	0.09	0.01
Distal Phalanx, Index Finger - Temperature Sensor	0.08	0.02

Table A.4 One-tailed paired t-test p-values for force tests where H_0: X = Y and H_a: X > Y

X \ Y	Proximal Phalanx, Middle Finger - Standard EDA Electrode	Medial Phalanx, Middle Finger - Standard EDA Electrode	Proximal Phalanx, Index Finger - Flexible EDA Electrodes	Distal Phalanx, Index Finger - Temperature Sensor
Proximal Phalanx, Middle Finger - Standard EDA Electrode		0.12	0.02	0.02
Medial Phalanx, Middle Finger - Standard EDA Electrode			0.00	0.01
Proximal Phalanx, Index Finger - Flexible EDA Electrodes				0.36
Distal Phalanx, Index Finger - Temperature Sensor				

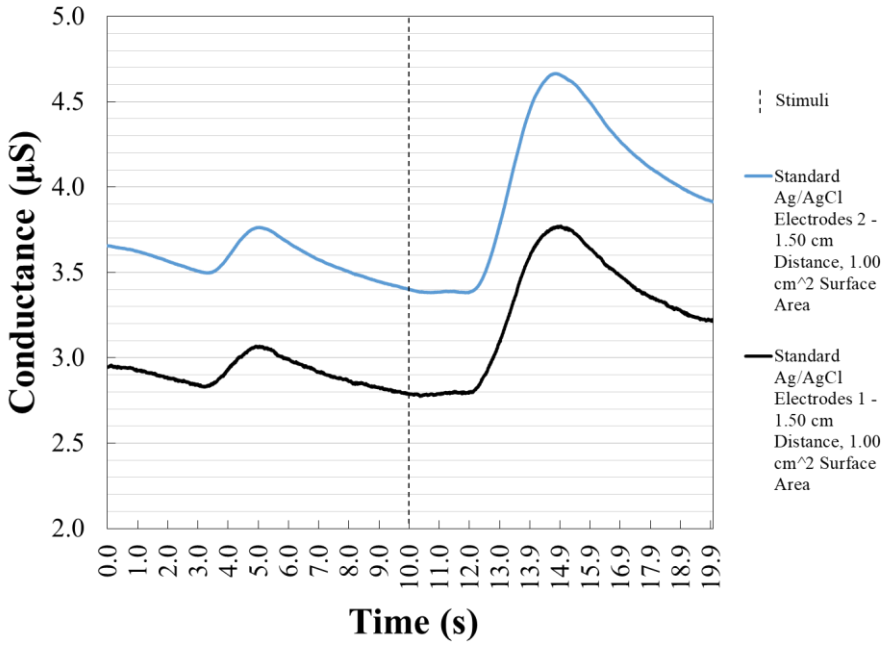

Figure A.1 EDA stimulus responses for dry commercial electrodes (1.00 cm^2 surface area, 1.50 cm distance) when compared to another set of dry commercial electrodes (1.00 cm^2 surface area, 1.50 cm distance). Pearson correlation coefficient is 0.998 when comparing the EDA signals from both sets of standard electrodes.

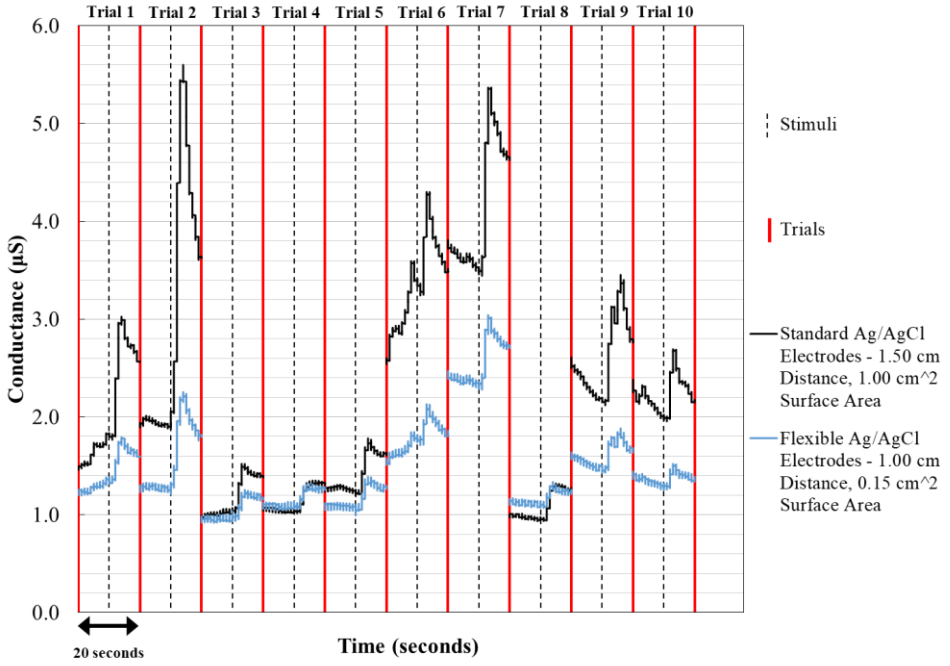

Figure A.2 All EDA stimulus responses for dry flexible electrodes (0.15 cm^2 surface area, 1.00 cm distance) when compared to dry commercial electrodes (1.00 cm^2 surface area, 1.50 cm distance).

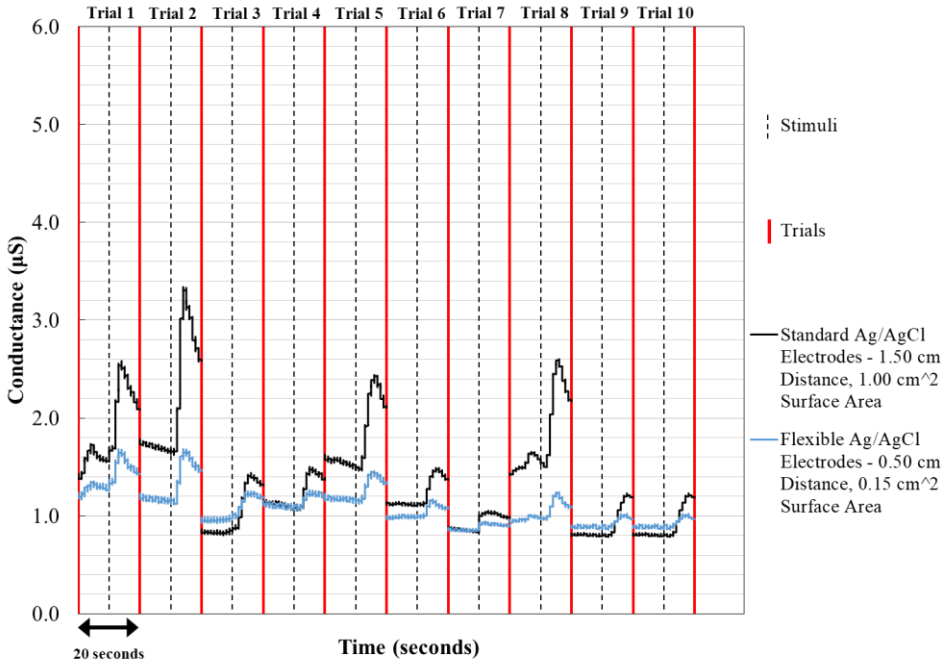

Figure A.3 All EDA stimulus responses for dry flexible electrodes (0.15 cm^2 surface area, 0.50 cm distance) when compared to dry commercial electrodes (1.00 cm^2 surface area, 1.50 cm distance).

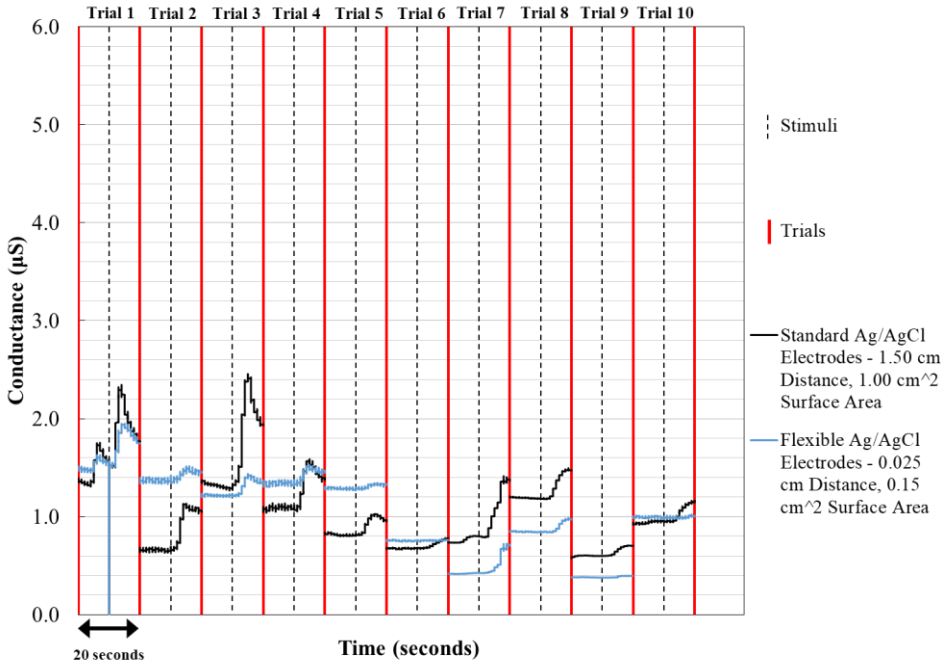

Figure A.4 All EDA stimulus responses for dry flexible electrodes (0.15 cm^2 surface area, 0.025 cm distance) when compared to dry commercial electrodes (1.00 cm^2 surface area, 1.50 cm distance).

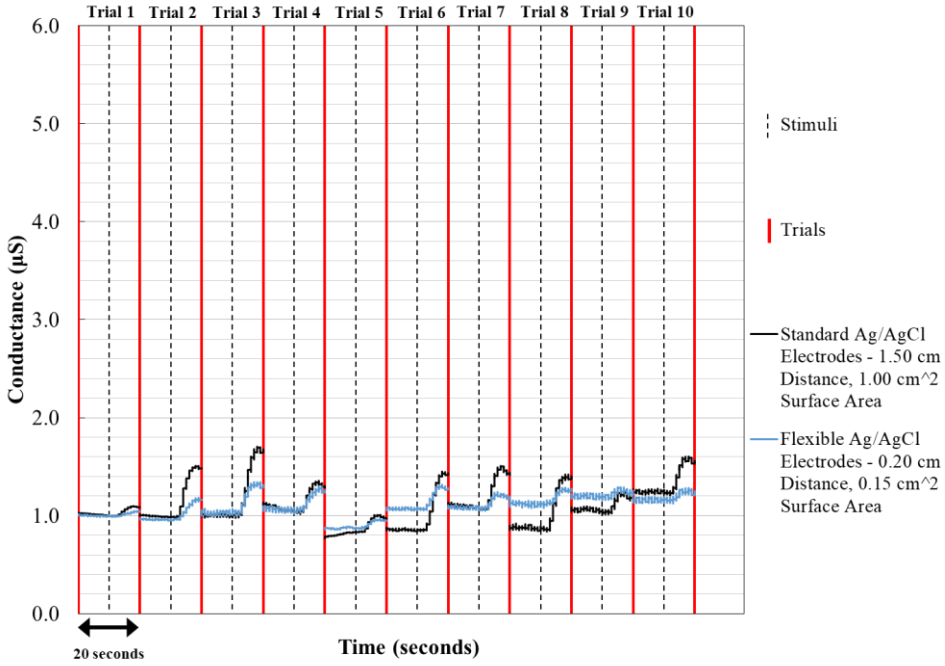

Figure A.5 All EDA stimulus responses for dry flexible electrodes (0.15 cm^2 surface area, 0.20 cm distance) when compared to dry commercial electrodes (1.00 cm^2 surface area, 1.50 cm distance).

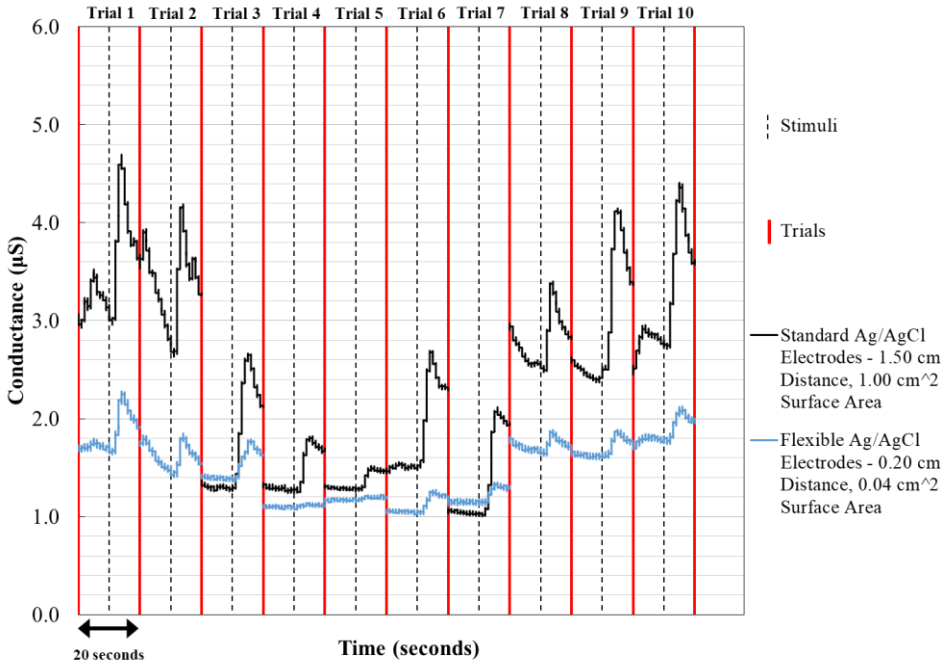

Figure A.6 All EDA stimulus responses for dry flexible electrodes (0.04 cm^2 surface area, 0.20 cm distance) when compared to dry commercial electrodes (1.00 cm^2 surface area, 1.50 cm distance).

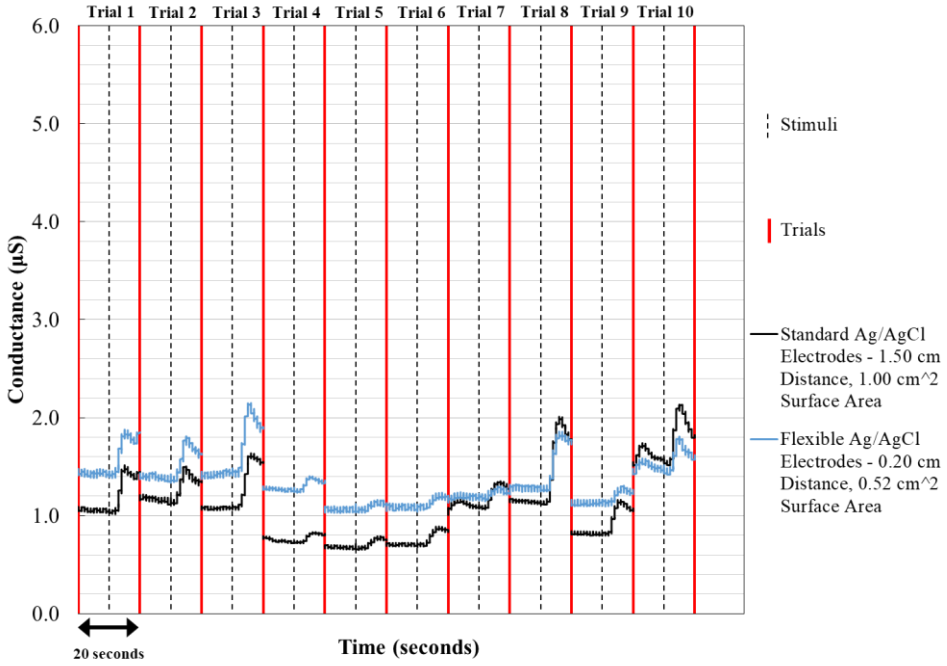

Figure A.7 All EDA stimulus responses for dry flexible electrodes (0.52 cm^2 surface area, 0.20 cm distance) when compared to dry commercial electrodes (1.00 cm^2 surface area, 1.50 cm distance).

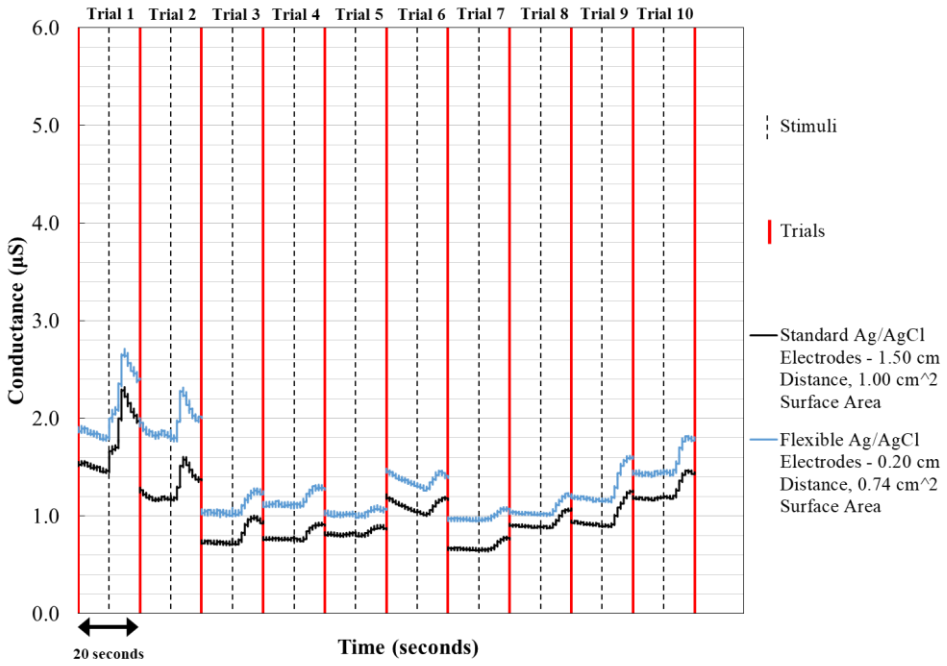

Figure A.8 All EDA stimulus responses for dry flexible electrodes (0.74 cm^2 surface area, 0.20 cm distance) when compared to dry commercial electrodes (1.00 cm^2 surface area, 1.50 cm distance).

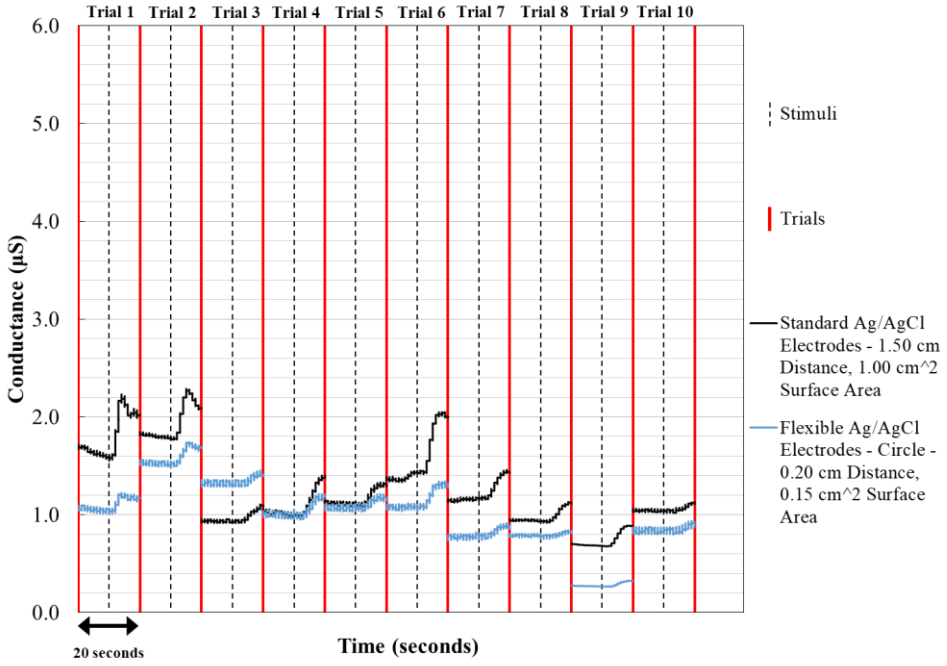

Figure A.9 All EDA stimulus responses for dry flexible electrodes of circular geometry (0.15 cm^2 surface area, 0.20 cm distance) when compared to dry commercial electrodes (1.00 cm^2 surface area, 1.50 cm distance).

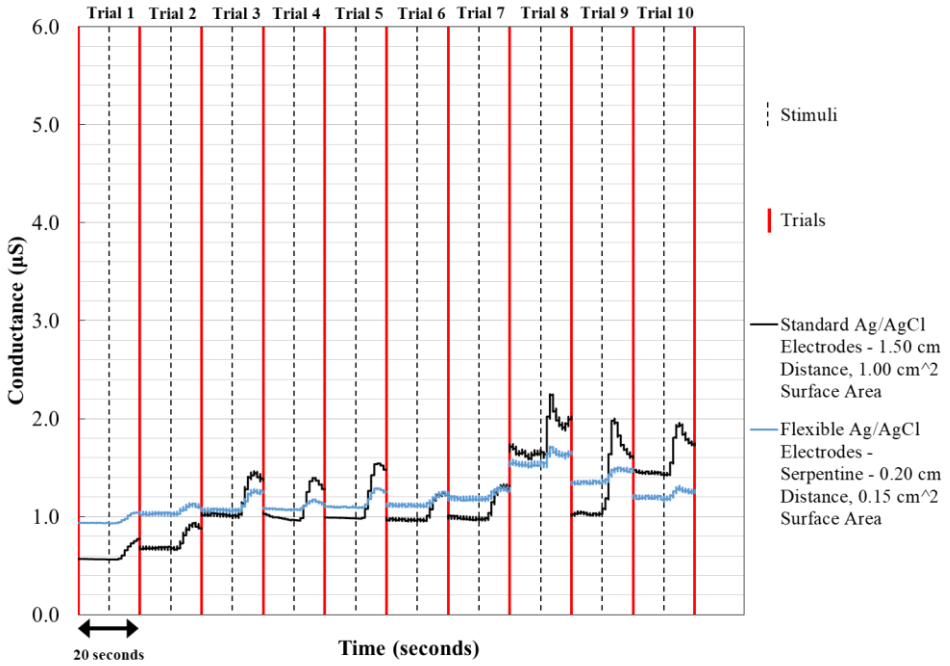

Figure A.10 All EDA stimulus responses for dry flexible electrodes of serpentine geometry (0.15 cm^2 surface area, 0.20 cm distance) when compared to dry commercial electrodes (1.00 cm^2 surface area, 1.50 cm distance).

Table A.5 Pearson correlation coefficients when comparing EDA stimulus response detected by electrodes with different distances (0.15 cm^2 surface area) to EDA response recorded by standard electrodes

Distance Between Electrodes (cm)	Trial 1	Trial 2	Trial 3	Trial 4	Trial 5	Trial 6	Trial 7	Trial 8	Trial 9	Trial 10
0.025	0.923	0.951	0.984	0.981	0.930	0.431	0.949	0.959	0.903	0.271
0.20	0.956	0.987	0.984	0.970	0.971	0.993	0.979	0.965	0.900	0.953
0.50	0.976	0.996	0.988	0.976	0.991	0.943	0.971	0.986	0.954	0.954
1.00	0.995	0.997	0.979	0.982	0.990	0.989	0.992	0.946	0.979	0.939

Table A.6 Pearson correlation coefficients when comparing EDA stimulus response detected by electrodes with different surface areas (0.20 cm distance) to EDA response recorded by standard electrodes

Surface Area of Electrodes (cm^2)	Trial 1	Trial 2	Trial 3	Trial 4	Trial 5	Trial 6	Trial 7	Trial 8	Trial 9	Trial 10
0.04	0.963	0.930	0.974	0.695	0.820	0.968	0.977	0.955	0.984	0.985
0.15	0.956	0.987	0.984	0.970	0.971	0.993	0.979	0.965	0.900	0.953
0.52	0.994	0.985	0.974	0.904	0.943	0.968	0.902	0.995	0.960	0.987
0.74	0.998	0.970	0.986	0.983	0.908	0.977	0.977	0.991	0.994	0.998

Table A.7 Pearson correlation coefficients when comparing EDA stimulus response detected by electrodes with different geometries (0.15 cm^2 surface area, 0.20 cm distance) to EDA response recorded by standard electrodes

Geometry	Trial 1	Trial 2	Trial 3	Trial 4	Trial 5	Trial 6	Trial 7	Trial 8	Trial 9	Trial 10
Circle	0.980	0.974	0.930	0.975	0.950	0.984	0.953	0.767	0.994	0.828
Rectangle	0.956	0.987	0.984	0.970	0.971	0.993	0.979	0.965	0.900	0.953
Serpentine	0.996	0.977	0.993	0.989	0.998	0.976	0.972	0.975	0.957	0.955

Table A.8 Average Pearson correlation coefficients and total sweat gland coverage for all electrode designs

Electrodes	Average Pearson Correlation	Standard Deviation	Sweat Glands Between Electrodes	Sweat Glands Under Electrodes	Total Sweat Glands
Rectangular, SA: 0.15 cm^2, D: 0.0025 cm	0.828	0.256	9.553	69.90	79.45
Rectangular, SA: 0.04 cm^2, D: 0.20 cm	0.925	0.094	68.502	18.64	87.14
Circular, SA: 0.15 cm^2, D: 0.20 cm	0.934	0.075	31.688	69.90	101.59
Rectangular, SA: 0.52 cm^2, D: 0.20 cm	0.961	0.035	68.502	242.32	310.82
Rectangular, SA: 0.15 cm^2, D: 0.20 cm	0.966	0.027	68.502	69.90	138.40
Rectangular, SA: 0.15 cm^2, D: 0.50 cm	0.974	0.018	172.42	69.90	242.32
Rectangular, SA: 0.74 cm^2, D: 0.20 cm	0.978	0.026	68.502	344.84	413.34
Rectangular, SA:0.15 cm^2, D: 1.00 cm	0.979	0.020	344.84	69.90	414.74
Serpentine, SA: 0.15 cm^2, D: 0.20 cm	0.979	0.015	180.109	69.90	250.01

Note: Utilized 233 sweat glands per cm^2 on the palms of adults.

Table A.9 One-tailed paired t-test p-values for average Pearson correlation coefficients for flexible electrode designs where H_0: X = Y and H_a: X > Y

X \ Y	Serpentine, SA: 0.15 cm^2, D: 0.20 cm	Rectangular, SA:0.15 cm^2, D: 1.00 cm	Rectangular, SA: 0.74 cm^2, D: 0.20 cm	Rectangular, SA: 0.15 cm^2, D: 0.50 cm	Rectangular, SA: 0.15 cm^2, D: 0.20 cm	Rectangular, SA: 0.52 cm^2, D: 0.20 cm	Circular, SA: 0.15 cm^2, D: 0.20 cm	Rectangular, SA: 0.04 cm^2, D: 0.20 cm	Rectangular, SA: 0.15 cm^2, D: 0.0025 cm
Serpentine, SA: 0.15 cm^2, D: 0.20 cm		0.500	0.481	0.350	0.190	0.096	0.040	0.066	0.043
Rectangular, SA:0.15 cm^2, D: 1.00 cm			0.480	0.252	0.192	0.128	0.018	0.063	0.043
Rectangular, SA: 0.74 cm^2, D: 0.20 cm				0.142	0.093	0.087	0.065	0.042	0.052
Rectangular, SA: 0.15 cm^2, D: 0.50 cm					0.056	0.168	0.073	0.083	0.045
Rectangular, SA: 0.15 cm^2, D: 0.20 cm						0.378	0.118	0.120	0.063
Rectangular, SA: 0.52 cm^2, D: 0.20 cm							0.190	0.094	0.075
Circular, SA: 0.15 cm^2, D: 0.20 cm								0.423	0.107
Rectangular, SA: 0.04 cm^2, D: 0.20 cm									0.167
Rectangular, SA: 0.15 cm^2, D: 0.0025 cm									

Appendix B - Additional Figures and Tables for Flexible and Breathable Electronic Textile EDA Electrode Development Research

Table B.1 Resistance per cm of original silver coated nylon yarn and the silver/silver chloride yarns fabricated at different applied currents

	Sample Location (cm)	Original Ag yarn (Ω/cm)	Ag/AgCl yarn at 0.5 mA (Ω/cm)	Ag/AgCl yarn at 0.75 mA (Ω/cm)	Ag/AgCl yarn at 1.0 mA (Ω/cm)	Ag/AgCl yarn at 1.25 mA (Ω/cm)
	1	1.9	3.2	8.1	26.6	> 1 M
	2	1.6	2.7	14.5	32.6	> 1 M
	3	2.1	4.6	9.7	31.8	> 1 M
	4	2.2	3.7	11.7	46.6	> 1 M
	5	1.8	3.9	14.6	46.1	> 1 M
	6	2.0	5.4	11.9	55.3	> 1 M
	7	3.6	6.2	10.3	54.4	> 1 M
	8	1.7	4.6	13.3	37.7	> 1 M
	9	1.7	5.0	16.2	30.6	> 1 M
	10	1.8	4.4	13.2	37.9	> 1 M
Average		**2.0**	**4.4**	**12.4**	**40.0**	**N/A**
Standard Deviation		**0.6**	**1.0**	**2.5**	**10.1**	**N/A**

Table B.2 One-tailed paired t-test p-values for resistance per cm of the different conductive yarns where H_0: X = Y and H_a: X > Y

X \ Y	Ag/AgCl yarn at 1.0 mA	Ag/AgCl yarn at 0.75 mA	Ag/AgCl yarn at 0.5 mA	Original yarn Ag
Ag/AgCl yarn at 1.0 mA		< 0.01	< 0.01	< 0.01
Ag/AgCl yarn at 0.75 mA			< 0.01	< 0.01
Ag/AgCl yarn at 0.5 mA				< 0.01
Original yarn Ag				

Table B.3 Resistance per cm of the silver/silver chloride yarns fabricated at an applied current of 0.75 mA with different trials

Sample Location (cm)	Trial 1 (Ω/cm)	Trial 2 (Ω/cm)	Trial 3 (Ω/cm)	Overall Average	Overall Standard Deviation Between
1	8.1	16.2	10.8	**11.0**	**1.8**
2	14.5	17.1	6.0		
3	9.7	11.6	12.0		
4	11.7	10.1	8.2		
5	14.6	15.7	10.1		
6	11.9	14.8	6.1		
7	10.3	9.4	9.5		
8	13.3	8.0	8.0		
9	16.2	7.1	9.6		
10	13.2	6.4	9.9		

Table B.4 Two-tailed paired t-test p-values for resistance per cm of the different trials for the silver/silver chloride yarns fabricated at 0.75 mA where H_0: X = Y and H_a: X ≠ Y

X \ Y	Trial 1	Trial 2	Trial 3
Trial 1		0.67	0.02
Trial 2			0.12
Trial 3			

Table B.5 Resistance of original silver coated nylon yarns at different total lengths

Total Length (cm)	Trial 1 (Ω)	Trial 2 (Ω)	Trial 3 (Ω)	Average (Ω)	Standard Deviation (±Ω)
1	1.8	1.7	1.7	1.7	0.1
2	3.2	3.1	3.3	3.2	0.1
3	4.5	4.4	4.9	4.6	0.3
4	6.3	5.6	6.3	6.1	0.4
5	7.5	6.9	8.0	7.5	0.6
6	9.5	8.4	9.4	9.1	0.6
7	10.5	9.4	11.2	10.4	0.9
8	12.2	10.8	12.6	11.9	0.9
9	13.7	12.3	13.6	13.2	0.8
10	15.5	13.7	15.3	14.8	1.0

Table B.6 Resistance of optimal silver/silver chloride coated nylon yarns at different total lengths

Total Length (cm)	Trial 1 (Ω)	Trial 2 (Ω)	Trial 3 (Ω)	Average (Ω)	Standard Deviation (±Ω)
1	12.7	13.8	12.6	13.0	0.7
2	23.6	29.6	23.4	25.5	3.5
3	36.5	40.6	36.9	38.0	2.3
4	46.9	54.1	46.0	49.0	4.4
5	58.7	61.2	62.5	60.8	1.9
6	65.9	76.2	70.6	70.9	5.2
7	73.7	83.0	80.6	79.1	4.8
8	84.0	96.4	89.1	89.8	6.2
9	94.1	109.1	100.9	101.4	7.5
10	102.7	125.2	110.8	112.9	11.4

Table B.7 Contact resistances for silver coated nylon yarns and for silver/silver chloride coated nylon yarns

	Length 1 (cm)	Length 2 (cm)	Contact Resistance for Ag Yarn (Ω)	Contact Resistance for Ag/AgCl Yarn (Ω)
	1	2	0.1	0.3
	2	4	0.2	1.0
	3	6	0.1	2.6
	4	8	0.1	4.1
	5	10	0.0	4.4
Average			**0.11**	**2.46**
Standard Deviation			**0.05**	**1.81**

Note: One-tailed paired t-test p-value of 0.02 between averages, therefore contact resistance determined for Ag coated yarn is greater than for Ag/AgCl yarn

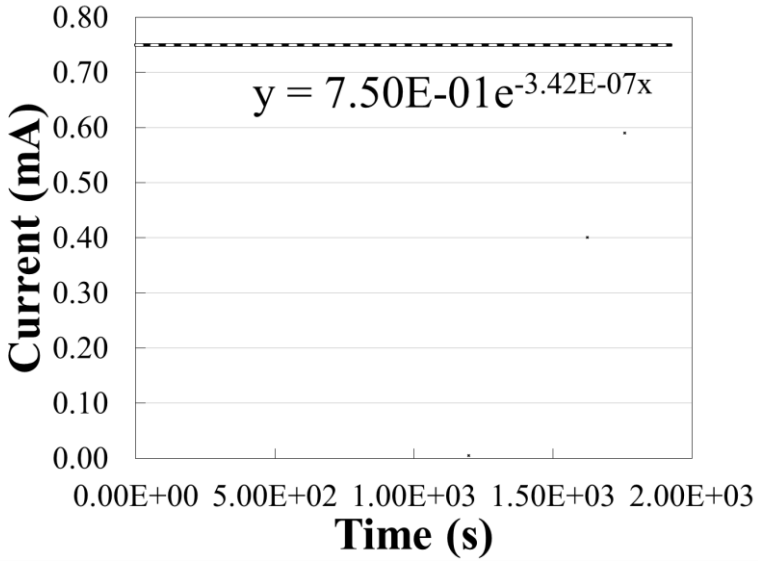

Figure B.1 Current versus time for the roll-to-roll electrochemical fabrication of optimal silver/silver chloride coated nylon yarn with an exponential trend line and equation indicated.

Table B.8 Maximum load at break and tenacity for silver and optimal silver/silver chloride yarns

	Trial	Ag Yarn (N)	Ag Yarn (N/tex)	Ag/AgCl Yarn (N)	Ag/AgCl Yarn (N/tex)
	1	12.74	0.54	10.53	0.44
	2	11.33	0.48	11.80	0.50
	3	12.50	0.53	12.17	0.51
Average		**12.19**	**0.52**	**11.50**	**0.48**
Standard Deviation		**0.75**	**0.03**	**0.86**	**0.04**

Note: Two-tailed paired t-test p-value of 0.48 and 0.38 between N averages and N/tex averages, respectively. Ag yarn dtex is 234 and Ag/AgCl yarn is 238 dtex.

Table B.9 Breathability testing parameters for different textile substrates

Textile Substrate Trials	Average Temperature (°C)	Standard Deviation Between Trials (± °C)	Average RH (%)	Standard Deviation Between Trials (± %)	Average Air Flow (FPS)	Standard Deviation Between Trials (± FPS)
Cotton	22.63	0.44	28.55	5.80	0.97	0.01
Nylon	22.82	0.41	26.99	1.38	0.97	0.02
Polyester	22.78	0.41	28.26	2.24	0.97	0.03
Overall Average	**22.74**		**27.93**		**0.97**	
Standard Deviation Between Textile Trials	**0.10**		**0.83**		**0.00**	

Table B.10 Breathability testing results for different textile substrates

Textile Substrate	Permeability (g/Pa·s·m)	Standard Deviation Between Trials (g/Pa·s·m)	Permeance (g/Pa·s·m^2)	Standard Deviation Between Trials (g/Pa·s·m^2)	Average Rate of Water Vapor Trans-mission (g/h·m^2)	Standard Deviation Between Trials (± g/h·m^2)
Cotton	**7.02E-10**	**2.69E-11**	**6.50E-06**	**2.49E-07**	**46.09**	**5.97**
Nylon	**6.50E-10**	**1.85E-11**	**6.70E-06**	**1.91E-07**	**49.04**	**3.53**
Polyester	**4.05E-10**	**1.18E-11**	**6.23E-06**	**1.82E-07**	**44.62**	**2.66**

Table B.11 One-tailed paired t-test p-values for permeability of the different textile substrates where H_0: X = Y and H_a: X > Y

X / Y	Cotton	Nylon	Polyester
Cotton		0.03	< 0.01
Nylon			< 0.01
Polyester			

Table B.12 Water droplet contact angles for different textile substrates and silver/silver chloride material

Trial	Nylon Side 1 (°)	Nylon Side 2 (°)	Nylon Average (°)	Polyes-ter Side 1 (°)	Polyes-ter Side 2 (°)	Polyes-ter Average (°)	Ag/AgCl Side 1 (°)	Ag/AgCl Side 2 (°)	Ag/AgCl Average (°)	Cotton (°)
1	126	122	124	126	106	116	55	57	56	0
2	127	119	123	127	106	116	55	69	62	0
3	128	122	125	126	113	120	61	63	62	0
Average			124			117			60	0
Standard Deviation			1			2			3	0

Table B.13 One-tailed paired t-test p-values for water droplet contact angles of the different textile substrates and silver/silver chloride material where H_0: X = Y and H_a: X < Y

X / Y	Cotton	Ag/AgCl	Polyester	Nylon
Cotton		0.00	0.00	0.00
Ag/AgCl			0.00	0.00
Polyester				0.01
Nylon				

Table B.14 Bending rigidity and hysteresis values for textile substrates

	Cotton		Nylon		Polyester	
	Bending Rigidity Average (Nm/m x 10^{-4})	**Bending Hysteresis (Recoverability) Average (N/m x 10^{-2})**	**Bending Rigidity Average (Nm/m x 10^{-4})**	**Bending Hysteresis (Recoverability) Average (N/m x 10^{-2})**	**Bending Rigidity Average (Nm/m x 10^{-4})**	**Bending Hysteresis (Recoverability) Average (N/m x 10^{-2})**
Trial 1	0.0306	0.0302	0.0814	0.0573	0.0995	0.0090
Trial 2	0.0320	0.0319	0.0799	0.0504	0.1005	0.0100
Trial 3	0.0326	0.0297	0.0784	0.0530	0.0976	0.0095
Overall Average	**0.0317**	**0.0306**	**0.0799**	**0.0535**	**0.0992**	**0.0095**
Standard Deviation Between Trials	**0.0010**	**0.0011**	**0.0015**	**0.0035**	**0.0015**	**0.0005**

Table B.15 One-tailed paired t-test p-values for bending rigidity values where H_0: X = Y and H_a: X < Y

X \ **Y**	**Cotton**	**Nylon**	**Polyester**
Cotton		0.00	0.00
Nylon			0.00
Polyester			

Table B.16 One-tailed paired t-test p-values for bending hysteresis values where H_0: X = Y and H_a: X < Y

X \ **Y**	**Polyester**	**Cotton**	**Nylon**
Polyester		0.00	0.00
Cotton			0.01
Nylon			

Table B.17 Success rate for prototyping e-textile EDA electrode straps with textile substrates

Substrate Material	**Success Rate (%)**	**Overall Success Rate (%)**
Cotton Textile	50% (3/6)	50%
Nylon Textile	50% (3/6)	
Polyester Textile	50% (3/6)	

Table B.18 Resistances from electrical connector to end of e-textile electrodes for e-textile EDA electrode straps with textile substrates

Proto-type	Cotton Textile Substrate		Nylon Textile Substrate		Polyester Textile Substrate		Overall Average	Overall Standard Deviation
	Electrode 1 (Ω)	Electrode 2 (Ω)	Electrode 1 (Ω)	Electrode 2 (Ω)	Electrode 1 (Ω)	Electrode 2 (Ω)		
1	99.60	55.00	81.40	83.70	43.10	87.40	80.96	26.53
2	53.10	150.70	83.40	73.50	98.60	84.20		
3	36.20	91.70	105.30	94.80	58.10	77.50		

Table B.19 Compressive force test results for sensors at different locations

Location	Average (N)	Standard Deviation Between (±N)
Proximal Phalanx, Middle Finger - Standard EDA Electrode	0.15	0.01
Medial Phalanx, Middle Finger - Standard EDA Electrode	0.13	0.02
Distal Phalanx, Middle Finger - E-textile EDA Electrodes	0.07	0.00
Distal Phalanx, Index Finger - E-textile EDA Electrodes	0.07	0.01
Distal Phalanx, Ring Finger - Temperature Sensor	0.07	0.01
Distal Phalanx, Little Finger - E-textile EDA Electrodes	0.06	0.01

Table B.20 One-tailed paired t-test p-values for force tests where H_0: X = Y and H_a: X > Y

X \ Y	Proximal Phalanx, Middle Finger - Standard EDA Electrode	Medial Phalanx, Middle Finger - Standard EDA Electrode	Distal Phalanx, Middle Finger - E-textile EDA Electrodes	Distal Phalanx, Index Finger - E-textile EDA Electrodes	Distal Phalanx, Ring Finger – Tempera-ture Sensor	Distal Phalanx, Little Finger - E-textile EDA Electrodes
Proximal Phalanx, Middle Finger - Standard EDA Electrode		0.12	0.01	0.00	0.00	0.00
Medial Phalanx, Middle Finger - Standard EDA Electrode			0.01	0.01	0.01	0.02
Distal Phalanx, Middle Finger - E-textile EDA Electrodes				0.42	0.23	0.31
Distal Phalanx, Index Finger - E-textile EDA Electrodes					0.42	0.24
Distal Phalanx, Ring Finger - Temperature Sensor						0.36
Distal Phalanx, Little Finger - E-textile EDA Electrodes						

Table B.21 Sweat gland density experimental results at different locations

Trial	Distal Phalanx, Little Finger	Distal Phalanx, Middle Finger	Distal Phalanx, Index Finger	Proximal Phalanx, Middle Finger	Medial Phalanx, Middle Finger
1	434	349	314	274	217
2	416	353	320	242	258
3	425	355	336	248	223
Average	**425**	**352**	**323**	**255**	**233**
Standard Deviation	**9**	**3**	**11**	**17**	**22**

Table B.22 One-tailed paired t-test p-values for sweat gland density tests at different locations where H_0: X = Y and H_a: X > Y

X \ Y	Distal Phalanx, Little Finger	Distal Phalanx, Middle Finger	Distal Phalanx, Index Finger	Proximal Phalanx, Middle Finger	Medial Phalanx, Middle Finger
Distal Phalanx, Little Finger		0.00	0.00	0.00	0.00
Distal Phalanx, Middle Finger			0.01	0.01	0.01
Distal Phalanx, Index Finger				0.02	0.01
Proximal Phalanx, Middle Finger					0.20
Medial Phalanx, Middle Finger					

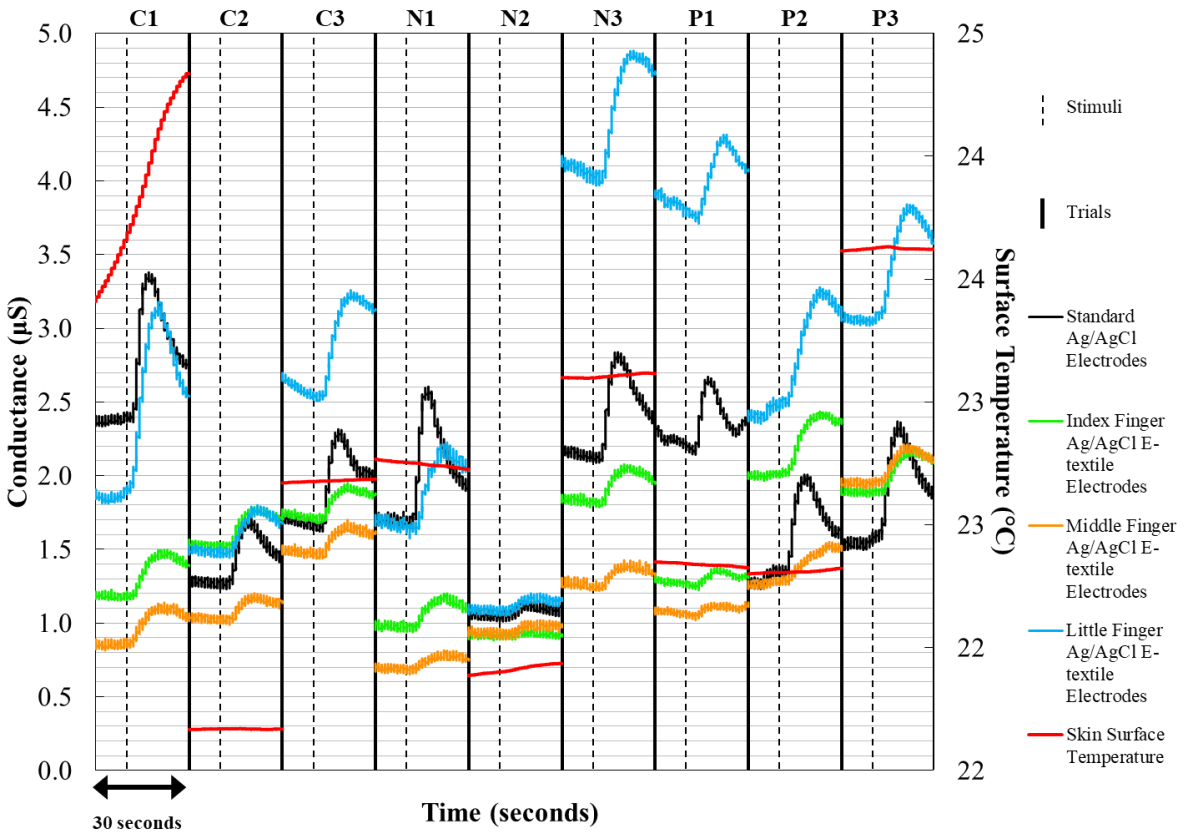

Figure B.2 All EDA stimulus responses for dry e-textile electrodes (0.12 cm^2 surface area, 0.40 cm distance) on the distal phalanx of the little, middle and index fingers compared to dry commercial electrodes (1.00 cm^2 surface area, 1.50 cm distance) on the medial and proximal phalanges of the middle finger. Skin surface temperature indicated and all trials for cotton (C), nylon (N) and polyester (P) are shown.

Table B.23 Pearson correlation coefficients when comparing EDA stimulus response detected by e-textile electrodes with different textile substrates at different locations on the hand to the EDA response recorded by standard electrodes

Substrate	Index Finger	Middle Finger	Little Finger
Cotton Trial 1	0.859	0.865	0.935
Cotton Trial 2	0.942	0.940	0.915
Cotton Trial 3	0.927	0.934	0.874
Nylon Trial 1	0.746	0.686	0.658
Nylon Trial 2	0.820	0.860	0.901
Nylon Trial 3	0.920	0.904	0.832
Polyester Trial 1	0.705	0.723	0.503
Polyester Trial 2	0.849	0.766	0.824
Polyester Trial 3	0.866	0.909	0.893

Table B.24 Average Pearson correlation coefficients for all e-textile EDA electrodes at different locations with different textile substrates

	Distal Phalanx of Index Finger		Distal Phalanx of Middle Finger		Distal Phalanx of Little Finger	
	Average	**Standard Deviation**	**Average**	**Standard Deviation**	**Average**	**Standard Deviation**
Cotton Textile Substrate	0.909	0.044	0.913	0.041	0.908	0.031
Nylon Textile Substrate	0.828	0.087	0.817	0.115	0.797	0.125
Polyester Textile Substrate	0.807	0.089	0.799	0.097	0.740	0.208

Table B.25 One-tailed paired t-test p-values for all average Pearson correlation coefficients for all e-textile EDA electrodes at different locations with different textile substrates where H_0: X = Y and H_a: X > Y

Distal Phalanx of Index Finger p-values			
X \ Y	**Cotton**	**Nylon**	**Polyester**
Cotton		0.08	0.03
Nylon			0.24
Polyester			

Cotton Textile Substrate p-values			
X \ Y	**Index**	**Middle**	**Little**
Index		0.15	0.49
Middle			0.45
Little			

Distal Phalanx of Middle Finger p-values			
X \ Y	**Cotton**	**Nylon**	**Polyester**
Cotton		0.08	0.06
Nylon			0.35
Polyester			

Nylon Textile Substrate p-values			
X \ Y	**Index**	**Middle**	**Little**
Index		0.36	0.32
Middle			0.31
Little			

Distal Phalanx of Little Finger p-values			
X \ Y	**Cotton**	**Nylon**	**Polyester**
Cotton		0.16	0.17
Nylon			0.23
Polyester			

Polyester Textile Substrate p-values			
X \ Y	**Index**	**Middle**	**Little**
Index		0.19	0.22
Middle			0.71
Little			

Table B.26 Minimum to maximum EDA stimulus response signal percent change per sweat gland when recording with e-textile EDA electrodes at different locations

	Distal Phalanx of Index Finger	Distal Phalanx of Middle Finger	Distal Phalanx of Little Finger
Cotton Textile Substrate	0.0709%	0.0806%	0.1011%
	0.0517%	0.0503%	0.0466%
	0.0429%	0.0440%	0.0541%
Nylon Textile Substrate	0.0677%	0.0565%	0.0687%
	0.0245%	0.0360%	0.0298%
	0.0432%	0.0410%	0.0441%
Polyester Textile Substrate	0.0337%	0.0305%	0.0328%
	0.0596%	0.0585%	0.0664%
	0.0456%	0.0381%	0.0503%
Average	**0.0489%**	**0.0484%**	**0.0549%**
Standard Deviation	**0.0153%**	**0.0152%**	**0.0218%**

Table B.27 One-tailed paired t-test p-values for all average minimum to maximum EDA stimulus response signal percent change per sweat gland at different locations where H_0: X = Y and H_a: X > Y

X / Y	Distal Phalanx of Little Finger	Distal Phalanx of Middle Finger	Distal Phalanx of Index Finger
Distal Phalanx of Little Finger		0.03	0.06
Distal Phalanx of Middle Finger			0.42
Distal Phalanx of Index Finger			

Table B.28 Signal percent change over a 4-hour EDA recording experiment

Time (h)	Skin Surface Temperature Signal Change (%)	E-textile Ag/AgCl Electrodes Baseline Signal Change (%)	Standard Ag/AgCl Electrodes Baseline Signal Change (%)
1	12%	22%	26%
2	33%	25%	54%
3	52%	45%	110%
4	60%	28%	61%